WOOD AND FIBER SCIENCE

The Sustainable Natural Materials Journal

Volume 57, Number 4, 2025 (ISSN 0735-6161)

Open Access

JOURNAL OF THE

SWST – International Society of Wood Science and Technology

WOOD AND FIBER SCIENCE

Wood and Fiber Science is published quarterly in January, April, July, and October by the Society of Wood Science and Technology, P.O. Box 6155, Monona, WI 53716-6155

There are three classes of membership (electronic only) in the Society: Members – dues $150; Retired Members – dues $75; Student Members – dues $25. We also have a membership category for individuals from Emerging Countries where individual members pay $30, individual students pay $10; Emerging Groups of 10 pay $290, and Student Groups of 10 pay $90. Institutions and individuals who are not members pay $300 per volume (electronic only). Applications for membership and information about the Society may be obtained from the Executive Director, Society of Wood Science and Technology, P.O. Box 6155, Monona, WI 53716-6155 or found at the website https://www.swst.org.

Site licenses are also available with a charge of:

$300/yr for single online membership, access by password and email
$500/yr for institutional subscribers with 2–10 IP addresses
$750/yr for institutional subscribers with 11–50 IP addresses
$1000/yr for institutional subscribers with 51–100 IP addresses
$1500/yr for institution subscribers with 101–200 IP addresses
$2000/yr for institutions subscribers with over 200 IP addresses.

New subscriptions begin with the first issue of a new volume. All subscriptions are to be ordered through the Executive Director, Society of Wood Science and Technology. The Executive Director, at the Business Office shown below or by email to execdir@swst.org, should be notified 30 days in advance of a change of email address.

Business Office: Society of Wood Science and Technology, P.O. Box 6155, Monona, WI 53716-6155.
Editorial Office: Jeff Morrell, jeff.morrell@oregonstate.edu
Copy Editor, *Wood and Fiber Science* and *BioProducts Business*: Caryn M. Davis, Cascadia Editing, Philomath, OR USA

EDITORIAL AND PUBLICATION POLICY

Wood and Fiber Science as the official publication of the Society of Wood Science and Technology publishes open access papers with both professional and technical content. Original papers of professional concern, or based on research of international interest dealing with the science, processing, and manufacture of wood and composite products of wood or wood fiber origin will be considered.

All manuscripts are to be written in US English, the text should be proofread by a native speaker of English prior to submission. Any manuscript submitted must be unpublished work not being offered for publication elsewhere.

Papers will be reviewed by referees selected by the editor and will be published in approximately the order in which the final version is received. Research papers will be judged on the basis of their contribution of original data, rigor of analysis, and interpretations of results; in the case of reviews, on their relevancy and completeness.

Color photos/graphics will be offered at no additional cost to authors. The Open Access fee will be $1800/article for SWST members and $2000/article for nonmembers. Reduced rates are available for authors based in developing countries.

Technical Notes

Authors are invited to submit Technical Notes to the Journal. A Technical Note is a concise description of a new research finding, development, procedure, or device. The length should be **no more than two printed pages in WFS**, which would be five pages or less of double-spaced text (TNR12) with normal margins on 8.5 x 11 paper, including space for figures and tables. In order to meet the limitation on space, figures and tables should be minimized, as should be the introduction, literature review and references. The Journal will attempt to expedite the review and publication process. As with research papers, Technical Notes must be original and go through a similar double-blind, peer review process.

On-line Access to *Wood and Fiber Science* Back Issues

SWST is providing readers with a means of searching all articles in *Wood and Fiber Science* from 1968 to present.

Visit the SWST website at https://www.swst.org and go to Wood & Fiber Science Online. Click on either SWST Member Publication access (SWST members) or Subscriber Publication access (Institution Access). All must login with their email and password on the https://www.swst.org site or use their ip authentication if they have a site license.

As an added benefit to our current subscribers, you can now access the electronic version of every printed article along with exciting enhancements that include:

- IP authentication for institutions (only with site license)
- Enhanced search capabilities
- Email alerting of new issues
- Custom links to your favorite titles

(ISSN 0735-6161)

WOOD AND FIBER SCIENCE

JOURNAL OF THE SOCIETY OF WOOD SCIENCE AND TECHNOLOGY

VOLUME 57 OCTOBER 2025 NUMBER 4

CONTENTS

Articles

Democratizing essential wood identification information for Central American timber markets with an ergonomically designed, interactive, bilingual smartphone app

Kyatt G. Spessert
Graduate Research Assistant
Department of Sustainable Bioproducts, Mississippi State University
Mississippi State, MS 39762-9820; Email: kgs211@msstate.edu

*Frank C. Owens**†*
Associate Professor
Department of Sustainable Bioproducts, Mississippi State University
Mississippi State, MS 39762-9820; Email: fco7@msstate.edu

Adriana Costa†*
Assistant Professor
Department of Sustainable Bioproducts, Mississippi State University
Mississippi State, MS 39762-9820; Email: adc751@msstate.edu

Rafael Arévalo
Botanist and Collections Manager
Center for Wood Anatomy Research, USDA Forest Products Laboratory
Madison, WI 53726-2398; Email: jorge.arevaloburbano@usda.gov

Alex C. Wiedenhoeft
Research Botanist and Team Leader
Center for Wood Anatomy Research, USDA Forest Products Laboratory, Madison, WI 53726-2398
and
Department of Botany, University of Wisconsin, Madison, WI 53706-1313
and
Department of Sustainable Bioproducts, Mississippi State University, Starkville, MS 39762-9820
and
Department of Forestry and Natural Resources, Purdue University, West Lafayette, IN 47907-2061
and
Departamento de Ciências Biológicas (Botânica), Universidade Estadual Paulista—Botucatu
São Paulo, Brasil; Email: alex.c.wiedenhoeft@usda.gov

(Received 14 May 2025)

Abstract. In 2022, scientists from the Center for Wood Anatomy Research at the USDA Forest Products Laboratory published a field manual entitled *Identification of Central American, Mexican, and Caribbean Woods*. Bilingual with English and Spanish side-by-side on each page, this publication provided step-by-step processes with simple tools to enable readers with no previous experience in wood anatomy or identification to identify woods of the region. In use, the manual presented potential ergonomic challenges in both print and PDF formats. The objective of this project was to eliminate these challenges by transforming the field manual into a smartphone app. The *WhatWood? Central America* app was built in Visual Studio 2022 using Microsoft's .NET Multi-platform App UI (.NET MAUI). The app is available as a free download on both Android and iOS platforms and can run without an internet connection. Ergonomic modifications included small-screen-optimization, adjustable text, image zooming and panning, and a colorblind viewing option. Dichotomous key navigation was automated, removing the need for manual page turning. Quizzes were added to reinforce the learning of anatomical features. The settings page was configured to show only one language at a time to eliminate the potential for confusion caused by parallel translations. Transforming the original source material into a smartphone application has democratized essential wood identification information for the Central American, Caribbean, and Mexican timber markets by making it available at no cost to virtually anyone in the world with a mobile device, delivering content in both Spanish and English, eliminating potential barriers for operators with mild visual impairments, and providing interactive functionality for self-study.

Keywords: Smartphone app; Wood identification; Illegal logging; Mexico; Caribbean; Central America; Quiz

* Corresponding author
† Society of Wood Science & Technology member

Introduction

Exercising due diligence in the responsible management of forest products supply chains requires the assessment and mitigation of risk (PEFC 2020; Wang et al. 2023). Mexico and large parts of Central America[1] and the Caribbean[2] have come under scrutiny in recent years over concerns about illegal logging and wood trade. A 2022 assessment by Forest Trends, a nonprofit organization based in Washington, D.C., categorized 24 out of 27 countries[3] in these regions as medium- or higher-risk for illegal logging and associated trade (Table 1).

Multiple studies have offered evidence suggesting that illegal logging is a problem in Mexico, Central America, and the Caribbean (Buffum 2006; Miller 2011; Mulligan and Bennear 2015; Richards et al. 2003; Torres-Rojo 2021; Vardeman and Runk 2020). Torres-Rojo (2021) estimated that, in Mexico, in the economic census years of 2009, 2014, and 2019, the roundwood-equivalent volume of sawn wood from illegally harvested sources exceeded that of legally harvested materials. Miller (2011) cited studies conducted by the Ministerio de Ambiente y Energía (MINAE) (MINAE 2001) and the Tropical Agricultural Research and Training Center (CATIE) (Campos Arce et al. 2001) reporting that approximately 25%–35% of wood cut and commercialized in Costa Rica is illegal. Richards et al. (2003) estimated that approximately 50% of hardwood timber and 40%–45% of softwood timber produced in Nicaragua are of undocumented origin, and, in Honduras, 75%–85% and 30%–50%, respectively. Vardeman and Runk (2020) highlighted an uptick in illegal logging of cocobolo rosewood (*Dalbergia retusa*) in Panama from the early 2010s. Mulligan and Bennear (2015) estimated that over US$21 million of logs of cedar (*Cedrela odorata*), mahogany (*Swietenia macrophylla*), and rosewood (*Dalbergia* spp.), including Honduran rosewood (*Dalbergia stevensonii*), were illegally harvested in Belize from 2010 to 2012. Buffum (2006) suggested that illegal logging was a major problem in the Forêt des Pins forest reserve in Haiti.

In 2023, the collective export value of fuelwood, industrial roundwood, sawn wood, further-processed wood, wood products for domestic/decorative use, and wood furniture from Central America, Mexico, and the Caribbean exceeded US$2.6 billion (FAOSTAT 2025). As exports of wood products are substantial, concern that illegally harvested materials could be moving between countries in these regions or finding their way into the greater global market is justifiable.

To assist customs inspectors and other control officers in the identification of endangered or controlled species from Central America, Mexico, and the Caribbean, scientists from the Center for Wood Anatomy Research at the USDA Forest Service, Forest Products Laboratory published a revised and expanded

Table 1. Illegal Logging and Associated Trade (ILAT) risk scores and categories for Mexico and countries/territories in Central America and the Caribbean (Forest Trends 2022).

Region	Country/Territory	ILAT Score *	Risk Category
Mexico	Mexico	69.6	Higher
Central America	Honduras	85.7	Higher
	Nicaragua	79.7	Higher
	Guatemala	79.6	Higher
	Belize	65.0	Higher
	El Salvador	54.0	Higher
	Panamá	41.4	Medium
	Costa Rica	30.3	Medium
Caribbean	Haiti	88.7	Higher
	Cuba	65.8	Higher
	Dominican Republic	59.9	Higher
	Trinidad and Tobago	51.4	Higher
	Jamaica	39.8	Medium
	Grenada	39.5	Medium
	Saint Kitts and Nevis	37.5	Medium
	Dominica	37.3	Medium
	Puerto Rico	36.3	Medium
	Antigua and Barbuda	34.9	Medium
	Bahamas	34.3	Medium
	Saint Vincent and the Grenadines	33.9	Medium
	Barbados	31.6	Medium
	Saint Lucia	31.5	Medium
	Aruba	25.4	Medium
	Cayman Islands	28.7	Medium
	Anguilla	17.5	Lower
	Martinique	16.1	Lower
	U.S. Virgin Islands	15.6	Lower

* ILAT scores are based on political, business, government, and corruption data from sources such as the World Bank, United Nations, and others. Scores less than 25 are categorized as "lower-risk," between 25 and 50 as "medium-risk," and greater than 50 as "higher-risk," but scores are relative and should not be interpreted as absolute measures. A summary of data and the methodology used by Forest Trends and the Environmental Investigation Agency (EIA) to determine scores can be found at https://www.forest-trends.org/wp-content/uploads/2021/08/Methodology-for-State-ILAT-Project-Aug-2021-1.pdf.

1. Belize, Costa Rica, El Salvador, Guatemala, Honduras, Nicaragua and Panamá.
2. Anguilla; Antigua and Barbuda; Aruba; Bahamas; Barbados; Bonaire, Sint Eustatius, and Saba; British Virgin Islands; Cayman Islands; Cuba; Curaçao; Dominica; Dominican Republic; Grenada; Guadeloupe; Haiti; Jamaica; Martinique; Montserrat; Puerto Rico; Saint Barthélemy; Saint Kitts and Nevis; Saint Lucia; Saint Vincent and the Grenadines; Sint Maarten (French and Dutch parts); Trinidad and Tobago; Turks and Caicos Islands; and U.S. Virgin Islands.
3. Nine of the total 36 mentioned in footnote 2 did not have a risk score or category.

second edition of a field manual for macroscopic identification of common commercial woods from these regions (Arévalo and Wiedenhoeft 2022). Bilingual in English and Spanish, this publication was intended to provide step-by-step processes with simple tools to enable customs officials with no previous experience in wood anatomy or identification to screen wood products with a hand lens and flag suspicious shipments for further forensic investigation in a laboratory. Available in both print and PDF formats, the manual can be used as a tool in both law enforcement and academia, yet it presents potential ergonomic challenges in both paper and electronic formats. To address these challenges, this project reimagined the original publication by transforming it into a smartphone application with added functionality.

Project background

In the late 2000s, the CITES management authorities of Nicaragua and Honduras requested assistance, as part of a Central America-Dominican Republic Free Trade Agreement (CAFTA-DR) implementation plan, from the U.S. Forest Service International Programs. Beginning in 2007, trainers were sent to Central America to teach wood identification workshops on CITES species to customs, military, and government officials responsible for enforcing timber trade regulations in their countries. When author Wiedenhoeft taught a workshop in Honduras, he met with the chief of the newly established National Institute of Forest Conservation, Protected Areas and Wildlife (ICF), Ramón Álvarez, as well as ICF employees Oscar Oqueli and Carla de Martinez, who, having seen the CITES identification guide (Environment Canada 2002), expressed a greater need for a wood identification field manual that covered not only controlled species but also species commonly traded among Central American nations.

To address this need, the U.S. Agency for International Development (USAID), under the CAFTA-DR Environmental Cooperation Agenda, provided funding via the U.S. Forest Service (USFS) International Programs to author a field manual for Central American species from CAFTA-DR countries, with additional support from the U.S. Forest Service, Forest Products Laboratory (FPL) and the Forest Products Society (Wiedenhoeft 2011). Fully bilingual, the publication was laid out in two columns—Spanish on the left and English on the right (Wiedenhoeft 2011). Intended as a tool for customs inspectors and other officials to monitor woods going in and out of their countries, the manual featured an introduction to wood anatomy, step-by-step instructions on how to conduct field identifications with a hand lens, a wood identification key, and species description pages (Wiedenhoeft 2011).

Following the initial publication, workshops across Latin America were supported by USFS International Programs. Although the manual was not intended to be used as an academic reference, it was taken up by some wood anatomy professors at universities in the region (V. Angyalossy, personal communication, June 25, 2013). Chapters of the manual also contributed content to subsequent field identification manuals (Wiedenhoeft and Kretschmann 2014; Arévalo et al. 2020). Several years later, USFS International Programs provided additional funding to expand the number and regional coverage of wood species in the manual from Central America to Mexico and the Caribbean (Arévalo and Wiedenhoeft 2022). This fully revised and expanded second edition increased the number of taxa to 373 species grouped into 138 wood groups or timbers, and more rationally encompassed a coherent biogeographical region.

While the field manual remains a scientifically grounded guide for customs inspectors and other officers to conduct first-level screenings of wood materials with a hand lens, it is not without potential ergonomic challenges in the field. Weighing 1.6 kg, the printed manual is heavier to carry than the typical smartphone (e.g., iPhone 16: 170 g, Apple 2025; Samsung Galaxy S25: 162 g, Samsung 2025) and necessitates manual page turning. Entire PDF pages cannot be legibly viewed on the screens of smaller smartphones, thus requiring users to zoom and pan by pinching and dragging with two hands to view content. The side-by-side bilingual format can be distracting and difficult to navigate, especially for monolingual users. Reformatting the content into a smartphone app has the potential to improve the manual's utility, availability, and accessibility in the field.

Computer-aided wood identification programs

Computer-aided wood identification began in the early 1980s. As innovations such as the personal computer, the graphic user interface, the worldwide web, cellular networks, handheld smart mobile devices, and artificial intelligence emerged over the next four decades, platforms and program features evolved to provide better functionality, availability, accessibility, and interactivity (see Table S1 in the supplement for a more detailed timeline).

Starting in 1980 with IDENT4 (Miller 1980), computer-aided wood identification programs became accessible on time-sharing mainframe computers; by the end of the decade, they had migrated to personal computers, after the release of the IBM PC in 1981, the Apple MacIntosh in 1984, and Windows 1.0 in 1985. Throughout this decade of personal computer innovation and into the mid-1990s, numerous programs and databases,

many of which were based on edge-notched/edge-punched cards, were developed for these emerging platforms, e.g., SEARCH (Pearson and Wheeler 1981), CATWI (Tochigi et al. 1984), CARDBOX (Ilic and Hillis 1984), IDENT (Kuroda and Shimaji 1984), IDENT6 (Wheeler and Pearson 1985; Miller et al. 1987), INTKEY (Dallwitz and Paine 1986), MEKA (Duncan and Meacham 1986; Meacham n.d.), GUESS (LaPasha and Wheeler 1987), IAWA-Search (Miller et al. 1987), CARDBOX-PLUS (Ilic 1987; Ilic 1990), SOGEN (Izumoto et al. 1987b, 1988b), IDENTIFY (Kuroda 1987), COMEX (Izumoto et al. 1988a), WIP89 (Jiaju and Fang 1990; Jiaju et al. 2001), IDINEX (Lee and Chun 1990), CSIROID (Ilic 1993), TISS (Chun et al. 1994), and UniWoods 2.0 (Brunner et al. 1995). These early programs introduced much of the functionality that appeared in future wood identification programs and applications, including: on-screen suggestions for characters useful in eliminating remaining taxa, e.g., IDENT4 (Miller 1980), IDENT6 (Wheeler and Pearson 1985; Miller et al. 1987), INTKEY (Dallwitz and Paine 1986), "Microcomputer-based identification program" (Zhang et al. 1986), and CSIROID (Ilic 1993); large databases containing thousands of woods, e.g., SEARCH (Pearson and Wheeler 1981), CARDBOX (Ilic and Hillis 1984), GUESS (LaPasha and Wheeler 1987), IAWA-Search (Miller et al. 1987), CARDBOX-PLUS (Ilic 1987; Ilic 1990), and CSIROID (Ilic 1993); backtracking to and cancelling previous character inputs, e.g., CARDBOX (Ilic and Hillis 1984), IDENT (Kuroda and Shimaji 1984), INTKEY (Dallwitz and Paine 1986), CARDBOX-PLUS (Ilic 1987; Ilic 1990), and CSIROID (Ilic 1993); displaying example images of wood anatomical features, e.g., "Microcomputer-assisted Wood Identification System" (Izumoto et al. 1987a; Izumoto and Hayashi 1990), SOGEN (Izumoto et al. 1987b, 1988b), and WIP89 (Jiaju and Fang 1990; Jiaju et al. 2001); and, providing detailed, written explanations of wood anatomical features, e.g., "Microcomputer-assisted Wood Identification System" (Izumoto et al. 1987a; Izumoto and Hayashi 1990), SOGEN (Izumoto et al. 1987b, 1988b), and CSIROID (Ilic 1993).

With the advent of the Worldwide Web in the 1990s, web-based applications began to appear in the early 2000s, e.g., Commercial Timbers (Richter and Dallwitz 2000 onwards), Anatomy of European and North American Woods (Heiss n.d.), Wood Database of the Forestry and Forest Products Research Institute (Forestry & Forest Products Research Institute n.d.), InsideWood (InsideWood 2004 onwards; Wheeler 2011; Wheeler et al. 2020), and Wood Anatomy of Central European Species (Schoch et al. 2004). Following the release of the Apple iPhone in 2007 and the first version of the Android operating system in 2008, the first smartphone-based wood ID program launched on iOS in 2009: I.D. Wood (Jordan Silberman 2009). Smartphones offered numerous advantages over previous platforms, including improved portability, single-handed operation, optimized displays, adjustable text sizes, automatic updates, and now near ubiquitous availability. Publishing of manual, key-based apps continued through the 2010s and into the 2020s, e.g., macroHOLZdata (Sven Koch 2016), Xylorix PocketWood (Agritix Sdn Bhd 2020a,b), CITESwoodID (Sven Koch 2020), and ID Maderas (UNODC 2021). In 2018, automated wood identification programs using computer vision also began to emerge, e.g., MyWoodPremium (formerly MyWood-ID; INSTITUT PENYELIDIKAN DAN PERHUTANAN MALAYSIA 2018), Xylorix Inspector (Agritix Sdn Bhd 2018), AIKO-KLHK (AIKO-KLHK Dev 2019), Xylorix Enforcer (Agritix Sdn Bhd 2022), and WoodID App (Khanh Nguyen Trong 2024).

While computer-vision-based applications provided a means for users less familiar with conventional macroscopic techniques to perform wood identifications, there remained a need for traditional key-based programs. For example, the ISO 17020:2012 workflow and instructions for the Timber Industry Development Division (TIDD) of the Ghana Forestry Commission timber inspectors still prescribe the use of manual inspection techniques (Eshun et al. 2017) and rely on a specific publication (Arévalo et al. 2020) for their wood identification work.

Project objectives

The objective of this project was to improve the utility, availability, accessibility, and flexibility of the original wood identification field manual Identification of Central American, Mexican, and Caribbean Woods (Arévalo and Wiedenhoeft 2022) by utilizing smartphone app functionality to eliminate potential ergonomic challenges inherent to static print and PDF publication formats. The project's specific goals were to:

1. Release the app in both Spanish and English to maximize linguistic accessibility.
2. Present content one language at a time to prevent the potential for confusion caused by parallel translations and the resultant diminution of text size or need for panning when languages are presented side-by-side.
3. Adapt the manual's visual and textual elements to automatically fit any smartphone or tablet display.
4. Equip the app with adjustable accessibility settings for users with mild visual impairments.
5. Empower users to navigate and scroll using only one hand.
6. Automate decision-tree routing for the wood identification key.

7. Enhance the wood identification key with zoom- and pan-capable reference images.
8. Enable automatic dissemination of content updates to users' smartphones.
9. Simplify the revision process, allowing authors to continually improve content as a result of #8.
10. Offer the app free of charge on both Android and iOS platforms.
11. Supply all content within a native app, eliminating the need for internet access in the field post-installation.
12. Introduce interactive functionality for learning wood anatomical features through quizzes.

Materials and methods

Source publication

WhatWood? Central America Edition is largely based on the original source publication entitled *Identification of Central American, Mexican, and Caribbean Woods* (hereafter "the field manual," or simply "the manual"; Arévalo and Wiedenhoeft 2022). Organized into eight chapters, the manual covers topics such as basic wood anatomy, features and techniques used in wood identification, surface preparation of specimens, proper hand lens use, description pages for 138 species groups (hereafter "woods"), and a dichotomous wood identification key.

Images

The high-resolution PDF version of the manual was the source of all specimen images. Each was extracted and saved with Adobe Acrobat at a resolution of 721×721p. Screenshots were taken of all figures and tables at 1920×1080p. In all, 929 specimen images and 59 screenshots of figures and tables were used in the app.

Text

The field manual was also the source of most of the app's text. The text concerning wood anatomy and macroscopic wood identification from Chapters 1 through 5 and Chapter 8 was saved as resource (.resx) files with Adobe Acrobat. Using the same software, the text for the wood identification key (Chapter 6), species description pages (Chapter 7), and anatomical feature index was saved as text files (.txt), along with the key's navigation routes.

Framework

Visual Studio 2022 was used to build the app with Microsoft's .NET Multi-platform App UI (.NET MAUI). This framework allows projects to be complied into native Android, iOS, macOS, Windows, and Samsung Tizen apps by a single code base (alvinashcraft et al. 2025; davidbritch et al. 2025) using XAML for markup and C# for code-behind. Of these platforms, the authors chose to compile and distribute the app for Android, iOS, and macOS. Resulting .NET MAUI apps are backward compatible to Android version 5.0 (Lollipop), iOS version 12.2, and macOS version 11.0.

Database

Resource and text file data were imported into an SQLite database (SQLite Developers 2025). The database was managed by Microsoft's Entity Framework Core (EF Core) object-relational mapper (SamMonoRT et al. 2024), allowing the .NET MAUI app to interact with and retrieve data from the database.

Anatomical feature quizzes

To familiarize users with the wood anatomical features referenced in the manual's dichotomous identification key, two interactive quizzes were created: a choice quiz and a feature selection quiz. In the choice quiz, users are shown pictures of two different woods and prompted to choose the wood that displays a particular anatomical feature. In the feature selection quiz, users are shown a single picture of one wood and asked to choose from a list all anatomical features that appear in the image.

To enable image queries based on anatomical characteristics, numerical codes for the features detailed in the species descriptions were added to the database for every wood. For instance, *Cedrela* spp. were coded for the presence of distinct growth ring boundaries (coded as 1); semi-ring-porosity (coded as 4); medium-to-narrow rays (coded as 97); average ray abundance (coded as 115); apotracheal diffuse parenchyma (coded as 76); paratracheal vasicentric parenchyma (coded as 79); and marginal parenchyma (coded as 89). Anatomical features were also grouped by category. For instance, the features "distinct growth ring boundaries" and "indistinct or absent growth ring boundaries" were assigned to the category "growth ring boundaries," while the features "narrow rays," "medium-to-narrow rays," "wide rays," and "very wide rays" were assigned to the category "ray width."

Choice quiz. The choice quiz generates question pages through an in-app initialization process. First, a random anatomical feature code (e.g., 89) is chosen. The question is created by displaying that feature's name ("marginal parenchyma") after the phrase "Which species displays…" (see Figure 1, upper right). Next, the app queries the database with this code to randomly select two woods: one with the feature (e.g., *Cedrela*

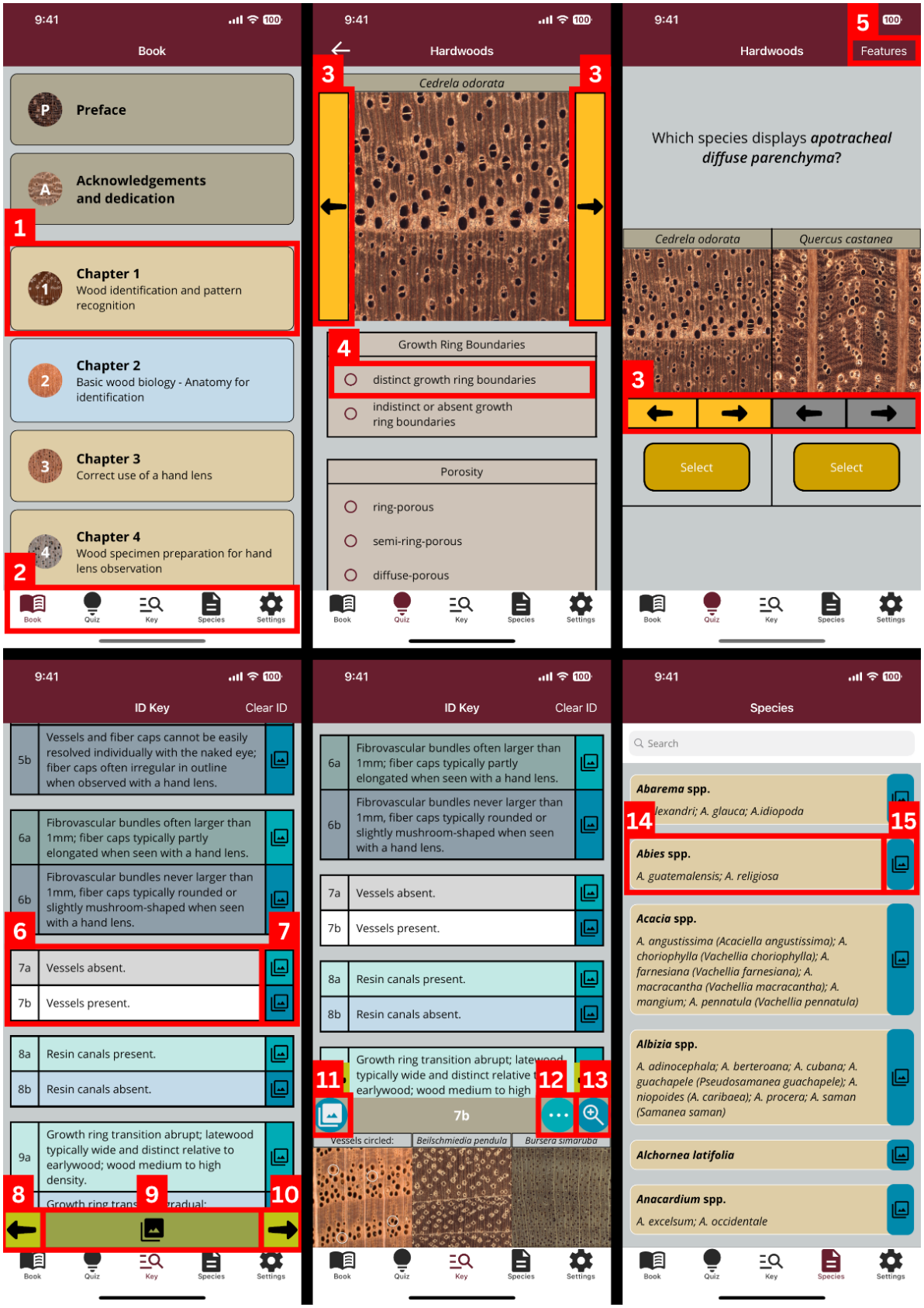

Figure 1. Buttons that appear in the *WhatWood? Central America Edition* app. (1) Chapter button. (2) Tab bar. (3) Arrow buttons. (4) Check box. (5) Features button. (6) Option buttons. (7) Example buttons. (8) Back button. (9) Image button. (10) Forward button. (11) Round image button. (12) More button. (13) Zoom button. (14) Wood button. (15) Preview button.

sp.) and one without (e.g., *Vochysia* sp.). Then, an image for each wood is retrieved via the database. The image showing the feature is randomly positioned on the left or right, with the other image filling the remaining spot. Both images are labeled with their scientific names. Finally, after the user selects an image, a results screen indicates if the answer is correct. New questions are then generated using the same initialization process.

Feature selection quiz. The question pages for the feature quiz are generated through a disparate in-app initialization process. First, a random database query returns a list of anatomical features for a particular wood (e.g., *Cedrela* sp.: distinct growth ring boundaries, semi-ring-porosity, medium-to-narrow rays, average ray abundance, apotracheal diffuse parenchyma, paratracheal vasicentric parenchyma, and marginal parenchyma). A second query makes a list of categories those features represent (i.e., the categories of growth ring boundaries, porosity, ray width, ray abundance, apotracheal axial parenchyma, paratracheal axial parenchyma, and banded parenchyma). A third query makes a list of all possible features for every feature category represented. A final query returns a list of images of the selected wood. To fill out the page, an initial image of that wood is positioned near the top, headed by its scientific name (Figure 1, upper middle). Below the image appears a scrollable list of features separated into sections by category. Each section contains two or more anatomical features belonging to that category formatted as check boxes. After the user makes his/her feature selections and taps submit, the result is displayed. The initialization process repeats for each subsequent question.

Beginning each initialization with a random query reduces the likelihood that the same questions with the same images will appear in the same order. This ensures a novel experience every time a new quiz is started.

Results

The app, *WhatWood? Central America Edition,* is available free of charge on the Google Play Store[4] and Apple App Store.[5] It is downloadable to both Android and iOS devices with a minimum available storage of 190 MB and 342 MB, respectively. Once installed, the app can run without an internet connection. The .NET MAUI source code can be viewed on GitHub at (https://github.com/msu-whatwood).

4. Google Play Store: https://play.google.com/store/apps/details?id=com.MSUwoodID.camcwoods&hl=en_US)
5. Apple App Store: https://apps.apple.com/iq/app/whatwood-central-america-ed/id6737476229

The user-interface (UI)

Figure 1 shows the button types that appear in the app. References to these button types are bolded in the paragraphs below.

The app is organized into five sections, each accessible from the **tab bar** at the bottom of every screen: (1) "Book" (represented by the book icon) containing all the text and images from the original field guide organized by chapter; (2) "Quiz" (lightbulb icon) offering two self-study quizzes on anatomical features; (3) "Key" (magnifying glass icon) providing the interactive dichotomous wood identification key; (4) "Species" (dog-eared document icon) including all the individual species description pages from the original manual; and (5) "Settings" (gear icon) where users can customize the app's interface and find the credits.

Book tab

The Book tab provides access to the complete contents of the original field manual, including text and images, except for Chapters 6 and 7, which are represented by the key tab and species tab, respectively. The main page presents a table of contents by chapter (Figure 2A). The user can open any chapter by tapping its **chapter button** (Figures 2A and 2B). Tapping on an image will open it in a separate screen where the user can zoom (pinch gesture) and pan (drag gesture) for closer examination.

Quiz tab

To aid users in recognizing the kinds of anatomical features described in the dichotomous key, the Quiz tab provides two interactive learning modes: the choice quiz and the feature selection quiz. The choice quiz (Figure 3A) displays an anatomical characteristic and a pair of images. The user is asked to select the image exhibiting that characteristic. The **arrow buttons** below each image enable the user to browse additional images of the same woods. Each selection results in a pop-up message indicating whether the answer was right and showing a running total of correct responses (Figures 3B and 3C).

Accessible via the **features button** in the top right of the choice quiz (Figure 3A), the feature selection quiz (Figure 3D) presents an image of one wood and asks the user to identify all features exhibited in that image by selecting the corresponding **check boxes**. Similar to the choice quiz, **arrow buttons** allow the user to view other images of the same wood. After each attempt, a pop-up message provides feedback on the number of correctly identified features (out of the total possible) as well as tallies of any correct features missed and any incorrect features chosen (Figures 3E and 3F).

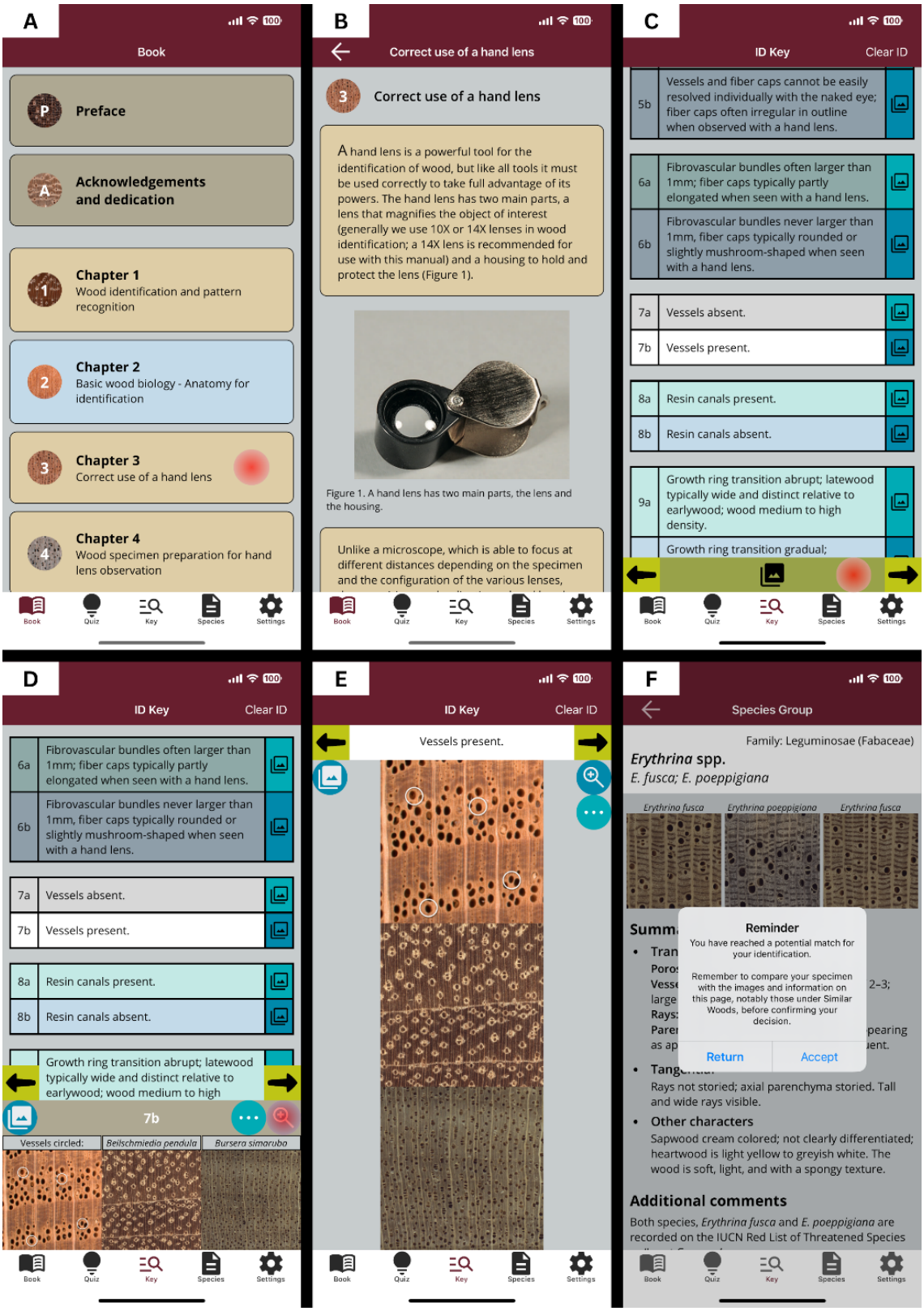

Figure 2. Pages in the Book tab (A, B) and the Key tab (C, D, E, F) of the *WhatWood? Central America Edition* app. Circular red highlights on A, C, and D signify a user's tap and the following in-app navigation to a subsequent page. (A) Book tab showing the first part of the table of contents (the rest of the TOC can be accessed by scrolling down the screen). (B) Book page for Chapter 3. (C) Dichotomous wood identification key. **Option buttons** appear in couplets, requiring the user to choose one to proceed to the next couplet. (D) Exemplar images in expanded view in the interactive dichotomous key. (E) Full-screen exemplar images in the interactive dichotomous key. The images can be examined in detail by zooming and panning with pinch and drag gestures, respectively. (F) Pop-up message reminding the user to compare their specimen with the images, information, and similar woods listed on the description page before confirming the classification.

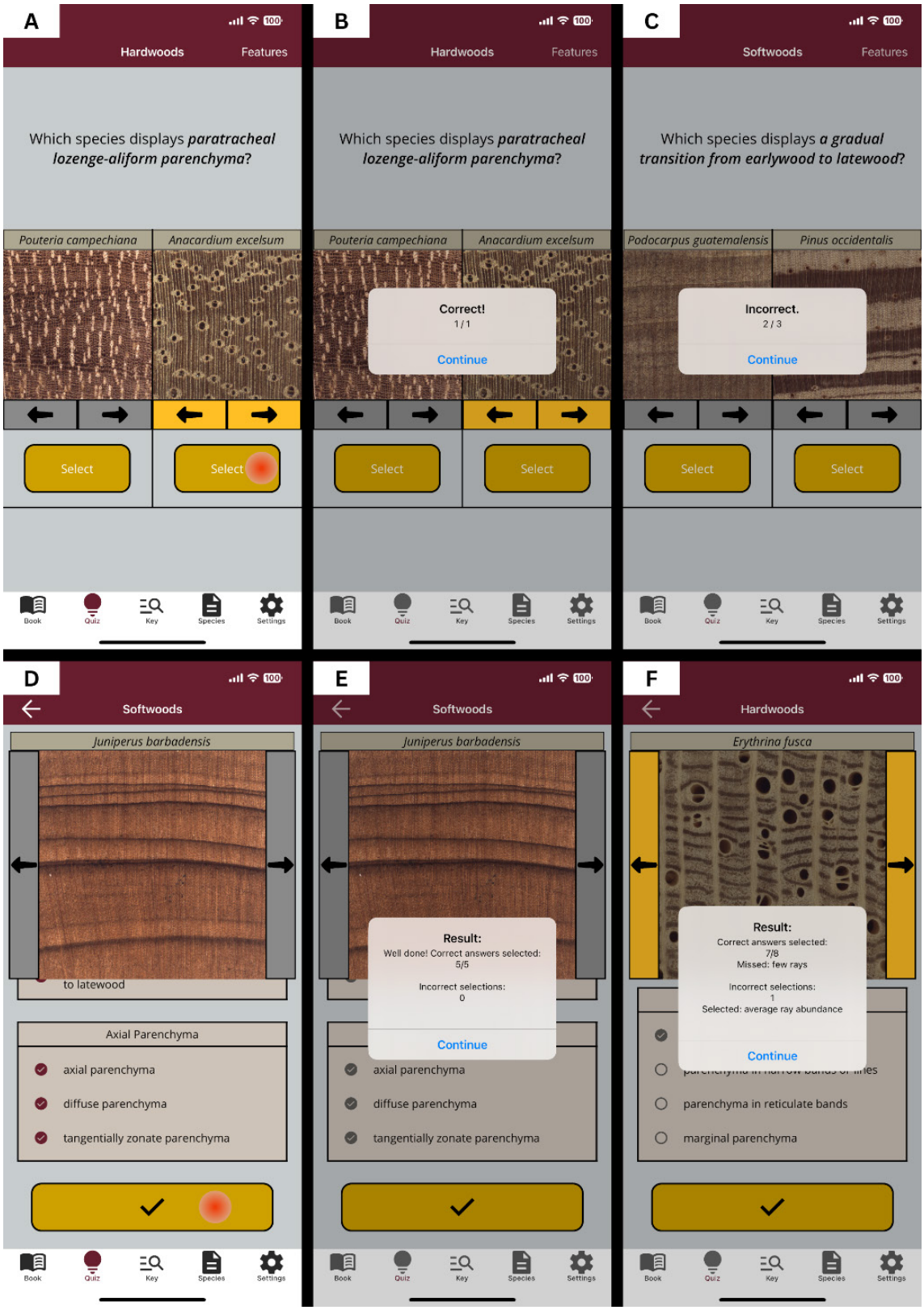

Figure 3. The choice quiz page (A, B, C) and the feature selection quiz page (D, E, F) in the *WhatWood? Central America Edition* app. Circular red highlights on A and D signify a user's tap and the following in-app navigation to a subsequent page. (A) Choice quiz. Arrow buttons under the images allow users to cycle through additional images of each wood. (B) Pop-up message for the choice quiz with running total of correct responses per total attempted questions. (C) Pop-up message for the choice quiz following two correct responses and a final incorrect response. (D) Feature selection quiz. (E) Pop-up message for the feature selection quiz following a user selecting every correct feature and no incorrect features. (F) Pop-up message for the feature selection quiz stating the numbers of correct and incorrect features selected as well as listing the correct features missed and the incorrect features selected.

Key tab

The Key tab provides access to the interactive dichotomous wood identification key. It opens to a scrollable series of **option buttons** arranged in pairs. Each button is labeled with an anatomical feature description representing one of two choices. When an option is selected, the interface automatically scrolls to the next pair of choices in the decision tree, skipping the no-longer-relevant options *en route*. The black-on-green **back** and **forward buttons** just above the **tab bar** (Figure 2C) allow users to backtrack or return one or more steps in the key without having to restart from the beginning.

Tapping the dark green **image button** with the black image icon centered just above the **tab bar** (Figure 2C) opens an expanded view revealing specimen images to supplement the feature descriptions in each **option button**. Users can alternate between image sets for each feature description by tapping the **blue example button** with the black image icon to the right of each **option button** (Figure 2D). For each feature description with more than one associated image set, the **more button** appears at the top of the expanded view, allowing users to view additional specimen images for the same description. By tapping the **magnifying glass button** (Figures 2D and 2E), users are able to zoom and pan images in a separate full screen page (Figure 2D). Tapping the **blue image button** in the upper left of the expanded view (Figures 2D and 2E) causes it to close.

Upon making a terminal decision, a species page automatically opens along with a pop-up message encouraging users to compare their specimen with the information and images on that page before finalizing their conclusion (Figure 2F). To facilitate additional comparisons, similar woods are illustrated at the bottom of the page.

Species tab

The Species tab gives users the option to select and view description pages for each wood. Navigation begins on the index page where users can choose from a series of **wood buttons**, each labeled with the included scientific names (Figure 4A). Each **wood button** can be expanded to reveal three exemplar images by tapping the **blue preview button** on the right (Figure 4A). By tapping an exemplar image, the user can view a larger version in full screen where it can be zoomed and panned. Woods can be filtered by scientific name by using the search bar at the top of the index page (Figure 4B). Users can open a species description page by tapping the **wood button** for that taxon (Figure 4C). Images of lookalike woods appear at the bottom of each page (when applicable) to facilitate comparisons. User notes can be saved in the large text box at the bottom of each species page, and these notes are carried over when the user changes the language setting.

Settings tab

The Settings tab provides customization options for the app's appearance (Figure 4D) and access to the author credits via a dedicated button (Figure 4F). From here, users can adjust the font size (8–24 point) or increase the visual contrast of elements in the tab bar and navigation bar by switching to colorblind mode, improving usability for individuals with color vision deficiency (CVD) (Jamil and Denes 2024) (Figure 4E). To further support users with CVD, all buttons in the app exhibit icons or text labels to ensure color is not the only way to convey information or distinguish elements (World Wide Web Consortium 2024). The scrolling animation for the wood identification key can be toggled on (default) or off from this page. When enabled, tapping an **option button** executes a scroll animation to the next couplet; when disabled, the key advances to the next couplet without scrolling. Users can also select their preferred launch from among the Key (default), Book, Quiz, or Species tabs.

Discussion

Without rigorous field trials or comparative assessments—neither of which were feasible at present due to logistical and cost limitations—it was not possible to draw definitive, scientific conclusions about the degree to which *WhatWood? Central America Edition* has improved or enhanced the user experience. Until such testing can be conducted, the authors offer the following summary of objectives achieved. Any statements of improvement or enhancement presented herein are either logical outcomes of the app design or expected impacts.

Available free of charge on both the Google Play Store and the Apple App Store, anyone with an Android or iOS device can now download *WhatWood? Central America Edition* at no cost from virtually anywhere on the planet at any time, effectively democratizing access to the content first presented in *Identification of Central American, Mexican, and Caribbean Woods* (Arévalo and Wiedenhoeft 2022). Unlike print or PDF publications, the app can receive content updates automatically. This has the potential to make the revision process less burdensome, costly, and time consuming for developers. Once installed, the native app can function without an internet connection even in the remotest of areas.

Ergonomic modifications have the potential to improve the app's usability and accessibility over print and PDF versions. Choosing a language on the Settings tab removes the

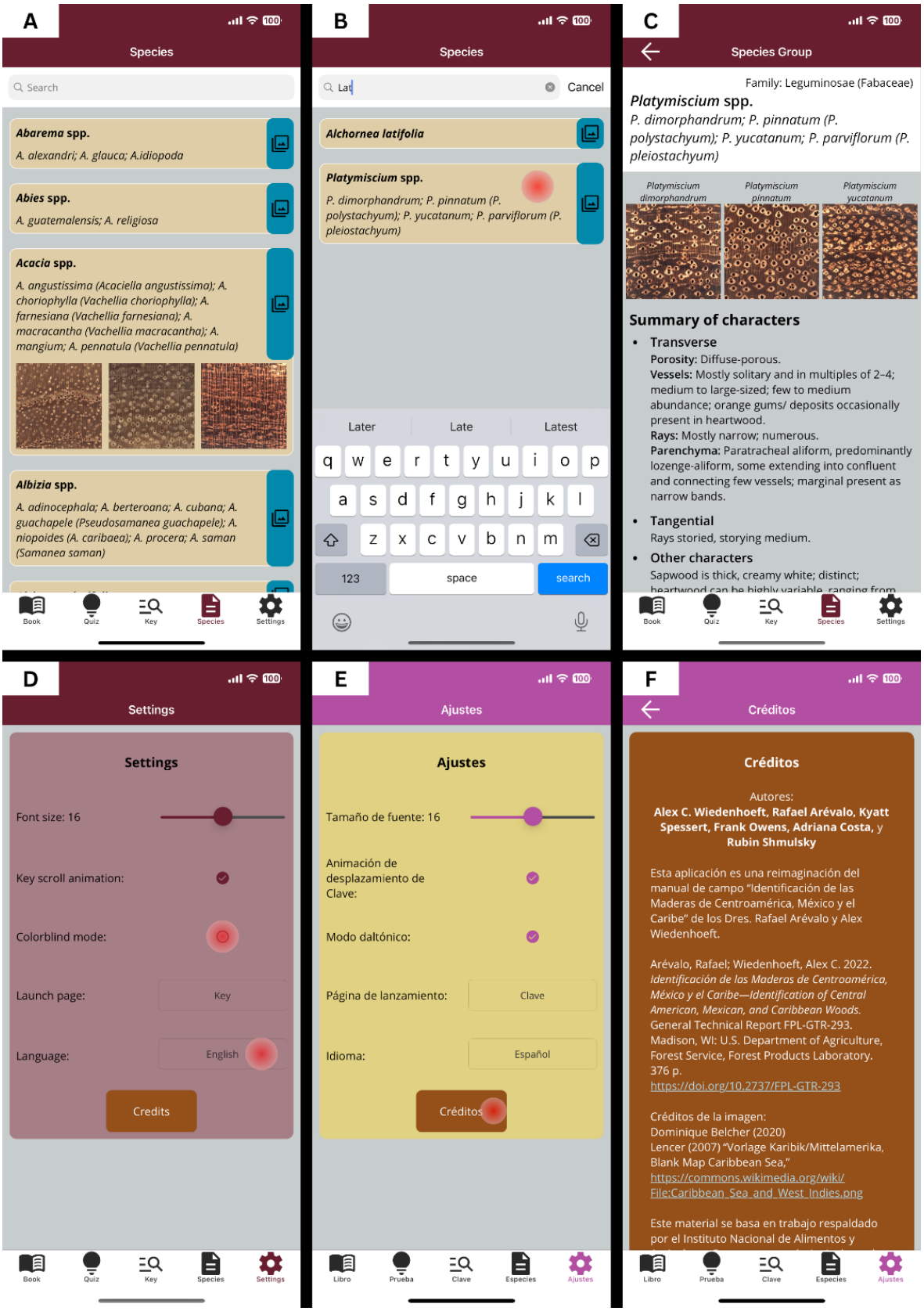

Figure 4. Pages in the Species tab (A, B, C) and the Settings tab (D, E, F) of the *WhatWood? Central America Edition* app. Circular red highlights on B, D, and E signify a user's tap and the following in-app navigation to the subsequent page. (A) Species index page with preview images for *Acacia* spp. revealed. (B) Example search for "Lat" on the species index page. (C) Species description page for *Platymiscium* spp. including images and descriptions. (D) Settings page. (E) Settings page with colorblind mode enabled and Spanish language selected. (F) Credits page with colorblind mode enabled and Spanish language selected.

Figure 5. One-handed use of *WhatWood? Central America Edition.*

other language from the interface, eliminating any potential difficulties resulting from side-by-side Spanish and English translations. The content is thus available not only to native speakers of Spanish and English but also to the millions of potential users for whom Spanish or English is an additional language. Owing to the automatic optimization of text and images to fit smartphone or tablet screens of any size, users no longer have to pinch and drag to view and navigate page content, yet the addition of expanded views and full screen images allows for zooming and panning when needed. Font sizes are no longer fixed, allowing users with visual impairments to enlarge text via the Settings page. For users with CVD, a high-contrast colorblind mode is also available. Manual page turning has been replaced by finger scrolling. Dichotomous key navigation can be executed with one hand via automatic decision routing, potentially reducing the likelihood of human error and allowing the user to hold a specimen or hand lens in the opposite hand (Figure 5). Terminal decisions result in the automatic opening of species description pages expediting access to critical information. Static, conventional learning of essential anatomical features from the Book tab has been supplemented with interactive quizzes that can turn even a few minutes of free time into a focused study session.

Suggestions for future work

Enhancing the educational components of *WhatWood? Central America Edition* could potentially add greater value. To improve engagement, understanding, and retention (Bai et al. 2020; Hamari et al. 2014; Kapp 2012), the interactive functionality of the anatomical feature quizzes could be further expanded to include gamified elements such as badges, personal best scores, skill rankings, etc. Video content could also be incorporated into the app to provide quick-start usage tutorials and more in-depth visual descriptions of anatomical characteristics. As many of the woods that appear in the app are also common to Brazil, the addition of a third language, Portuguese, might increase the size of its audience substantially.

Future integration with computer-vision wood identification (de Andrade et al. 2020; Hwang and Sugiyama 2021; Ravindran et al. 2020; Yi Tou et al. 2007) could be employed in conjunction with the inspector's manual identification as a preliminary identification or a final step to bolster field identification.

Conclusion

Transforming the original source material into a smartphone application has democratized essential wood identification information for the Central American, Caribbean, and Mexican timber markets by making it available at no cost to virtually anyone in the world with a mobile device, delivering content in both Spanish and English, minimizing potential barriers for operators with mild visual impairments, and providing interactive functionality for self-study. *WhatWood? Central America Edition* has also demonstrated the potential for converting and enhancing a wide array of print publications into more modern, accessible, intuitive, and ergonomic digital products that can further empower the frontline defenders policing illegal logging and commercial fraud.

Acknowledgments

This material is based upon work that is supported by the National Institute of Food and Agriculture (NIFA), U.S. Department of Agriculture, McIntire-Stennis project under accession number 7004014. This publication is a contribution of the Forest and Wildlife Research Center, Mississippi State University.

The authors wish to gratefully acknowledge the specimen preparation and imaging efforts of Richard Soares, Patricia Vega, Jennifer Baccam, Nic Bargren, Karl Kleinschmidt, and Caitlin Gilly.

All authors (Kyatt Spessert, KS; Frank Owens, FO; Adriana Costa, AC; Rafael Arévalo, RA; Alex Wiedenhoeft, AW) contributed actionable feedback that improved the presentation of the paper. KS, AW, AC, and FO wrote the paper. The authors declare that the research was conducted in the absence of any commercial or financial relationships that could be construed as a potential conflict of interest.

The authors ask that any use or adaptation of the code for *WhatWood? Central America Edition* will include clear reference to and citation of this paper, and credit for the app source code.

References

Agritix Sdn Bhd (2018) Xylorix Inspector. Version 3.3.2. Kuala Lumpur, Malaysia. App Store (https://apps.apple.com/us/app/xylorix-inspector/id1380163985), Play Store (https://play.google.com/store/apps/details?id=com.xylorixinspectorreact&hl=en_US). (10 March 2025).

Agritix Sdn Bhd (2020a) Xylorix PocketWood. Version 1.9.2. Kuala Lumpur, Malaysia. App Store (https://apps.apple.com/us/app/xylorix-pocketwood/id1536371454). (10 March 2025).

Agritix Sdn Bhd (2020b) Xylorix PocketWood. Version 1.9.1. Kuala Lumpur, Malaysia. Play Store (https://play.google.com/store/apps/details?id=com.xylorixpocketwoodreact&hl=en_US). (10 March 2025).

Agritix Sdn Bhd (2022) Xylorix Enforcer. Version 1.10.0. Kuala Lumpur, Malaysia. App Store (https://apps.apple.com/my/app/xylorix-enforcer/id1618671537), Play Store (https://play.google.com/store/apps/details?id=com.xylorixenforcerreact&hl=en_US). (10 March 2025).

AIKO-KLHK Dev (2019) AIKO-KLHK. Version 2.2.0. Bogor City, West Java, Indonesia. Play Store (https://play.google.com/store/apps/details?id=id.codepresso.woodid&hl=en_US). (10 March 2025).

alvinashcraft, jwmsft, eelnivla (2025) Build Windows apps with .NET MAUI. Microsoft. https://learn.microsoft.com/en-us/windows/apps/windows-dotnet-maui/. (26 March 2025).

Apple Inc. (2025) iPhone 16 and iPhone 16 Plus Technical Specifications. https://www.apple.com/in/iphone-16/specs/ (08 July 2025).

Arévalo R, Ebanyenle E, Ebeheakey AA, Kofi E, Bonsu KA, Lambog O, Soares R, Wiedenhoeft AC (2020) Field Identification Manual for Ghanaian Timbers. Gen Tech Rep FPL-GTR-277. USDA For Serv Forest Prod Lab, Madison, WI. 130 p. https://research.fs.usda.gov/treesearch/60264

Arévalo R, Wiedenhoeft AC (2022) Identification of Central American, Mexican, and Caribbean Woods. Gen Tech Rep FPL-GTR-293. USDA For Serv Forest Prod Lab, Madison, WI. 376 p. In English and Spanish. https://research.fs.usda.gov/treesearch/64547

Bai S, Hew KF, Huang B (2020) Does gamification improve student learning outcome? Evidence from a meta-analysis and synthesis of qualitative data in educational contexts. Educ Res Rev-Neth 30:100322. https://doi.org/10.1016/j.edurev.2020.100322.

Brunner M, Kučera LI, Zürcher E (1995) Major Timber Trees of Guyana - A Lens Key. IAWA J 16(1):101–103. https://doi.org/10.1163/22941932-90001396.

Buffum B (2006) Managing a Forest Reserve Severely Affected by Illegal Logging and Farming. Based on Research in Haiti. University of Rhode Island, South Kingstown, RI. https://digitalcommons.uri.edu/nrs_facpubs/923.

Campos Arce JJ, Camacho M, Villalobos R, Rodríguez CM, Gómez M (2001) Illegal logging in Costa Rica: An analysis for discussion. Centro Agronómico Tropical de Investigación y Ense-ñanza (CATIE), Turrialba, Costa Rica. 70 p. In Spanish, with summary in English. https://www.researchgate.net/publication/283266480_La_tala_ilegal_en_Costa_Rica_un_analisis_para_la_discusion

Chun SK, Kim MJ, Lee WC (1994) The TISS system: A computer search routine for wood identification and physical or mechanical property information. Pp 212–213 *in* BG Butterfield, L Donaldson, and A Singh, eds. The Third Pacific Regional Wood Anatomy Conference, 20–24 November 1994, Rotorua, New Zealand. IAWA J 15(3):212–213. https://doi.org/10.1163/22941932-90000598

Dallwitz MJ, Paine TA (1986) User's Guide to the DELTA System: A General System for Processing Taxonomic Descriptions. 3rd edition. CSIRO Aust Div Entomol Rep No 13: 106 p.

davidbritch, thimanshu1993, mhrastegari, jonpryor, Banovvv, jconrey (2025) What is .NET MAUI?. Microsoft. https://learn.microsoft.com/en-us/dotnet/maui/what-is-maui?view=net-maui-9.0. (11 February 2025).

de Andrade BG, Basso VM, de Figueiredo Latorraca JV (2020) Machine vision for field-level wood identification. IAWA J 41(4):681–698. https://doi.org/10.1163/22941932-bja10001

Duncan T, Meacham CA (1986) Multiple-entry keys for the identification of Angiosperm families using a microcomputer. Taxon 35(3):492–494. https://doi.org/10.2307/1221902

Environment Canada (2002) CITES Identification Guide – Tropical Woods: Guide to the Identification of Tropical Woods Controlled under the Convention on International Trade in Endangered Species of Wild Fauna and Flora. Canadian Cataloguing in Publication Data, Ottawa, ON, Canada. 210 p. In English, French, Spanish, and Turkish. https://cites.org/eng/node/133877

Eshun AA, Quansah JH, Donkor BN (2017) Work Instructions for Square-Edge Sawn Timber Inspection and Grading. Ghana Forestry Commission, Accra, Ghana. 6 p.

FAOSTAT (2025) FAOSTAT: Forestry Production and Trade. Food and Agriculture Organization of the United States (FAO), Washington, DC. https://www.fao.org/faostat/en/#data/FO.

Forest Trends (2022) Forest Trends' 2022 Illegal Logging and Associated Trade (ILAT) Risk Scores and Categories. Forest Trends, Washington, DC. https://www.forest-trends.org/wp-content/uploads/2022/03/2022-Risk-Scores-IDAT.xlsx.

Forestry & Forest Products Research Institute (n.d.) Wood Database of the Forestry & Forest Products Research Institute. Forestry and Forest Products Research Institute, Tsukuba, Ibaraki, Japan. https://db.ffpri.go.jp/WoodDB/index-E.html. (9 April 2025).

Hamari J, Koivisto J, Sarsa H (2014) Does Gamification Work? – A Literature Review of Empirical Studies on Gamification. Pp 3025–3034 *in* 47th Hawaii International Conference on System Sciences, 6-9 January 2014, Waikoloa, HI. IEEE Comp Soc, Washington, D.C. 9 p. https://doi.org/10.1109/HICSS.2014.377

Heiss AG (n.d.) Anatomy of European and North American Woods—An Interactive Identification Key. https://web.archive.org/web/20220627150501/http://www.holzanatomie.at/. (21 April 2025).

Hwang SW, Sugiyama J (2021) Computer vision-based wood identification and its expansion and contribution potentials in wood science: A review. Plant Methods 17(47). https://doi.org/10.1186/s13007-021-00746-1

Ilic J (1987) The CSIRO Family Key for Hardwood Identification. Commonwealth Scientific and Industrial Research Organization (CSIRO), Melbourne, Australia. 171 p.

Ilic J (1990) The CSIRO macro key for hardwood identification. Commonwealth Scientific and Industrial Research Organization (CSIRO) Australia, Highett, Victoria, Australia. 125 p.

Ilic J (1993) Computer Aided Wood Identification Using Csiroid. IAWA J 14(4):333–340. https://doi.org/10.1163/22941932-90000587

Ilic Y, Hillis WE (1984) Wood identification in CSIRO Australia. Pp 138–140 *in* S Sudo, ed Proceedings of the Pacific Regional Wood Anatomy Conference, 1–7 October 1984, Tsukuba, Ibaraki, Japan. Forestry and Forest Products Research Institute, Tsukuba, Ibaraki, Japan.

InsideWood (2004 onwards) InsideWood. http://insidewood.lib.ncsu.edu/search. (9 April 2025).

INSTITUT PENYELIDIKAN DAN PERHUTANAN MALAYSIA (2018) MyWoodPremium. Version 1.0.0. Kuala Lumpur, Malaysia. App Store (https://apps.apple.com/us/app/mywoodpremium/id1457421688). (10 March 2025).

Izumoto Y, Ojika T, Kakimoto T, Watanabe T (1987a) Identification System of Wood Assisted by Microcomputer. Memoirs of Osaka Kyoiku University III. Natural science and applied science 35(2):193–201. In Japanese with summary in English. https://opac-ir.lib.osaka-kyoiku.ac.jp/webopac/TD00005708

Izumoto Y, Ojika T, Hashimoto T (1987b) Expert System for Wood Identification(I). Memoirs of Osaka Kyoiku University III. Natural science and applied science 36(1):39–46. In Japanese with summary in English.

Izumoto Y, Ojika T, Hashimoto T, Higuchi T (1988a) Expert System for Wood Identification(II). Memoirs of Osaka Kyoiku University III. Natural science and applied science 36(2):201–209. In Japanese with summary in English.

Izumoto Y, Ojika T, Hashimoto T, Higuchi T (1988b) Expert System for Wood Identification(III). Memoirs of Osaka Kyoiku University III. Natural science and applied science 37(1):65–74. In Japanese with summary in English.

Izumoto Y, Hayashi S (1990) Identification System of Wood Assisted by Microcomputer(II). Memoirs of Osaka Kyoiku University III. Natural science and applied science 39(1):87–102. In Japanese with summary in English. https://opac-ir.lib.osaka-kyoiku.ac.jp/webopac/TD00005798

Jamil A, Denes G (2024) Investigating Color-Blind User-Interface Accessibility via Simulated Interfaces †. Computers 13(2):53. https://doi.org/10.3390/computers13020053

Jiaju Y, Fang C (1990) A Computerised System for Features Image Display and Identification of Woods from China. IAWA J 11(1):105–105. https://doi.org/10.1163/22941932-90001154

Jiaju Y, Fang C, HongJun L (2001) Initiation of Microcomputer Wood Identification. China Wood Industry 15(3):31–32. In Chinese with summary in English.

Jordan Silberman (2009) ID Wood. Version 4.1.4. Carson City, Nevada. App Store (https://apps.apple.com/us/app/i-d-wood/id325838725). (10 March 2025).

Kapp KM (2012) The Gamification of Learning and Instruction: Game-based Methods and Strategies for Training and Education, 1st ed. Pfeiffer & Company, Hoboken, NJ. 336 p.

Khanh Nguyen Trong (2024) WoodID App. Version 1.0.6. App Store (https://apps.apple.com/gb/app/woodid-app/id6504000600). (10 March 2025).

Kuroda K, Shimaji K (1984) Computerization of hardwood identification. Pp 171–173 *in* S Sudo, ed Proceedings of the Pacific Regional Wood Anatomy Conference, 1–7 October 1984, Tsukuba, Ibaraki, Japan. Wood Res Inst, Kyoto Univ, Uji, Kyoto 611, Japan.

Kuroda K (1987) Hardwood Identification Using a Microcomputer and Iawa Codes. IAWA J 8(1). http://dx.doi.org/10.1163/22941932-90001030

LaPasha CA, Wheeler EA (1987) A Microcomputer Based System for Computer-Aided Wood Identification. IAWA J 8(4):347–354. https://doi.org/10.1163/22941932-90000454

Lee W, Chun SK (1990) Computer - Aided Korean Wood Identification. Journal of Korean Wood Science and Technology 18(2): 49-66. In Korean with summary in English. https://koreascience.kr/article/JAKO199000238218093.page

Meacham CA (n.d.) The MEKA Home Page. Berkeley, CA. https://ucjeps.berkeley.edu/meacham/meka/. (15 April 2025).

Miller MJ (2011) Persistent Illegal Logging in Costa Rica: The Role of Corruption Among Forestry Regulators. J Environ Dev 20(1):50–68. https://doi.org/10.1177/1070496510394319

Miller RB (1980) Wood Identification Via Computer. IAWA J 1(4):154–160. https://doi.org/10.1163/22941932-90000714

Miller RB, Pearson RG, Wheeler EA (1987) Creation of a Large Database with Iawa Standard List Characters. IAWA J 8(3):219–232. https://doi.org/10.1163/22941932-90001049

MINAE (Ministerio de Ambiente y Energía) (2001) National plan for forest development 2001-2010. Ministerio de Ambiente y Energía/ONF/FONAFIFO/PROFOR, San José, Costa Rica. 81 p. In Spanish. https://www.sirefor.go.cr/pdfs/tematicas/Especies/PNDF_2001-2010.pdf

Mulligan F, Bennear L (2015) Illegal Logging in Belize: Policy & Enforcement Mechanisms for a Sustainable Future. MEM thesis, Duke University, Durham, NC. 28 p. https://core.ac.uk/outputs/37750713/?source=oai

Pearson RG, Wheeler EA (1981) Computer Identification of Hardwood Species. IAWA J 2(1): 37–40. https://doi.org/10.1163/22941932-90000392

PEFC (Programme for the Endorsement of Forest Certification) (2020) PEFC ST 2002:2020, Chain of Custody of Forest and Tree Based Products – Requirements. PEFC General Assembly, virtual. 35 p. https://cdn.pefc.org/pefc.org/media/2020-02/66954288-f67f-4297-9912-5a62fcc50ddf/23621b7b-3a5d-55c9-be4d-4e6a5f61c789.pdf

Ravindran P, Thompson BJ, Soares RK, Wiedenhoeft AC (2020) The XyloTron: Flexible, Open-Source, Image-Based Macroscopic Field Identification of Wood Products. Front Plant Sci 11:01015. https://doi.org/10.3389/fpls.2020.01015

Richards M, Wells A, Del Gatto F, Contreras-Hermosilla A, Pommier D (2003) Impacts of illegality and barriers to legality: a diagnostic analysis of illegal logging in Honduras and Nicaragua. Int For Rev 5(3):282–292. https://doi.org/10.1505/IFOR.5.3.282.19153

Richter HG, Dallwitz MJ (2000 onwards) Commercial Timbers: Descriptions, Illustrations, Identification, and Information Retrieval. https://www.delta-intkey.com/wood/en/index.htm

SamMonoRT, AndriySvyryd, Rick-Anderson, stamminator, dennisseders, smitpatel, roji, riccikl, divega, gurmeetsinghdke, tdykstra, mairaw, bricelam, rowanmiller, mjmilan (2024) Entity Framework Core. Microsoft. https://learn.microsoft.com/en-us/ef/core/. (10 February 2025).

Samsung Electronics Co., Ltd. (2025) Samsung Galaxy S25 & S25+ Specs. https://www.samsung.com/my/smartphones/galaxy-s25/specs/ (08 July 2025).

Schoch W, Heller-Kellenberger I, Schweingruber F, Kienast F, Schmatz D (2004) Wood Anatomy of Central European Species. Swiss Federal Institute for Forest, Snow, and Landscape Research (WSL), Birmensdorf, Switzerland. http://www.woodanatomy.ch/authors.html

SQLite Developers (2025) About SQLite. https://www.sqlite.org/about.html. (10 February 2025).

Sven Koch (2016) macroHOLZdata. Version 2.1.3. Hamburg, Germany. App Store (https://apps.apple.com/us/app/macroholzdata/id1120922391), Play Store (https://play.google.com/store/apps/details?id=de.thuenen.macroHOLZdata&hl=en_US). (10 March 2025).

Sven Koch (2020) CITESwoodID. Version 1.1.2. Hamburg, Germany. App Store (https://apps.apple.com/us/app/citeswoodid/id1534768227), Play Store (https://play.google.com/store/apps/details?id=de.bfn.CITESwoodID&hl=en_US). (10 March 2025).

Tochigi T, Shiokura T, Lantican CB, Salud CG, Madamba CB (1984) Computer assisted tropical wood identification (CATWI). Pp 174–176 *in* S Sudo, ed Proceedings of the Pacific Regional Wood Anatomy Conference, 1–7 October 1984, Tsukuba, Ibaraki, Japan. Forestry and Forest Products Research Institute, Tsukuba, Ibaraki, Japan.

Torres-Rojo JM (2021) Illegal Logging and the Productivity Trap of Timber Production in Mexico. Forests 12(7):838. https://doi.org/10.3390/f12070838

UNODC (2021) ID Maderas. Version 1.0.20. Vienna, Austria. Play Store (https://play.google.com/store/apps/details?id=com.rrgonu.idmaderas&hl=en_CA). (10 March 2025).

USDA Forest Service (2025a) Center for Wood Anatomy Research: Overview. USDA For Serv Forest Prod Lab, Madison, WI. https://research.fs.usda.gov/fpl/centers/war#overview

USDA Forest Service (2025b) Center for Wood Anatomy Research: Research. USDA For Serv Forest Prod Lab, Madison, WI. https://research.fs.usda.gov/fpl/centers/war#research

Vardeman E, Runk JV (2020) Panama's illegal rosewood logging boom from Dalbergia retusa. Global Ecol Conserv 23: e01098. https://doi.org/10.1016/j.gecco.2020.e01098

Wang M, Radics R, Islam S, Hwang K (2023) Towards Forest Supply Chain Risks. Operations and Supply Chain Management: An International Journal 16(1):97–108. http://doi.org/10.31387/oscm0520375

Wheeler EA, Pearson RG (1985) A Critical Review of the Iawa Standard List of Characters Formatted for the Ident Programs. IAWA J 6(2):151–160. https://doi.org/10.1163/22941932-90000926

Wheeler EA (2011) InsideWood – A Web Resource For Hardwood Identification. IAWA J 32(2):199–211. https://doi.org/10.1163/22941932-90000051

Wheeler EA, Gasson PE, Baas P (2020) Using The InsideWood Web Site: Potentials And Pitfalls. IAWA J 41 (4):412–462. https://doi.org/10.1163/22941932-bja10032

Wiedenhoeft AC (2011) Identification of Central American Woods. Forest Products Society, Madison, WI. 167 p. In English and Spanish. https://research.fs.usda.gov/treesearch/60337

Wiedenhoeft AC, Kretschmann DE (2014) Species Identification and Design Value Estimation of Wooden Members in Covered Bridges. Gen Tech Rep FPL-GTR-228. USDA For Serv Forest Prod Lab, Madison, WI. 94 p. https://research.fs.usda.gov/treesearch/46745.

World Wide Web Consortium (W3C) (2024) Web Content Accessibility Guidelines (WCAG) 2.1. https://www.w3.org/TR/WCAG21/. (20 March 2025).

Yi Tou J, Yee Lau P, Haur Tay Y (2007) Computer Vision-based Wood Recognition System. Pp 197–202 *in* Proc. Int'l Workshop on Advanced Image Technology, 8–9 January 2007, Bangkok, Thailand. Thai Embedded Systems Association (TESA), Ratchathewi, Bangkok, Thailand. https://www.researchgate.net/publication/264886592

Zhang QC, Cheng F, Lian YH (1986) Microcomputer identification of hardwood species. Scientia Silvae Sinicae 22(2):213–217. In Chinese, with summary in English.

Supplement: Table S1. Summary of computer-aided wood identification programs.

Date	Same-year historical milestones	Program name	Developer(s)	Platform or OS	References *	Purpose	Scope	Functionality
1980		IDENT4	L.E. Morse	Time-sharing computers	Morse 1971; Morse 1974; Miller 1980	General taxonomic ID	Hardwoods (number & regions unspecified)	Int. M-E Key; lists useful characters for separating remaining taxa & allows setting a character mismatch limit.
1981	IBM PC released	SEARCH	R.G. Pearson & E.A. Wheeler	Mainframe computer	Pearson and Wheeler 1981	Hardwood ID based on Metcalfe & Chalk's perforated cards (1950)	4724 hardwood entries, global	Non-Int. M-E Key that performs batch operations; allows specifying a minimum number of matches for entered characters.
1983		Adaption of IDENT4	J.T. Quirk	Time-sharing computers	Quirk 1983	ID of commercial Asian & Australian Leguminosae species	39 species of Asian & Australian Leguminosae	Int. M-E Key; lists useful characters for separating remaining taxa & allows setting a character mismatch limit.
1983		"Domestic Hardwood Identification System"	M. Hasegawa	NEC PC-8801	Hasegawa 1984	Microscopic ID of Japanese hardwoods based on Sudo's punched cards (1959)	59 domestic Japanese hardwood species	Non-Int. M-E Key that performs batch operations; allows entering unknown/"wildcard" characters.
1984	Apple releases Macintosh	Computer Assisted Tropical Wood Identification (CATWI)	T. Tochigi, T. Shiokura, C.B. Lantican, C.G. Salud, & C.B. Madamba	Hitachi PC-9801	Tochigi et al. 1984	Tropical hardwood ID intended for non-expert wood anatomists; based on set theory	Tropical hardwoods (number & regions unspecified)	M-E Key that presents characters in order of their ease of observation & suitability for separating remaining woods in two.
1984		CARDBOX (CSIRO Microcomputer Wood Identification Database)	CSIRO Australia	CP/M-80	Ilic and Hillis 1984	Hand lens & microscopic ID of primarily southwest Pacific & Australian woods	About 5000 taxa, primarily of the southwest Pacific & Australia; 14 total macro/micro keys	Int. M-E Key that allows sorting taxa by presence or absence of characters, searching for terms used in taxa descriptions, & backtracking to previous character inputs.
1984		IDENT	K. Kuroda & K. Shimaji	CP/M, NEC PC-9801, & Fujitsu FACOM OS IV/F4	Kuroda and Shimaji 1984	Commercial Japanese hardwood ID based on Sudo's punched cards (1959) & coded according to the IAWA Standard List (1981)	Commercial Japanese hardwoods reported by Sudo (1959) (number unspecified)	Int. M-E Key that displays the number of remaining taxa & allows backtracking to previous character inputs; accessible in Japan via telephone call.
1985	Microsoft releases Windows 1.0	IDENT6	Department of Wood and Paper Science, North Carolina State University	PC	Wheeler and Pearson 1985; Miller et al. 1987	Further iteration of the IDENT4 program featuring usability improvements	Hardwoods (number & regions unspecified)	Same as IDENT4, w/ improvements: users can enter more characters at once, search for exact matches of characters, & obtain individual taxa descriptions & character states.
1986		INTeractive KEY (INTKEY)	M.J. Dallwitz & T.A. Paine	Mainframe computers & microcomputers	Dallwitz and Paine 1986	General taxonomic ID using DEscription Language for TAxonomy (DELTA) formatting	General biological taxonomy	Int. M-E Key that allows entering multiple characters, obtaining possible matches at any time, & viewing useful features for distinguishing remaining taxa.
1986		Multiple-Entry Key Algorithm (MEKA)	T. J. Rosatti, R. Phillips, D. Hough, T. Duncan, & C.A. Meacham	CP/M & MS-DOS	Duncan and Meacham 1986; Meacham n.d.	Hardwood ID to family based on punched-card key data of Hansen and Rahn (1969, 1972, 1979) and of Simpson and Janos (1974)	Global angiosperm & dicot families of the Western Hemisphere, south of North America (number unspecified)	M-E Key that provides IDs to one or a set of taxa, listing taxa lacking up to five entered characters; lists shared & individual characters among sets of taxa.
1986		General Unknown Entry and Search System (GUESS)	C.A. LaPasha	DOS & Macintosh	LaPasha and Wheeler 1987	General taxonomic ID; derived from the SEARCH program	5260 entries of global hardwoods, softwoods, & fibers	M-E Key that performs batch operations & allows mismatches.

Supplement: Table S1. Summary of computer-aided wood identification programs (*continued*).

Date	Same-year historical milestones	Program name	Developer(s)	Platform or OS	References *	Purpose	Scope	Functionality
1986		"Microcomputer-based identification program"	Q.C. Zhang, F. Cheng, & Y.H. Lian	Microcomputers	Zhang et al. 1986	Microscopic Chinese hardwood ID based on punched-card keys of the Wood Industry Research Institute of the Chinese Academy of Forestry (1983)	Chinese hardwoods (number unspecified)	M-E Key that allows searching by characters and species names, specifying character absence, & obtaining characters for narrowing remaining taxa; uses an indexed DB for quick searching.
1987		IAWA-Search	C.A. LaPasha	PC	Miller et al. 1987	Searching the IAWA-OPN DB of global hardwoods; derived from the SEARCH program	~3500 hardwood species, global scope; SEARCH's DB adapted to the IAWA Standard List (1981)	M-E Key that searches its DB quicker than the IDENT4 & IDENT6 programs but lacks some of their features.
1987		"Microcomputer-assisted Wood Identification System"	Y. Izumoto, T. Ojika, T. Kakimoto, & T. Watanabe	NEC PC-9801	Izumoto et al. 1987a	Macroscopic Japanese wood ID & display of wood images & diagrams, aimed at beginner/non-expert wood anatomists	32 hardwood & 18 softwood species of Japan	Interactive dichotomous key that displays diagrams of wood characters, includes a glossary & written tutorials on its use & interpreting characters, & provides microphotographs & color surface images of included woods.
1987		CARDBOX-PLUS (CSIRO Family Key)	CSIRO Australia	PC	Ilic 1987	ID of hardwoods to family, w/ a focus on the southwest Pacific & Australia	152 hardwood families, primarily of the southwest Pacific; includes keys used in CARDBOX	Int. M-E Key that allows exclusion of characters, displaying the sequence of entered characters, & cancelling previous character inputs.
1987		SOGEN	Y. Izumoto, T. Ojika, & T. Hashimoto	NEC PC-9801UV2	Izumoto et al. 1987b	Macroscopic ID of domestic Japanese hardwoods	32 Japanese hardwood species	Int. M-E Key that presents characters in order of frequency & accommodates ambiguous characters.
1987		IDENTIFY	K. Kuroda	CP/M & MS-DOS	Kuroda 1987	Microscopic wood ID; coded according to the IAWA Standard List (1981)	180 domestic Japanese hardwood species	Int. M-E Key intended for use alongside a microscope; does not allow character mismatches.
1988		COMEX	Y. Izumoto, T. Ojika, T. Hashimoto, & T. Higuchi	Microcomputers	Izumoto et al. 1988a	Macroscopic Japanese hardwood ID; derived from a program for general disease diagnosis	Japanese hardwoods (number unspecified)	Int. M-E Key that presents characters in order of frequency & hides irrelevant/ redundant characters.
1988		Update of SOGEN	Y. Izumoto, T. Ojika, T. Hashimoto, & T. Higuchi	Microcomputers	Izumoto et al. 1988b	Macroscopic Japanese hardwood ID; update of SOGEN program to include character illustrations & descriptions	Japanese hardwoods (number unspecified)	Int. M-E Key that presents characters in order of frequency & provides illustrations & written descriptions for characters.
1990		Wood Identification Program 1989 (WIP89)	Jiaju & Fang	PC	Jiaju and Fang 1990	Wood ID, tree species indexing, & display of wood anatomical feature images	500 hardwood & 169 softwood species, primarily Chinese	Int M-E Key that allows searching families, genera, or species per-letter, displaying the character-code list, & showing example images of wood characters.
1990		Update of "Microcomputer-assisted Wood Identification System"	Y. Izumoto & S. Hayashi	PC	Izumoto and Hayashi 1990	Macroscopic Japanese wood ID & display of wood images & diagrams, aimed at beginner/non-expert wood anatomists	180 hardwood & 39 softwood species of Japan	Same as "Microcomputer-assisted Wood Identification System," w/ improvements: now an Int. M-E Key; allows backtracking to previous character inputs; includes tutorials w/ diagrams, microphotographs, & color surface images accessible during IDs.
1990		IDentification INformation EXpress (IDINEX)	W.Y. Lee & Su Kyoung Chun	DOS	Lee and Chun 1990	General taxonomic ID based on edge-punched card keys	Native Korean hardwoods & softwoods (number unspecified)	M-E Key that enables easy addition of new taxa & can process up to 229 characters per DB.

Supplement: Table S1. Summary of computer-aided wood identification programs (*continued*).

Date	Same-year historical milestones	Program name	Developer(s)	Platform or OS	References *	Purpose	Scope	Functionality
1990		CARDBOX-PLUS (CSIRO Macro Key)	CSIRO Australia	Windows, DOS, & CP/M	Ilic 1990	Hand lens wood ID w/ a focus on the southwest Pacific region & Australia	Woods primarily of the southwest Pacific & Australia (number unspecified)	Int. M-E Key that allows exclusion of characters, displaying the sequence of entered characters, & cancelling previous character inputs.
1991		Adaption of INTKEY	N. Espinoza de Pernia & R.B. Miller	Mainframe computers & microcomputers	Espinoza de Pernia and Miller 1991	Adaption of the IAWA List of Microscopic Features (1989) to the DELTA programs, including INTKEY	40 commercially important Venezuelan hardwoods	Int. M-E Key that allows entering multiple characters, obtaining possible matches at any time, & viewing useful features for distinguishing remaining taxa.
1993	World Wide Web became public domain	CSIROID	CSIRO Australia	MS-DOS	Ilic 1993; Wheeler and Baas 1998	Microscopic & hand lens wood ID; designed to replace CARDBOX-PLUS at CSIRO	Woods primarily of the southwest Pacific; 12 DBs including the CSIRO Family, Macro, & Eucalyptus keys	Int. M-E Key that provides detailed explanations of characters w/ a "feature help" option, allows removing entered characters, & provides "best subsequent features."
1994	Netscape 1.0 web browser released	Taxonomic Information Search System (TISS)	Su Kyoung Chun, M. J. Kim, & W. C. Lee	PC	Chun et al. 1994	Primarily for wood ID based on edge-punched cards, but can also be used to search DBs of physical & mechanical properties	Woods on Korean edge-punched cards (number & regions unspecified); includes DB of properties & uses for 382 tropical woods	Int. M-E Key that allows searching by scientific or common name, specifying mismatches, & searching data from multiple DBs at once.
1994	First smartphone IBM Simon released	UniWoods 2.0 (ENTRY2 and IDENT2)	O. Baumann	MS-DOS 3.0	Brunner et al. 1995	Two programs for hand lens wood ID; distributed w/ a reference manual w/ illustrated wood & character descriptions	115 hardwood species common to Guyana	ENTRY2 compares characters of a known wood to entries in the provided DB; IDENT2 keys out unknown characters.
1995	Amazon and Ebay launched; MS Internet Explorer released	Adaption of INTKEY	Institute for Wood Biology and Wood Protection, Federal Research Centre for Forestry and Forest Products (BFH)	Windows	Richter and Trockenbrodt 1995	Adaption of the DELTA programs, including INTKEY, for German & European hardwood ID & data storage/ retrieval w/ a German translation	180 commercial German and European wood species	Int. M-E Key that allows entering multiple characters, obtaining possible matches at any time, & viewing useful features for distinguishing remaining taxa.
1999	Blackberry 850 launched; Kyocera Visual Phone released w/ camera	Taxonomic Information Search System 2 (TISS 2)	Su Kyoung Chun	32-bit operating systems, including Windows 95	Chun 1999	Wood fiber ID using DELTA formatting, including microscopic fiber images; derived from TISS	124 fibers of hardwood & softwood species	Int. M-E Key that allows searching by scientific name & provides microscopic images of included fibers.
2000		Commercial timbers: descriptions, illustrations, identification, and information retrieval	H.G. Richter & M.J. Dallwitz	Web (https://tinyurl.com/5cxc6xry)	Richter and Dallwitz 2000 onwards; Silva et al. 2022	Adaption of the DELTA programs, including INTKEY, for international hardwood ID; provides example macroscopic & microscopic images of woods	409 internationally traded hardwood taxa	Int. M-E Key that allows entering multiple characters, obtaining possible matches at any time, & viewing useful features for distinguishing remaining taxa; includes detailed wood descriptions.
2000		Anatomy of European and North American Woods	A.G. Heiss	Web (https://tinyurl.com/57jw4c6m)	Silva et al. 2022; Heiss n.d.	Microscopic ID of European & North American woods, including illustrations	325 hardwood & 101 softwood species of Europe & North America	Int. M-E Key w/ example images & characters for palaeobotanical wood ID, including two DBs for modified & carbonized wood; currently defunct.
2001		Update of Wood Identification Program 1989 (WIP89)	Y. Jiaju, C. Fang, & L. HongJun	PC	Jiaju et al. 2001	Development of Wood Identification Program 1989 (WIP89) as an initiation of automated wood ID	570 hardwood & 171 softwood species, primarily Chinese	Same as Wood Identification Program 1989 (WIP89), w/ improvements: automated classification of softwood earlywood to latewood transitions & hardwood porosity domains.

Supplement: Table S1. Summary of computer-aided wood identification programs (*continued*).

Date	Same-year historical milestones	Program name	Developer(s)	Platform or OS	References *	Purpose	Scope	Functionality
2002	Friendster social network launched	macroHOLZdata	Department of Wood Biology, University of Hamburg & Holzfachschule, Bad Wildungen, Germany	PC	Heinz 2003; Silva et al. 2022	Hand lens wood ID, including images of woods from each plane of section; uses DELTA formatting	46 hardwood & 13 softwood commercial species (regions unspecified)	Int. M-E Key that allows querying of explanations & glossaries for wood biological & anatomical terms, structural features, properties, & applications.
2003	Myspace launched	Wood Database of the Forestry & Forest Products Research Institute	Forestry & Forest Products Research Institute, Ibaraki, Japan	Web (https://tinyurl.com/yvbkj4k3)	Silva et al. 2022; Forestry & Forest Products Research Institute n.d.	Microscopic ID of Japanese woods, including illustrations	781 Japanese woods	Int. M-E Key that includes features from the IAWA List of Microscopic Features (1989), w/ microscopic & macroscopic wood images.
2004	Facebook launched (Harvard only)	InsideWood	Libraries & Department of Forest Biomaterials of North Carolina State University, Raleigh, North Carolina	Web (https://tinyurl.com/3nenr9sw)	InsideWood 2004 onwards; Wheeler 2011; Wheeler et al. 2020; Silva et al. 2022	Microscopic ID of global woods, including illustrations	7849 global modern hardwoods, 2247 global fossil hardwoods, & 236 global modern softwoods	Three Int. M-E Keys for ID of modern hardwoods, fossil hardwoods, & modern softwoods; includes microscopic & macroscopic images of woods.
2004		Wood Anatomy of Central European Species	W. Schoch, I. Heller-Kellenberger, F. Schweingruber, F. Kienast, & D. Schmatz	Web (https://tinyurl.com/6pa82yvz)	Schoch et al. 2004; Silva et al. 2022	Microscopic ID of European woods, including illustrations	133 European hardwoods & softwoods	Microscopic ID key that lists characters for observation consecutively, including microscopic & macroscopic wood images & descriptions.
2005	YouTube launched	CITESwoodID	Institute of Wood Technology and Wood Biology, Federal Research Institute for Rural Areas, Forestry and Fisheries (vTI), Hamburg, Germany	Windows	Koch et al. 2011; Silva et al. 2022	Hand lens wood ID w/ a focus on CITES-listed woods; uses DELTA formatting	11 global hardwoods and 1 softwood listed in CITES, & 44 commercial look-a-like woods	Int. M-E Key that allows entering characters in any order & includes a character search bar; characters have detailed definitions, explanations for observation, & example images of woods.
2005		Key to a Selection of Arid Australian Hardwoods and Softwoods	J.A. Barker & B.A.H. Flinders	Web (https://tinyurl.com/3ryuarhj)	Silva et al. 2022; Barker and Flinders n.d.	Microscopic ID of Australian hardwoods & softwoods, including illustrations	58 Australian hardwoods & softwoods	Int. M-E Key that displays available & used characters, remaining taxa, & discarded taxa simultaneously; includes sub-keys for ID to species.
2009	ImageNet is created; Telia Sonera releases 4G network	I.D. Wood	Jordan Silberman	iOS (https://tinyurl.com/mrx4efvs)	Jordan Silberman 2009	Macroscopic ID of global woods, including illustrations, usage information, calculators & a glossary	205 global woods	Illustrated list of woods w/o a traditional key, but includes details on wood processing & utilization & a map for measuring land area.
2010	Apple releases iPad; Instagram launched	Brazilian Commercial Timbers	Forest Products Laboratory of the Brazilian Forest Service	Windows	Coradin et al. 2010; Forest Products Laboratory of the Brazilian Forest Service 2022; Silva et al. 2022	Adaption of the INTKEY program for Brazilian commercial wood ID	157 Brazilian wood species, primarily commercial	Int. M-E Key that allows entering multiple characters, obtaining possible matches at any time, & viewing useful features for distinguishing remaining taxa.
2011		Pl@ntWood	C. Sarmiento, P. Détienne, C. Heinz, J.-F. Molino, P. Grard, & P. Bonnet	Windows	Sarmiento et al. 2011; Silva et al. 2022	Microscopic ID of Amazonian hardwoods based on IDAO software, w/ illustrations	110 Amazonia hardwoods	Interactive ID tool w/ illustrations, designed to be user-friendly; uses a graphic interface and includes illustrated wood descriptions.

Supplement: Table S1. Summary of computer-aided wood identification programs (*continued*).

Date	Same-year historical milestones	Program name	Developer(s)	Platform or OS	References *	Purpose	Scope	Functionality
2014	VGGNet deep convolutional neural network released	CITESwoodID (web page)	H.G. Richter, K. Gembruch, & G. Koch	Web (https://tinyurl.com/jscf636b)	Richter et al. 2014 onwards; Silva et al. 2022	Adaption of the CITESwoodID program for hand lens ID of CITES-listed woods & look-a-likes, w/ illustrations	41 global CITES-listed woods & 31 commercial look-a-like woods	Int. M-E Key that allows entering multiple characters, obtaining possible matches at any time, & viewing useful features; includes detailed wood descriptions.
2016		macroHOLZdata (smartphone app)	Sven Koch	iOS (https://tinyurl.com/yc7se36a), Android (https://tinyurl.com/3cxdnays), macOS, & Windows	Sven Koch 2016	Adaption of the macroHOLZdata program for hand lens wood ID; uses DELTA formatting	153 global woods	Int. M-E Key that displays best & used characters, remaining taxa, & eliminated taxa simultaneously; includes illustrations, natural language descriptions, & a glossary of wood anatomical features.
2018		MyWoodPremium	Forest Research Institute Malaysia & Tunku Abdul Rahman University	iOS (https://tinyurl.com/yvxzdy8d)	INSTITUT PENYELIDIKAN DAN PERHUTANAN MALAYSIA 2018	Automated ID of Malaysian woods using computer vision	100 Malaysian woods	CVWID using a macro lens attached to the smartphone; requires internet.
2018		Xylorix Inspector	Agritix Sdn. Bhd.	iOS (https://tinyurl.com/u927ryfp) & Android (https://tinyurl.com/yc7ae5s6)	Agritix Sdn Bhd 2018	Automated wood ID using computer vision	45 woods from Malaysia, Madagascar, India, southeast Asia, Ghana, & France	CVWID using a macro lens attached to the smartphone; requires internet.
2019	Verizon released 5G network	AIKO-KLHK	Forest Products Research and Development Center, Bogor, Indonesia	Android (https://tinyurl.com/yc2tepac)	AIKO-KLHK Dev 2019	Automated ID of Indonesian woods using computer vision	823 Indonesian woods	CVWID using a macro lens attached to the smartphone; requires internet.
2020		Xylorix PocketWood	Agritix Sdn. Bhd.	iOS (https://tinyurl.com/yc6rczj7) & Android (https://tinyurl.com/5txxwkta)	Agritix Sdn Bhd 2020a, 2020b	Image-based macroscopic ID of global woods	455 global woods	Macroscopic wood ID by photographing the transverse surface of a wood w/o a macro lens, then comparing the image to included wood images; includes descriptions & uses of woods.
2020		CITESwoodID (smartphone app)	Sven Koch	iOS (https://tinyurl.com/yc6pcdyc), Android (https://tinyurl.com/ywtea8z5), macOS, & Windows	Richter et al. 2014 onwards; Sven Koch 2020	Adaption of the CITESwoodID program for hand lens ID of CITES-listed woods & look-a-likes, w/ illustrations	53 CITES-listed woods & 32 commercial look-a-like woods	Int. M-E Key that displays best & used characters, remaining taxa, & eliminated taxa simultaneously; includes illustrations, natural language descriptions, & a glossary of wood anatomical features.
2020		EyeWood	Wood Structure and Protection Innovation Team, Southwest Forestry University	Web (https://tinyurl.com/9ff7fu6f)	Southwest Forestry University 2020	Microscopic ID of hardwoods and softwoods; coded according to IAWA microscopic feature lists (1989, 2004)	7554 hardwoods & 356 softwoods (regions unspecified)	Int. M-E Keys for hardwoods & softwoods that display frequency of characters in remaining taxa, allow searching by family, genus, & species, & include taxa description pages.
2021		ID Maderas	United Nations Office on Drugs and Crime (UNODC)	Android (https://tinyurl.com/4xhzhbxh)	UNODC 2021	Hand lens ID of commercial Peruvian woods	20 commercial Peruvian woods	Two Int. M-E Keys: one for entering characters one-by-one & the other for entering any characters; includes glossaries for wood anatomical features & wood ID techniques.

Supplement: Table S1. Summary of computer-aided wood identification programs (*continued*).

Date	Same-year historical milestones	Program name	Developer(s)	Platform or OS	References *	Purpose	Scope	Functionality
2022		Xylorix Enforcer	Agritix Sdn. Bhd.	iOS (https://tinyurl.com/5du388bu) & Android (https://tinyurl.com/mupn632m)	Agritix Sdn Bhd 2022	Image-based macroscopic & automated wood ID; app suite that includes Xylorix Inspector & Xylorix PocketWood	465 global woods	CVWID using a macro lens attached to the smartphone (requires internet) & macroscopic wood ID by photographing the transverse surface of a wood w/o a macro lens, then comparing the image to included wood images.
2022	Open AI released Chat GPT	Brazilian Commercial Timbers (web page)	Forest Products Laboratory of the Brazilian Forest Service	Web (https://tinyurl.com/ywykp9fn)	Forest Products Laboratory of the Brazilian Forest Service 2022; Silva et al. 2022	Hand lens ID of Brazilian woods, including chemical & physical tests	275 Brazilian wood species	Int. M-E Key that displays available & used characters, remaining taxa, & discarded taxa simultaneously; includes macroscopic wood images & descriptions.
2024		WoodID App	Khanh Nguyen-Trong	iOS (https://tinyurl.com/4sbvht2n)	Khanh Nguyen Trong 2024	Automated ID of Vietnamese & African woods using computer vision	126 Vietnamese & African woods	CVWID using a macro lens attached to the smartphone; does not require internet.
2024		Wood Identifier: AI Scanner	Richard Schoerner	iOS (https://tinyurl.com/68yy4p27)	Richard Schoerner 2024	Automated wood & tree ID using computer vision	Woods & trees (number & regions unspecified)	Computer vision wood & tree ID w/o a macro lens attachment; requires internet.
2024		WhatWood? Central America Edition	Kyatt Spessert	iOS (https://tinyurl.com/4wxvxvzd), Android (https://tinyurl.com/59vp52hr), & macOS	Arévalo and Wiedenhoeft 2022; Kyatt Spessert 2024	Hand lens ID of Central American, Mexican, & Caribbean woods based on the *Identification of Central American, Mexican, and Caribbean Woods* field manual	138 Central American, Mexican, & Caribbean hardwoods, softwoods, & monocots	Dichotomous key that includes example images of woods for each decision couplet; provides instruction on performing macroscopic wood ID w/ a hand lens & explanations of wood anatomical features.
2025		WhatWood? Ghana Edition	Kyatt Spessert	iOS (https://tinyurl.com/4w4bmdhd), Android (https://tinyurl.com/yr87vx29), & macOS	Arévalo et al. 2020; Kyatt Spessert 2025; Author et al. *submitted*	Hand lens ID of Ghanaian woods based on the *Field Identification Manual for Ghanaian Timbers*	87 Ghanaian hardwoods, softwoods, & monocots	Dichotomous key that includes example images of woods for each decision couplet; provides instruction on performing macroscopic wood ID w/ a hand lens & explanations of wood anatomical features.
2025		Wood Id – Wood Identifier	iOS: Upasana Deshmukh Android: TLUTech	iOS (https://tinyurl.com/mtcw3skz) & Android (https://tinyurl.com/59xr954h)	Upasana Deshmukh 2025; TLUTech 2025	Automated wood ID using computer vision	Number & regions of woods unspecified	CVWID w/o a macro lens attachment; requires internet.
2025		Wood Identifier: AI Scanner (Artmvstd)	Artmvstd	Android (https://tinyurl.com/5xu2xxfs)	Artmvstd 2025	Automated ID of global woods & trees using computer vision	Global woods & trees (number unspecified)	Computer vision wood & tree ID w/o a macro lens attachment; requires internet.
2025		Wood Identifier AI Scanner (Nikhil Kumar)	Nikhil Kumar	iOS (https://tinyurl.com/ynj6dbh5)	Nikhil Kumar 2025	Automated ID of global woods using computer vision	Over 500 global woods	CVWID w/o a macro lens attachment; requires internet.
2025		Wood Identification App	DDR Technologies INC	Android (https://tinyurl.com/ykfr2ssx)	DDR Technologies INC 2025	Automated ID of global woods using computer vision	"Thousands" of global woods	CVWID w/o a macro lens attachment, including written explanations of model reasoning; does not require internet.

ID: Identification. M-E Key: Multi-entry key. Int. M-E Key: Interactive multi-entry key. Non-Int. M-E Key: Non-interactive multi-entry key. DB(s): Database(s). CVWID: Computer vision wood identification

* References can be found at https://github.com/MSU-WhatWood/Table-S1-References.

Compressive behavior of wood I-joist under elevated temperature

Byrne T. Miyamoto†
Structural Testing Coordinator
TallWood Design Institute
Oregon State University, Corvallis, OR 97331
Email: byrne.miyamoto@oregonstate.edu

*Arijit Sinha**†
Professor and JELD-WEN Chair
Department of Wood Science and Engineering
Oregon State University, Corvallis, OR 97331
Email: Arijit.sinha@oregonstate.edu

(Received 12 June 2025)

Abstract. Wood composite I-joists are commonly used in residential construction and light commercial buildings, particularly in floor and roof assemblies. These assemblies are often fire-rated, based on building design, to meet specific safety standards. Fire-rated assemblies are constructed using manufacturer-specified materials such as gypsum board and fire-retardant plywood. While I-joists may not be directly exposed to flames, they can still experience significant thermal exposure. This study investigates the effects of elevated temperatures on the compressive strength and modulus of elasticity (MOE) of I-joists, with 90 specimens tested across various temperatures and two exposure durations. Results indicate that significant degradation in mechanical properties occurs around 190°C, with OSB web buckling identified as the primary failure mechanism. A Sigmoidal model was applied to capture the temperature-dependent degradation, revealing critical property decline near 200°C and higher. This research provides insights into the thermal behavior of I-joists, with implications for maintaining structural integrity in high-temperature environments, and highlights the need for further studies on long-term exposure and temperatures above 200°C.

Keywords: Wood composite I-joist; Compression strength; Elevated temperature

Introduction

Wood-composite I-joists, first developed in the 1960s, gained widespread adoption in construction during the late 1980s and 1990s due to their efficiency and improved performance over traditional solid wood joists (Fisette 2000). These joists are constructed from two primary components, the flanges, typically made from laminated veneer lumber (LVL), which form the top and bottom horizontal sections, and the web, often made from oriented strand board (OSB), which forms the vertical section (Smulski 1997). This "I" cross-sectional shape, similar to that of steel I-beams, provides excellent load-bearing capabilities, making I-joists ideal for residential and light commercial applications.

The transition to wood-composite I-joists has been driven largely by their cost-effectiveness and superior mechanical performance compared to solid wood joists. I-joists are manufactured from lower-cost tree species and smaller-diameter logs, reducing material costs while maintaining comparable strength to solid wood. In addition, their engineered design minimizes natural defects such as knots and splits, which are common in solid wood, resulting in more reliable structural performance (APA 2024a; Forest Products Laboratory 2010). Despite their increased popularity, some countries, including the United Kingdom and Canada, have implemented restrictions on I-joist usage due to concerns over fire performance. In the United States, certain jurisdictions have also considered limitations, though the National Association of Home Builders (NAHB) has actively opposed such restrictions in 1999 and again in 2023 (NAHB 1999, 2023).

An important mechanical advantage of I-joists is that they span longer distances than traditional joists, allowing for larger open spaces in architectural designs, a feature that is highly valued in modern construction (APA 2024a). Moreover, I-joists exhibit superior dimensional stability, meaning they

* Corresponding author
† Society of Wood Science & Technology member

Wood and Fiber Science, 57(4), 2025, pp. 178–186
https://doi.org/10.22382/wfs-2025-15

are less prone to shrinkage, swelling, warping, and cupping, enhancing their long-term structural reliability (Forest Products Laboratory 2010). This combination of mechanical strength, stability, and cost-efficiency makes I-joists a common solution in both residential and commercial construction, particularly in applications that demand both flexibility and durability.

In construction, I-joists are commonly used in floors, roofs, and ceiling systems, although they may occasionally serve as wall studs or beams. Fire performance of these systems depends on the assembly in which they are installed, as I-joists themselves are not fire-rated. A common testing standard used to determine fire performance of materials is ASTM E119 (ASTM International 2020), where assemblies are exposed to a time-temperature curve under constant load to simulate real-world conditions (Sultan et al. 2007; APA 2024b). Under this standard, unprotected I-joist assemblies can fail in less than 15 minutes under fire testing conditions (APA 2007). For this reason, in most building systems, the fire protection of I-joists follows the guidelines from the International Residential Code (IRC) which includes the use of gypsum drywall, mineral wool insulation, or fire-treated plywood (ICC 2024). Following these guidelines, in proper fire-rated assemblies, under ASTM E119, I-joists can achieve fire ratings of one hour or more.

In building assemblies, the primary stresses experienced by I-joists are flexural stresses. Most research on I-joists has focused on their flexural properties. Studies by King et al. (2014) and Way et al. (2018) have shown that environmental factors, such as moisture and weathering, can degrade the flexural performance of I-joists. Similarly, studies by Morrissey et al. (2009) and Yeh and Herzog (2018) have investigated the impact of holes drilled for utilities on the structural integrity of I-joists. Although I-joists are not typically subjected to significant compressive forces in standard applications, localized compression can occur in scenarios such as short spans or improperly reinforced openings. While the compressive properties of I-joist web stock have been studied (e.g., Grandmont et al. 2010), little research has focused on the compressive performance of I-joists under uniform loads, particularly at elevated temperatures. Localized compressive stresses exacerbate failure at elevated temperatures, as was evident in Sultan et al. (2007), and therefore, further investigation is needed.

In fire conditions, even if I-joists are not exposed to direct flames, assemblies can still reach elevated temperatures that degrade the LVL and OSB components. Degradation has been observed at temperatures starting around 150°C (Sinha et al. 2011; Forest Products Laboratory 2010). Despite this, the effects of elevated temperatures on the compressive properties of wood-composite I-joists remain understudied.

This study aims to evaluate the compressive properties of wood-composite I-joists at elevated temperatures by applying a uniform vertical load to 301 mm x 304 mm specimens. The testing was conducted at nine temperatures ranging from 120°C to 200°C, with two exposure times. The objectives of the study were to:

- Compare the effects of exposure times at elevated temperatures on the compressive strength and stiffness of wood-composite I-joists.
- Investigate the compressive properties of wood-composite I-joists at elevated temperatures.
- Model the relationship between elevated temperature, exposure time, and compressive performance using a Sigmoidal model.

Materials

The testing was conducted on wooden I-joists procured from a local manufacturer with a country-wide distribution chain. These were then cut to dimensions of 301.6 mm (~1 ft) in depth and 304 mm (1 ft) in length. The I-joists consisted of an 11-mm-thick web made of OSB, while the flanges were constructed from Douglas-fir laminated veneer lumber (LVL) with a depth of 30 mm and a width of 50.8 mm. This specific I-joist size was selected because it is commonly used in industry. The measured specific gravity of the OSB used in the I-joist web was 0.59. The specimen size was based on ASTM D7672-14 (ASTM International 2014), the Standard Specification for Evaluating Structural Capacities of Rim Board Products and Assemblies, which prescribes a minimum length of 304 mm for vertical load testing. A total of 90 I-joists pieces were tested across nine different temperatures and two exposure times, as outlined in Table 1. The I-joists were conditioned at 20°C and 65% relative humidity until the material reached an approximate equilibrium moisture content of 12% (±3%), as seen in Figure 1a.

Table 1. Testing matrix for I-joist.

Exposure	Testing temperatures (°C)									Total
	120	130	140	150	160	170	180	190	200	
0 min.	5	5	5	5	5	5	5	5	5	45
50 min.	5	5	5	5	5	5	5	5	5	45
Total	10	10	10	10	10	10	10	10	10	90

Figure 1. Samples and compression test setup. (A) I-Joist conditioned room; (B) Testing setup with BEMCO installed within INSTRON testing frame; (C) Typical specimen installation with tested specimen and heating specimen.

Methods

Testing was conducted in accordance with ASTM D7672 (ASTM International 2014) Standard for Evaluating Structural Capacities of Rim Board Products and Assemblies. The tests were performed under uniform vertical load conditions using an INSTRON 5546, equipped with a Bemco environmental chamber integrated into the testing frame. The chamber had two access points, one at the top and the other at the bottom, allowing extension arms fitted with compression platens to extend from both the INSTRON testing base and crosshead, as shown in Figure 1b. This configuration allowed testing at elevated temperatures within the chamber while preventing any direct force from being applied to the Bemco chamber itself.

Thermocouples were installed in both the flange and web of the I-joists to monitor temperature. Two specimens were placed in the chamber, one for testing and the other for pre-heating (as shown in Figure 1c). Once the target temperature was reached for the specimen to be tested, the test was conducted. Afterward, the failed specimen was replaced by the pre-heated one, and a new specimen was placed in the chamber to pre-heat. A slight temperature drop occurred during the transfer, so the specimens were reheated to ensure uniformity before testing. The flange required approximately 20–30 minutes to heat, while the web took 10–15 minutes. This timing allowed sufficient time for testing before the next specimen reached the target temperature. Testing commenced once both the flange and web achieved the target temperature.

Tests were performed at nine temperatures, ranging from 120°C to 200°C, with 10°C increments. Two testing durations were used: one immediately after the specimen reached the prescribed temperature, and the other after 50 minutes of exposure. Once the specimen reached the target temperature and time, it was preloaded to approximately 170 N and tested at a rate of 1.25 mm/min until failure. Force measurements were taken from a 300 kN load cell attached to the INSTRON crosshead, and deflection was measured via crosshead displacement.

Following testing, both the compressive strength and compressive modulus of elasticity (MOE) of the I-joist were calculated.

Compressive strength (σc) was determined using the following equation:

$$\sigma_c = \frac{F_{max}}{A} \quad [1]$$

Where, σ_c is the compressive strength in MPa, F_{max} was the maximum applied force, and A is the cross-sectional area of the OSB web.

The compressive modulus of elasticity (E) was calculated using the following equation:

$$E = \frac{\Delta F}{d * \Delta \delta} \quad [2]$$

Where, E is the modulus of elasticity of the I-joist, ΔF is the change in load (N) within the elastic region, Δδ is the change in deflection (mm) in the elastic region, and d is the thickness of the OSB web in mm. The elastic range used for ΔF and Δδ, was approximately 10%–40% of the maximum force.

Results and Discussion

The results for compressive strength and compressive MOE of the I-joists are presented in Table 2 and Table 3, respectively. Table 2 provides the average compressive strength at each tested temperature, while Table 3 displays the average MOE for each temperature. These results offer a detailed comparison of how temperature affects both the strength and stiffness properties of the I-joists.

When examining the influence of exposure time on both compressive strength and stiffness, the results suggest that exposure duration did not significantly degrade these properties over time. This conclusion is supported by T-tests conducted at each temperature to compare the two exposure durations. For compressive strength, no significant differences were observed between exposure times except at 140°C (p-value = 0.01). A similar pattern was found for MOE, with a statistically significant difference only at 160°C (p-value = 0.02). These p-values are reported in Tables 2 and 3.

The stability of mechanical properties under elevated temperatures is likely due to the heat-resistant adhesive used in the I-joists, which meets ASTM D5055 (ASTM International 2021) standards and undergoes performance evaluation under ASTM D7247 (ASTM International 2017). Although the I-joists themselves are not rated for specific fire durations, their performance under high temperatures is considered during fire-rating assessments of complete assemblies.

To further investigate the effect of elevated temperatures on I-joist properties, a statistical analysis was conducted to assess whether significant differences exist across various temperature levels. The data was subsequently modeled using a Sigmoidal non-linear model to capture the temperature-dependent behavior of I-joists. The Sigmoidal function, which

Table 2. Average compressive strength of I-joists at elevated temperatures.

		Exposure temperature (°C)								
Time	Stats	120	130	140	150	160	170	180	190	200
0 min	Mean (MPa)	1369	1268	1481	1209	1223	1254	1098	1021	739
	StaDev (MPa)	116	120	134	68	147	140	113	59	32
50 min	Mean (MPa)	1452	1477	1431	1269	1365	1215	1189	1103	852
	StaDev (MPa)	123	90	105	45	157	46	91	108	97
T-test p-values		0.30	0.01	0.53	0.13	0.18	0.58	0.20	0.18	0.06

Table 3. Average compressive MOE of I-joists at elevated temperatures.

		Exposure temperature (°C)								
Time	Stats	120	130	140	150	160	170	180	190	200
0 min	Mean (MPa)	4520	3284	4449	4101	3938	3977	3723	3435	2377
	StaDev (MPa)	494	1934	268	444	101	512	313	391	150
50 min	Mean (MPa)	4955	4735	4720	4173	4607	4076	3978	3839	2810
	StaDev (MPa)	448	264	563	465	420	253	641	479	534
T-test p-values		0.26	0.28	0.36	0.79	0.02	0.77	0.52	0.33	0.15

exhibits an "S-shaped" curve, is typically applied to processes that start slowly, accelerate, and then slow down again, such as growth and dose-response relationships (Weisstein 2007; Sánchez-Jiménez et al. 2022). This model effectively fits the thermal degradation behavior of materials under increasing temperatures.

Prior to the statistical analysis, the data for compressive strength and stiffness were evaluated for homogeneity of variance (Flinger test, $\alpha = 0.05$) and normality (Shapiro-Wilk test, $\alpha = 0.05$). Both tests confirmed that the data met the assumptions of equal variance ($p > 0.05$) and normal distribution ($p > 0.05$). Subsequently, analysis of variance (ANOVA, $\alpha = 0.05$) was performed to detect significant differences in properties across temperature groups. The ANOVA revealed a significant influence of temperature on both compressive strength and stiffness, with clear trends emerging at each exposure time.

To further examine pairwise differences between temperatures, Tukey's post-hoc tests were applied. The results were then modeled using the Sigmoidal function:

$$\sigma_c or\ E = \frac{a}{\left(1 + exp(b * (t - c)\right)} \quad [3]$$

Where σc represents the compressive strength (kPa), E is the modulus of elasticity (MPa), a is the maximum property value observed at the lowest tested temperature, t is temperature (°C), b controls the rate of degradation after the critical temperature, and c denotes the critical temperature at which rapid degradation begins. Both b and c were estimated by fitting the model to the data using the Levenberg-Marquardt nonlinear algorithm in R (RStudio Team 2023). Model parameters and R^2 values are summarized in Table 4.

To visualize these results, boxplots were created for both compressive strength and MOE, showing the results of the Tukey tests. Each box is annotated with letters indicating statistical differences between temperatures; boxes sharing the same letters do not differ significantly. A red dashed line represents the fitted Sigmoidal model, with the equation and model parameters displayed in the top right corner of each plot, as seen in Figure 2.

Table 4. Fitted parameters for compressive strength and MOE.

	Strength Parameters				MOE Parameters			
exposure	a	b	c	R^2	a	b	c	R^2
0 min.	1345	0.066	204	0.871	4520	0.053	206	0.924
50 min.	1477	0.043	210	0.927	4813	0.050	210	0.883

The TUKEY test results for compressive strength revealed a predictable decline with increasing temperature, with significant degradation becoming apparent at 180°C. Specifically, beyond 180°C, compressive strength at higher temperatures showed statistically significant differences compared to lower temperatures, indicating the onset of notable thermal degradation. Similarly, the MOE exhibited a decreasing trend, with significant differences observed at 200°C for both exposure times.

The Sigmoidal model provided further insights into the degradation pattern. It demonstrated a gradual decline in compressive strength and MOE at lower temperatures, followed by accelerated degradation at higher temperatures. The model's critical temperature parameter (c) indicated that significant degradation occurred around or slightly above 200°C. The model fit the data well, with R^2 values ranging from 0.81 to 0.90, validating its suitability for representing the non-linear degradation trends observed in materials exposed to high temperatures. This approach aligns with previous studies on the thermal degradation of materials but has not been widely applied to wood-based composites (Pan et al. 2024; Li and Kasal 2022).

Both the statistical analysis (Tukey test) and the Sigmoidal model indicated a significant reduction in I-joist mechanical properties—compressive strength and MOE—between 190°C and 210°C. Compressive failures were primarily attributed to buckling of the OSB web, with some failures involving prying of the LVL, which was likely caused by OSB flexure, followed by buckling, as seen in Figure 3. These findings are consistent with established degradation patterns of OSB, which begins to degrade between 175°C and 200°C (Sinha et al. 2011; Sugahara et al. 2022; Miyamoto and Sinha 2025). The thermal degradation of OSB can be attributed to both the decomposition of wood components, such as hemicellulose, and the breakdown of adhesives. Hemicellulose degradation typically begins at 170°C to 200°C, contributing to the observed loss in mechanical properties (Dietenberger and Hasburgh 2016; Sinha 2013). Additionally, the dramatic drop in mechanical properties at 200°C may be linked to the degradation of the polymeric methylene diphenyl diisocyanate (PMDI) adhesive used in OSB, which also begins to degrade around 200°C (Desai and O'Dell 1989; Yang et al. 1986).

To assess whether the Sigmoidal model would also be effective at lower temperatures, it was fitted to both the elevated temperature data and manufacturer-supplied compressive

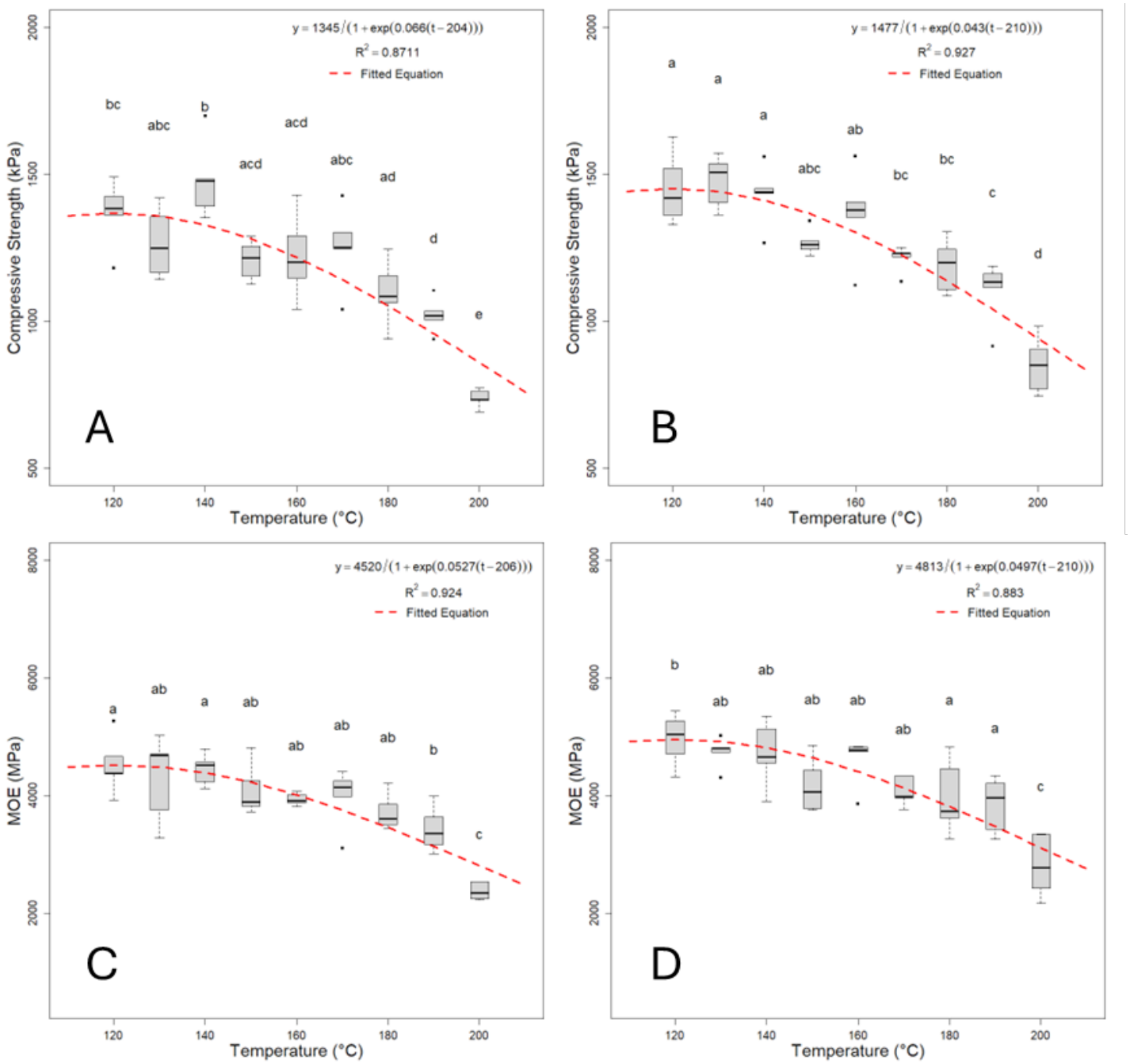

Figure 2. TUKEY test results for compressive strength at 0 min. (A) and 50 min (B) exposure times, and MOE at 0 min. (C) and 50 min. (D) exposure times, with the fitted Sigmoidal function model at both exposure times.

strength and MOE data for ambient conditions. This broader fitting provided a more comprehensive understanding of I-joist performance across a wide temperature range. The extended model results are shown in Figure 4.

The fitted parameters for the Sigmoidal model are shown in the top right corner of the graphs in Figure 4. The model demonstrated a good fit to the data, with R^2 values of 0.935 for compressive strength and 0.9147 for MOE. The shape of the curve is consistent with expectations, as thermal degradation is anticipated to commence at temperatures above 80°C and gradually progress, with accelerated degradation occurring at higher temperatures, such as 180°C to 200°C. While the model captures this general behavior, it may indicate the onset of thermal degradation at lower temperatures than expected. This model thus shows that it could be used as an empirical material model for thermal degradation.

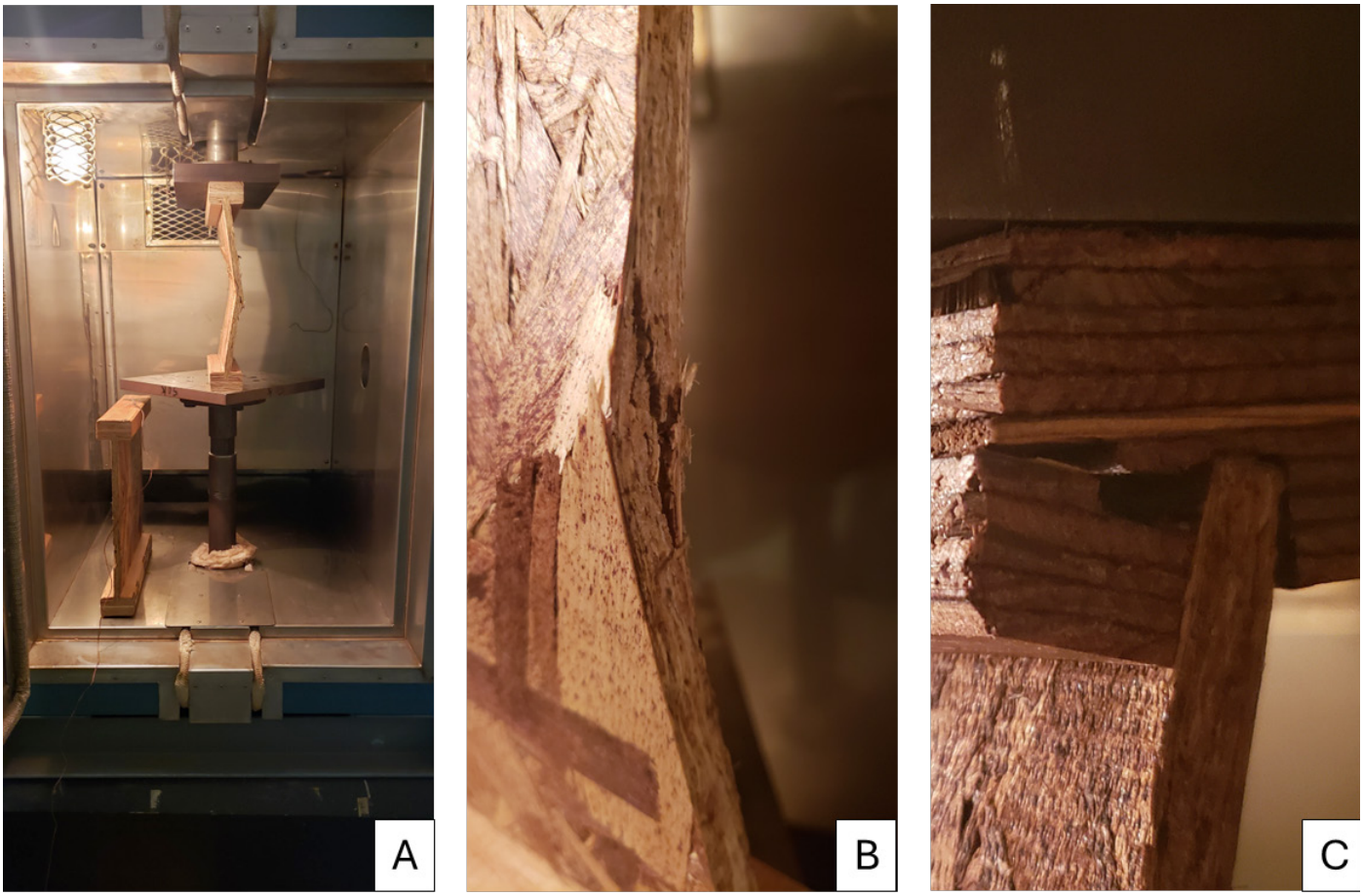

Figure 3. I-joist failure types. (A) Typical tested specimen failing in buckling; (B) OSB buckling failure; (C) LVL prying failure.

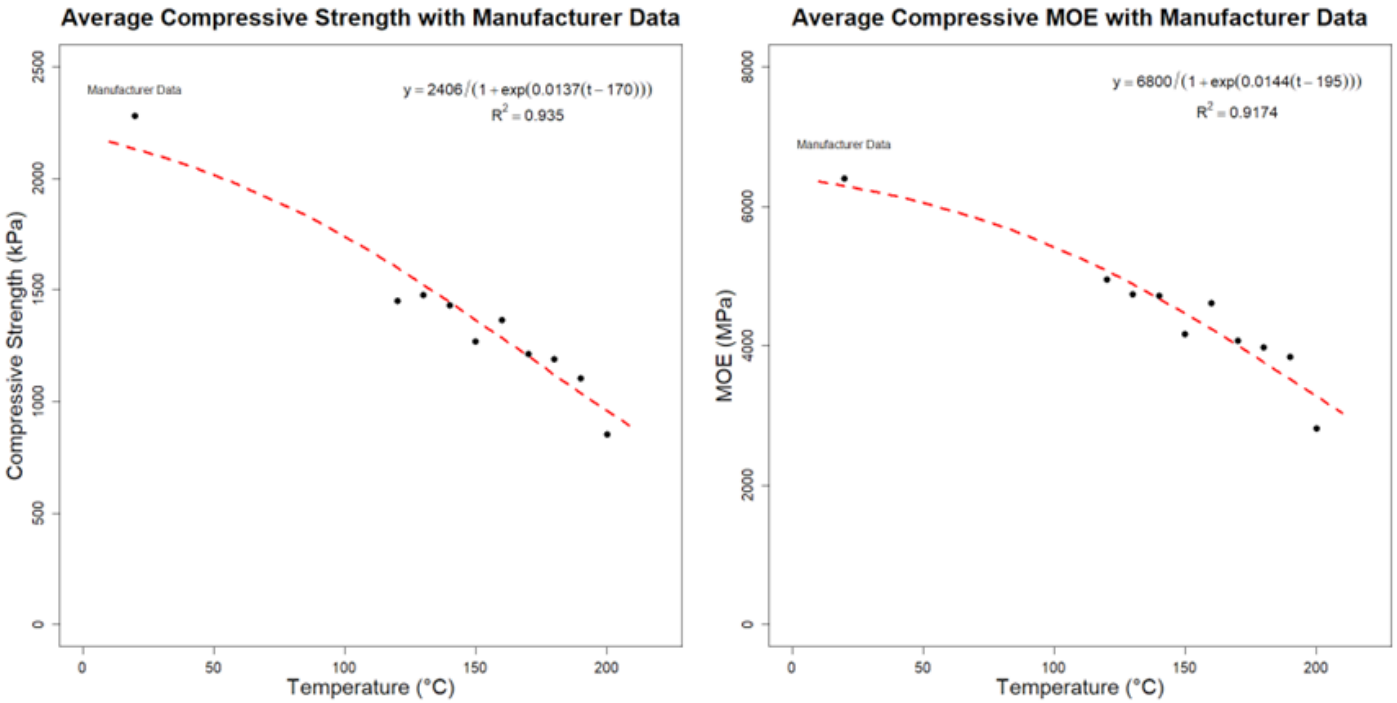

Figure 4. (A) Average compressive strength and (B) MOE at elevated temperatures and manufacturer data at room temperature with the fitted Sigmoidal function.

Conclusion

This study investigated the compressive properties of wooden I-joists under elevated temperatures. I-joists were tested at nine different temperatures, ranging from 120°C to 200°C, with two exposure times: one right when the specimen reached the target temperature and the other after 50 minutes of exposure. The tests followed a uniform vertical loading protocol in compression.

The results revealed that the OSB web was the primary failure mechanism, typically failing due to buckling. The two key properties evaluated were compressive strength and MOE. Both properties indicated significant thermal degradation beginning at approximately 190°C, with a drastic increase in degradation rates observed at 200°C. Interestingly, the comparison of the two exposure times showed no statistically significant differences. This suggests that temperature is the primary factor driving degradation, rather than the duration of exposure at high temperatures.

To further analyze the temperature-dependent behavior of the I-joists, a Sigmoidal model was fitted to the data. The model demonstrated a good fit, with R^2 values ranging from 0.81 to 0.90. The model also indicated that critical thermal degradation occurred primarily at temperatures of 200°C and above. An additional model fitting was performed, incorporating manufacturer data for I-joists tested at room temperature. This extended fit showed strong agreement, with R^2 values of 0.93 and 0.91 for compressive strength and MOE, respectively.

Future investigations into the compressive strength of I-joists at elevated temperatures should consider longer exposure durations to identify the critical time points at which compressive properties begin to degrade, as the two exposure times used in this study did not show significant differences. Additionally, testing at temperatures beyond 200°C, such as 220°C, would help validate the occurrence of thermal degradation at higher temperatures and could further refine the Sigmoidal model. Moreover, the effects of sustained constant loading on I-joists at elevated temperatures over extended exposure periods, such as 2 hours, should be explored to gain a deeper understanding of the long-term thermal behavior of these materials.

Acknowledgements

The authors would like to acknowledge the support of the Wood-Based Composites Center and the NSF INTERN program for funding this project.

References

APA – The Engineered Wood Association (2007) Wood I-joist floors, firefighters, and fire. APA – The Engineered Wood Association. Retrieved from https://www.apawood.org/Data/Sites/1/documents/fireprotection/fire-protection-requirements-for-IJ.pdf

APA – The Engineered Wood Association (2024a) PR-S259: Fire-rated assemblies for RFPI joists. Retrieved from https://www.apawood.org/download_pdf.ashx?pubid=80c89e03-9bb3-4c1c-bbfe-1f7496459874&bp=1

APA – The Engineered Wood Association (2024b) Performance Rated I-Joists Design and Construction Guide. https://www.apawood.org

ASTM International (2020) ASTM E119-20: Standard test methods for fire tests of building construction and materials. American Society for Testing and Materials, West Conshohocken, PA. USA. https://store.astm.org/standards/e119

ASTM International (2014) ASTM D7672-14: Standard specification for evaluating structural capacities of rim board products and assemblies. American Society for Testing and Materials, West Conshohocken, PA. USA. https://webstore.ansi.org/standards/astm/astmd767214

ASTM International (2021) ASTM D5055-21: Standard specification for establishing and monitoring structural capacities of prefabricated wood I-joists. American Society for Testing and Materials, West Conshohocken, PA. USA. https://store.astm.org/d5055-19e01.html

ASTM International (2017) ASTM D7247-17: Standard Test Method for Evaluating the Shear Strength of Adhesive Bonds in Laminated Wood Products at Elevated Temperatures. American Society for Testing and Materials, West Conshohocken, PA. https://store.astm.org/d7247-17.html

Desai HP, O'Dell JL (1989) Thermal stability and combustion characteristics of isocyanates in fire-retardant applications. Fire Mater 14(2):65–72.

Dietenberger MA, Hasburgh LE (2016) Wood Products: Thermal Degradation and Fire. In Reference Module in Materials Science and Materials Engineering (p. B9780128035818033385). Elsevier. https://doi.org/10.1016/B978-0-12-803581-8.03338-5

Grandmont J-F, Cloutier A, Gendron G, Desjardins R (2010) Effect of density on the properties of oriented strandboard web stock used in wood I-joists. For Prod J 60(7–8):592–598. https://doi.org/10.13073/0015-7473-60.7.592

ICC - International Code Council. (2024). ICC-ES Evaluation Report ESR-1336: Wood I-Joists (pp. 1–10). ICC Evaluation Service. https://cdn-v2.icc-es.org/wp-content/uploads/report-directory/ESR-1336.pdf

King DT, Sinha A, Morrell JJ (2014) Effects of outdoor exposure on properties of I-joists. Wood Fiber Sci 46(3):394–400. https://wfs.swst.org/index.php/wfs/article/view/264

Li J, Kasal B (2022) Effects of Thermal Aging on the Adhesion Forces of Biopolymers of Wood Cell Walls. Biomacromolecules 23(4):1601–1609. https://doi.org/10.1021/acs.biomac.1c01397

Miyamoto BT, Sinha A (2025) Time-temperature effects on early-stage primary thermal creep of plywood and oriented strand board (OSB) at elevated temperatures. Wood Fib Sci 57(1):15-26. https://doi.org/10.22382/wfs-2025-02

Morrissey GC, Dinehart DW, Dunn WG (2009) Wood I-Joists with Excessive Web Openings: An Experimental and Analytical Investigation. J Struct Eng 135(6):655–665. https://doi.org/10.1061/(ASCE)ST.1943-541X.0000013

NAHB - National Association of Home Builders (2023) Restrictions and bans on wood trusses and I-joists (Policy Resolution No. 2023/6-7). https://www.nahb.org/-/media/NAHB/advocacy/docs/policy-resolutions/construction-and-codes/2023-6-no-7-restrictions-and-bans-on-wood-trusses-and-i-joists.pdf?rev=675e5f2531264a8980b1f79b9dfd637b

NAHB - National Association of Home Builders (1999) Restrictions and bans on wood trusses and I-joists (Policy Resolution No. 1999/5-14). https://www.nahb.org/-/media/NAHB/advocacy/docs/policy-resolutions/construction-and-codes/1999-5-no14-restrictions-and-bans-on-wood-trusses-i-joists.pdf

Pan B, Shen F, Sampathkumar SR, Münstermann S (2024) Modeling strain hardening of metallic materials with Sigmoidal function considering temperature and strain rate effects. Materials 17(16):3950. https://doi.org/10.3390/ma17163950

RStudio Team (2023) RStudio: Integrated Development for R. RStudio, PBC. Retrieved from https://www.rstudio.com/

Sánchez-Jiménez PE, Perejón A, Arcenegui-Troya J, Pérez-Maqueda LA (2022) Predictions of polymer thermal degradation: Relevance of selecting the proper kinetic model. J Therm Anal Calorim 147(3):2335–2341. https://doi.org/10.1007/s10973-021-10649-x

Siimer K, Kaljuvee T, Pehk T, Lasn I (2010) Thermal behaviour of melamine-modified urea–formaldehyde resins. J Therm Anal Calorim 99(3):755–762. https://doi.org/10.1007/s10973-009-0617-z

Sinha A (2013) Thermal degradation modeling of flexural strength of wood after exposure to elevated temperatures. Wood Mater Sci Eng 8(2):111–118. https://doi.org/10.1080/17480272.2012.753950

Sinha A, Gupta R, Nairn JA (2011). Thermal degradation of bending properties of structural wood and wood-based composites. Holzforschung 65(2):221–229. https://doi.org/10.1515/hf.2011.001

Smulski S, ed. (1997) Engineered wood products: A guide for specifiers, designers & users. PFS Research Foundation. ISBN: 9780965673600

Sugahara E, Dias A, Arroyo F, Christoforo A, Costa ML, Botelho EC, Dias AMPG, Campos C (2022) Study of the influence of heat treatment on OSB panels produced with Eucalyptus wood in different layer compositions. Forests 13(12):2083. https://doi.org/10.3390/f13122083

Sultan MA, Seguin YP, Leroux P (2007) Fire resistance of wood-frame assemblies. Fire Technol 45(2):113–128. https://doi.org/10.1007/s10694-007-0038-0

Forest Products Laboratory (2010) Wood handbook: Wood as an engineering material. General Technical Report FPL-GTR-190. Madison, WI: U.S. Department of Agriculture, Forest Service, Forest Products Laboratory. https://www.fpl.fs.usda.gov/documnts/fplgtr/fpl_gtr190.pdfFisette, P (2000). The evolution of engineered wood I-joists. Building and Construction Technology. Retrieved from https://www.umass.edu/bct/publications/articles/the-evolution-of-engineered-wood-i-joists/

Way D, Sinha A, Kamke FA (2018) Laboratory and Outdoor Weathering of Wood-Composite I-Joists. J Mater Civ Eng 30(7):04018148. https://doi.org/10.1061/(ASCE)MT.1943-5533.0002327

Weisstein EW (2007) Sigmoid function. In MathWorld – A Wolfram Web Resource. Retrieved from https://mathworld.wolfram.com/SigmoidFunction.html

Yang WP, Macosko CW, Wellinghoff ST (1986) Thermal degradation of urethanes based on 4,4′-diphenylmethane diisocyanate and 1,4-butanediol (MDI/BDO). Polymer 27(8):1235–1240. https://doi.org/10.1016/0032-3861(86)90012-1

Yeh B, Herzog B (2018) Effect of holes on the structural capacities of laminated veneer lumber. In Proceedings of the 2018 World Conference on Timber Engineering. Seoul, Republic of Korea: APA – The Engineered Wood Association. Retrieved from https://www.apawood.org/Data/Sites/1/documents/technicalresearch/MAT-012-04_Effect-of-Holes-on-the-Structural-Capacities-of-LVL_FullPaper.pdf

Correlation between non-destructive assessment of wood veneers and the resulting laminated veneer lumber

Dalila Belaidi
Ph.D. Student, Department of Sustainable Bioproducts
Forest and Wildlife Research Center (FWRC), College of Forest Resources (CFR)
Mississippi State University, Starkville, MS 39762 USA
E-mail : db3049@msstate.edu

Mostafa Mohammadabadi *
Assistant Professor, Department of Sustainable Bioproducts
Forest and Wildlife Research Center (FWRC), College of Forest Resources (CFR)
Mississippi State University, Starkville, MS 39762 USA
E-mail : mm5132@msstate.edu

Fred França
Assistant Professor, Department of Sustainable Bioproducts
Forest and Wildlife Research Center (FWRC), College of Forest Resources (CFR)
Mississippi State University, Starkville, MS 39762 USA
E-mail : fn90@msstate.edu

Rubin Shmulsky
Professor and Head, Department of Sustainable Bioproducts
Forest and Wildlife Research Center (FWRC), College of Forest Resources (CFR)
Mississippi State University, Starkville, MS 39762 USA
E-mail : rs26@msstate.edu

Xiping Wang
Research Forest Products Technologist, USDA Forest Service
Forest Products Laboratory
US Department of Agriculture, Madison, WI 53706 USA
E-mail : xwang@fs.fed.us

Daniel Seale
Warren S. Thompson Professor of Wood Science and Technology
Department of Sustainable Bioproducts
Forest and Wildlife Research Center (FWRC), College of Forest Resources (CFR)
Mississippi State University, Starkville, MS 39762, USA
E-mail : rds9@msstate.edu

William Nkeuwa
Application Engineer
Engineered wood adhesives
Henkel, Inc., Blacksburg, VA 24060, USA
E-mail : william.nkeuwa@henkel.com

(Received 24 July 2025)

Abstract. This study investigated correlations between the mechanical properties of individual red maple *(Acer rubrum)* veneers and that of associated laminated veneer lumber (LVL). Veneers with an average thickness of 3.5 mm, width of 304 mm, and length of 2.44 m, were first subjected to a nondestructive test (NDT) using stress wave analysis. Dynamic modulus of elasticity (MOE_d) was used to classify 480 veneers into four equal groups: high-grade, medium-grade, low-grade, and a mixed group. Each LVL consisted of 12 veneers bonded with polyurethane (PUR) adhesive. All LVL billets were evaluated nondestructively to determine their dynamic modulus of elasticity. Two different measurement systems were employed: a Fakopp Microsecond Timer was used for a time-of-flight approach and a Hitman HM200 (resonance acoustics approach) applied the longitudinal stress wave method and assessed its reliability for predicting the mechanical performance of LVL billets. A strong correlation ($r = 0.85$ and $R^2 = 0.73$) was found between the average $MOE_{dVeneer}$ of veneers and that of the LVL billets (MOE_{dLVL}). There was a strong correlation between MOE_d from the Hitman HM200 device ($MOE_{dHitman}$) and that from the Fakopp device ($MOE_{dFakopp}$) ($r = 0.93$ and $R^2 = 0.86$).

Keywords: Hardwood; Red maple; Mechanical properties; Nondestructive evaluation (NDE); Dynamic modulus of elasticity (MOE_d); Longitudinal stress wave method; Fakopp; Hitman

* Corresponding author
† Society of Wood Science & Technology member

Wood and Fiber Science, 57(4), 2025, pp. 187–199
https://doi.org/10.22382/wfs-2025-16

Introduction

The concept of green building has gained significant traction in recent years (Pajchrowski et al. 2014; Xue and Hu 2013). However, the increasing reliance on fast-growing plantation trees has resulted in smaller logs with lower wood quality, making it difficult for traditional solid lumber to meet modern construction demands (Gao and Gong 2021; McGavin and Leggate 2019). In response to these challenges, engineered wood products (EWPs) have emerged as viable alternatives. The push toward sustainable construction has driven innovations in EWPs such as laminated veneer lumber (LVL), cross-laminated timber (CLT), and glulam, offering superior physical and mechanical performance compared to traditional solid lumber (Gong 2019). Corrugated wood-based panels, constructed from fibers and veneers, represent a novel solution that improves both the structural performance and resource efficiency of EWPs (Lamichhane et al. 2025)**.** These products promote greater resource efficiency and lower carbon emissions, aligning well with contemporary sustainable building practices (Winchester and Reilly 2020). In addition, techniques like densification have been shown to enhance mechanical characteristics, particularly stiffness and elasticity (Pradhan et al. 2024)

The orthotropic nature of wood must be taken into consideration when studying its behavior. Wood properties such as density, grain structure, and mechanical properties can vary significantly across different species, environmental conditions, and even among individual pieces from the same tree (Arriaga et al. 2023). These variations highlight the need for developing advanced methods to ensure reliable performance of EWPs like LVL in structural applications.

Since the 1960s, nondestructive evaluation (NDE) techniques have gained considerable attention, particularly for mechanical grading of wood (Divós and Tanaka 2005). NDE is also widely used to detect voids, irregularities, and other common defects in wood products (Del Menezzi et al. 2013). A major advantage of NDE is its ability to assess the mechanical and physical properties of wood without causing any damage, making it a valuable tool for wood quality assessment (Ross 2015; Miclea et al. 2002; Turkot et al. 2020; Liu et al. 2006).

Numerous studies have employed NDE to classify veneers, lumber, and logs for manufacturing EWPs. Teles et al. (2010) reported a strong coefficient ($R^2 = 0.95$) between the dynamic MOE of glulam and its laminae using the transverse vibration method. Similarly, Wang et al. (2003) demonstrated that ultrasonic wave propagation time and the corresponding MOE of red maple veneers were closely related to the strength and stiffness of LVL billets. Ross et al. (2004) further observed that the dynamic MOE values of red maple veneers followed a normal distribution, validating their applicability for LVL manufacturing.

While individual NDE methods have proven effective in evaluating the mechanical properties of wood, integrating multiple techniques can enhance the precision and reliability of the results (Divos and Tanaka 1997; Vössing and Niederleithinger 2018; Kloiber et al. 2016). Cavalli and Togni (2013) employed a combination of flexural and longitudinal vibration tests, stress wave transmission measurements, and Pilodyn penetration tests to evaluate the mechanical properties of silver fir timber, emphasizing that a single method was often insufficient for a comprehensive evaluation. Similarly, Chen and Guo (2016) combined stress wave timing with resistance drilling tests to evaluate the mechanical properties of Chinese fir and elm, finding strong linear correlations between nondestructive test parameters and key mechanical properties. This underscores the importance of exploring various NDT technologies to overcome the limitations of individual methods and achieve more reliable results.

Previous studies have investigated the potential of red maple (*Acer rubrum* L.) for structural applications, citing its favorable physical and mechanical properties (Ross et al. 2004; Kimmel and Janowiak 1995; Wang et al. 2004). However, red maple remains unexplored for use in EWPs due to limited commercial processing. Notably, few nondestructive evaluation studies have specifically targeted red maple, and most existing research relies on a single NDE technique.

To address this gap, the present research contributes to ongoing efforts to expand the market for this underutilized hardwood species by employing nondestructive test methods to accurately predict the structural performance of associated EWPs such as LVL.

In this study, we examined the relationships between the mechanical properties of individual veneers ($MOE_{dVeneer}$) and the overall structural performance of LVL (MOE_{dLVL}) using the longitudinal stress wave method. Two different measurement systems were employed: time-of-flight (ToF) approach, using a Fakopp Microsecond Timer, and resonance acoustics approach, using a Hitman HM200. The findings from this study contribute to a deeper understanding of how veneer-level mechanical characteristics affect the overall stiffness of LVL. The results have practical significance from an industrial perspective, as they may inform strategies for optimizing veneer

selection and layer configuration, thereby minimizing material waste and enabling the production of high-performance veneer-based products.

Materials and methods

Veneer

A total of 480 red maple veneer sheets (0.304 by 2.43 m (1 by 8 ft)) were selected for LVL fabrication from a larger population of 553 sheets reported in a previous study by Belaidi et al. (2025b). Seventy-three veneers were removed from the test because of prior damage. All veneer sheets were obtained from Great Lake Veneer (Marion, WI, USA). Prior to nondestructive evaluations, the density of all 480 veneers was determined by measuring their length, width, thickness, and mass (Table 1). The veneers were conditioned at 12% moisture content in a controlled environment to achieve a target equilibrium moisture content before the fabrication of LVL billets.

Grading process

The veneers were visually graded according to the International Hardwood Veneer Grading Rules (Redman 2020). The grading process, which considered various factors such as the number, size, and types of knots, checks, and splits, was used to assign each veneer a grade of A, B, C, or D. The grading process is explained in detail by Belaidi et al. (2025b).

LVL Fabrication and grading

To manufacture LVL billets with a target thickness of 38 mm (1.5 in), 12 layers of veneer were bonded using a one-component polyurethane (PUR) adhesive. LOCTITE UR5153 and its corresponding primer, LOCTITE PR3105 PURBOND (Henkel, Henrico, VA, USA) were applied using rollers to ensure uniform distribution on the bonding surface. The target application rate for this adhesive was 40 lb/1,000 ft^2 (200g/m^2). After applying the adhesive, the weighed veneers revealed an average application rate of approximately 220 g/m^2.

LOCTITE UR5153 had an opening time of 30 minutes and required a pressing time of 1 hour (Belaidi et al. 2025a). The manufacturing process involved pressing four LVL billets simultaneously at 150 psi. A total of 40 LVL billets were produced and trimmed, and the average dimensions (length, mass and width) were recorded to determine the density of LVL billets (Table 2).

To quantify the grading for the LVL billets, numerical values were assigned to each letter grade: 4 for Grade A, 3 for Grade B, 2 for Grade C, and 1 for Grade D; since each LVL billet was fabricated from veneers of different grades, it was not possible to assign a single letter grade to each veneer. These numerical values representing the grades were then summed to develop a single number representing the grade of the LVL billet. For example, if an LVL contained 6 Grade A veneers, 2 Grade B veneers, 3 Grade C veneers, and 1 Grade D veneer, the grading number was calculated as follows: (6×A) + (2×B) + (3×C) + (1×D) ≥ (6×4) + (2×3) + (3×2) + (1×1) = 37

The minimum possible grade number was 12, when all 12 veneers were Grade D, while the maximum number was 48, if all 12 veneers were Grade A.

Table 1. Average dimensions of red maple veneers.

Number of veneers measured	Thickness (mm)	Width (mm)	Length (mm)	Density (kg/m^3)
480	3.55	304.04	2441.96	584

Table 2. Average dimensions of LVL billets.

Number of LVL	Thickness (mm)	Width (mm)	Length (mm)	Density (kg/m^3)
40	39.96	280.50	2420.30	697

Nondestructive Characterization of LVL Billets

Time of Flight measurements

The veneers were nondestructively tested using the stress wave method to determine the dynamic modulus of elasticity. Each veneer was clamped at both ends using a specialized fixture (Figure 1a).

Ross (2015) noted that additional support was added under the veneer to maintain alignment and prevent damage at the contact point, which could affect the accuracy of the results. Each veneer was struck three times using an impact pendulum, and a portable stress wave timer, the Fakopp Microsecond Timer (Fakopp Enterprise, Hungary), was used to measure the transit time of the stress wave traveling from one end to the other. The average transit time, measured from three different longitudinal locations, was used to measure the stress wave velocity, using Equation 1, and the dynamic modulus of elasticity was then determined according to Equation 2.

$$\nu = L/\mathrm{t} \quad [1]$$

$$\mathrm{MOE_d} = \rho * \nu^2 \quad [2]$$

Where L is the length of the veneer (m), t is the transit time measured using the Fakopp device (s), ρ is the density of the veneer (kg/m^3), and ν is the velocity (m/s).

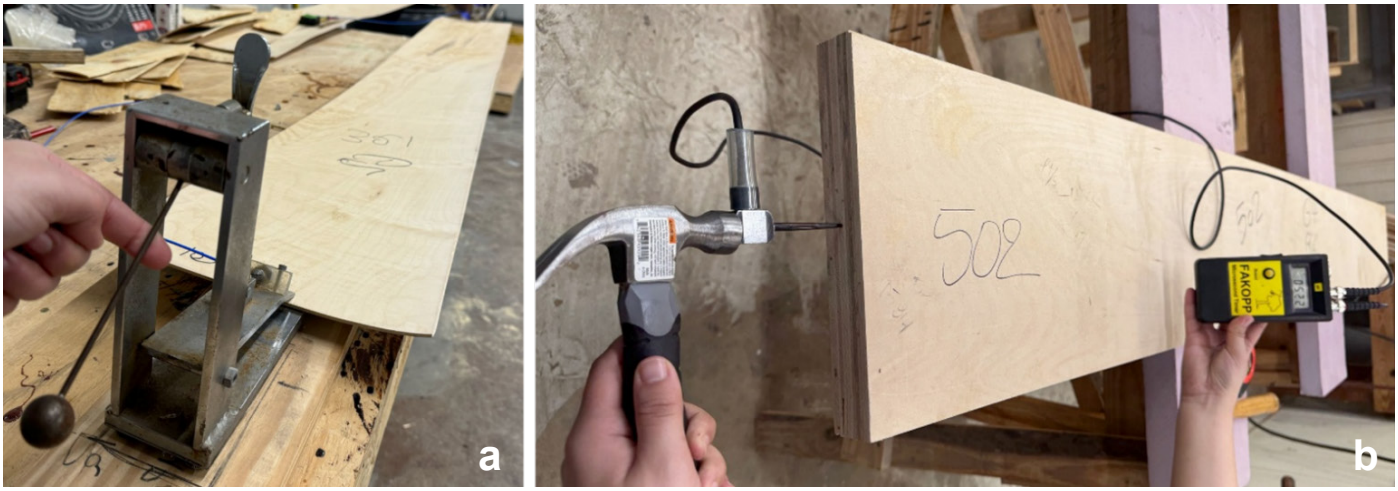

Figure 1. Setup for the stress wave measurement (a) using built-in pendulum; (b) using pins.

The same nondestructive method was applied to determine the dynamic modulus of elasticity of the LVL billets. Each billet was placed flatwise on two sawhorses, as shown in Figure 1(b). Pins were nailed at both ends of the billet, with the start pin struck by a small hammer to generate a stress wave that traveled the length of the billet. The Fakopp device recorded the transit time. The average transit time, measured from two different longitudinal locations, was used to determine the stress wave velocity and dynamic modulus of elasticity according to Equations 1 and 2, respectively.

Resonant acoustic measurement

Each LVL billet was placed flatwise on two sawhorses, positioned one-quarter of the total length from each end. A thin foam layer was placed between the billet and the sawhorses to reduce damping effects and improve measurement accuracy. A portable nondestructive device, the Hitman HM200 (Fibre-gen, Christchurch, New Zealand), was pressed against one end of the LVL billet, while the billet was hit with a hammer to generate longitudinal vibration. The Hitman device measures the stress wave velocity in the LVL billet. Average stress wave velocity, measured from two different longitudinal locations was used to calculate the dynamic modulus of elasticity, using Equation 2.

The Hitman HM200 was not suitable for the veneers due to their thinness, since the required contact area for the device exceeded the veneer thickness. While the vibration was propagated by the hammer, the small contact area could prevent the Hitman device from detecting the vibration, and as a result, affect the velocity measurement.

Statistical analysis

The statistical analyses were conducted using OriginPro software (Northampton, MA), at the significance level of 0.05 ($\alpha = 0.05$).

Results and discussion

Stress wave properties of the veneer

Dynamic modulus of elasticity (MOE_d) for the 480 veneers ranged from 10 to 26 GPa. The average MOE_d of the veneers was 19.10 GPa (± 2.97 GPa) and a coefficient of variance (COV) of 15.55%. According to Kolmogorov-Smirnov normality test, the resulting p-value 0.94 (>0.05), indicated that MOE_d values were normally distributed. The skewness of MOE_d was 0.0408, suggesting an approximate symmetric distribution. The visual grading distribution of the selected 480 veneers is shown in Figure 2.

Based on the MOE_d results, all 480 veneer samples were arranged in ascending order, and then evenly divided into three groups of 160 veneers each, as shown in Figure 3. The first

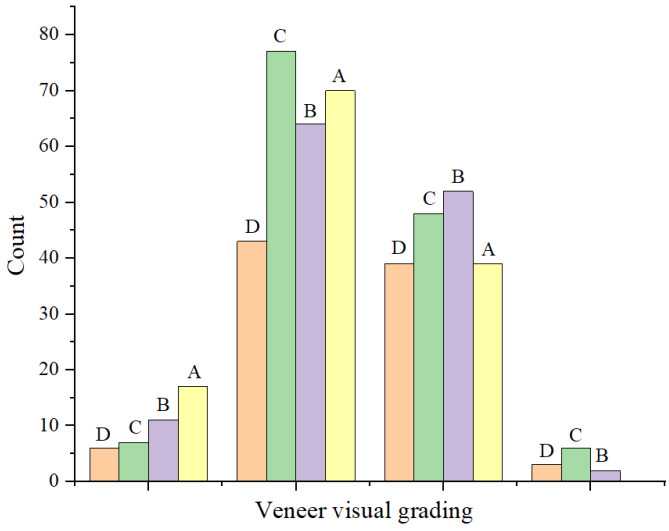

Figure 2. Distribution of the visual grades of 480 red maple veneer (letters on each bar indicate the assigned visual grade).

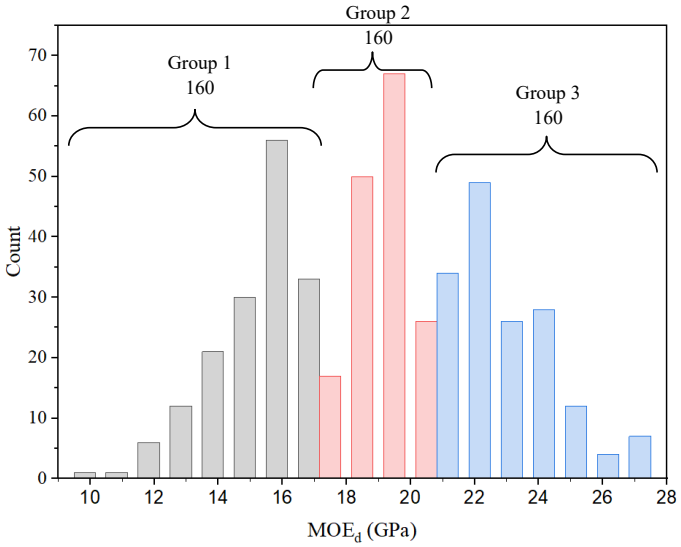

Figure 3. Distribution of MOE$_d$ into three equal groups.

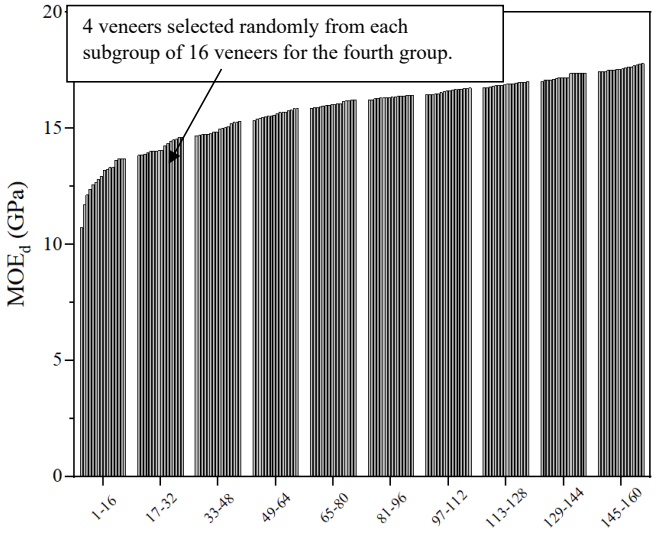

Figure 4. Sorting the veneers of the first group into 10 subgroups of 16 veneers each for random selection of 4 veneers from each subgroup into the fourth group.

group had MOE$_d$ values ranging from 10.73 to 17.79 GPa, the second group from 17.80 to 20.46 GPa, and the third group from 20.51 to 26.48 GPa. According to the MOE$_d$ values, the first group included high-MOE$_d$ veneers, the second contained medium-MOE$_d$ veneers, and the third consisted of low-MOE$_d$ veneers. An additional group, the fourth group, was created using a mix of veneers ranging from low to high MOE$_d$ values.

To ensure a representative distribution in the fourth group, each of the three original groups, ordered in ascending MOE$_d$, was subdivided into 10 subgroups of 16 veneers each (Figure 4). From each subgroup of 16 veneers, 4 veneers were randomly selected, resulting in 40 veneers from each original group and a total of 120 from all three groups. These 120 veneers, covering a wide range of MOE$_d$ values from low to high, were assigned to the fourth group. This selection resulted in four groups, each consisting of 120 veneers, ensuring an equal number across all groups.

The average MOE$_d$ of these 120 veneers in the fourth group was 19.05 GPa, which was similar to the average MOE$_d$ of all 480 veneers (Figure 5). The p-value of 0.52 (>0.05) obtained from Shapiro-Wilk normality test indicated a normal distribution for MOE$_d$ values. This confirmed that selecting 120 veneers with a normal distribution for the fourth group accurately represented the entire population.

Veneers from each group were used to manufacture 12-layer LVL billets, with 10 billets produced for each group, to investigate the impact of veneer MOE$_d$ on the structural performance of LVL. For the first three groups, 12 layers were randomly selected from each group, using a random number generator

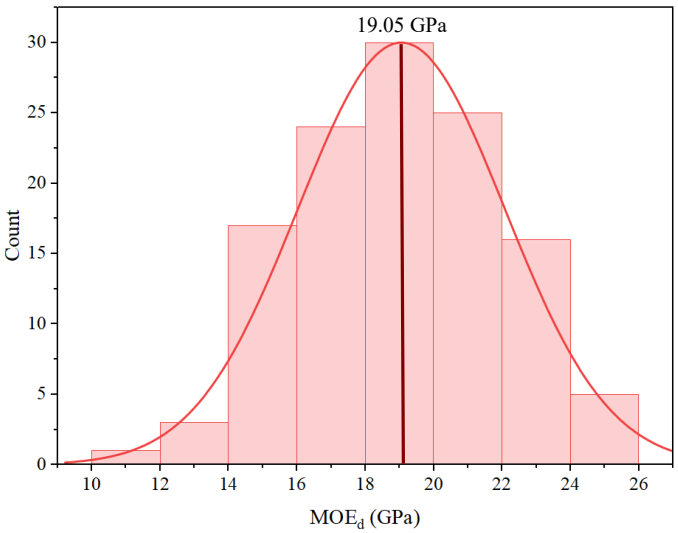

Figure 5. Distribution of the dynamic modulus of elasticity of 120 red maple veneers for the fourth group.

method, and stacked together, regardless of their MOE$_d$ and grade, to fabricate the LVL billet. For the fourth group, which was a combination of the first three groups, high-MOE$_d$ veneers from the third group were placed on the outer layers of the LVL, low-MOE$_d$ veneers from the first group were placed at the center, and medium-MOE$_d$ veneers from the second group were placed in between.

Stress Wave Properties of LVL billets

The distribution of the dynamic modulus of elasticity for the 40 LVL billets, obtained using the Fakopp device (Figure 6a), ranged from 13 to 17 GPa, with an average of 15.63 GPa (± 1.03 GPa) and a coefficient of variance (COV) of 6.5%. A

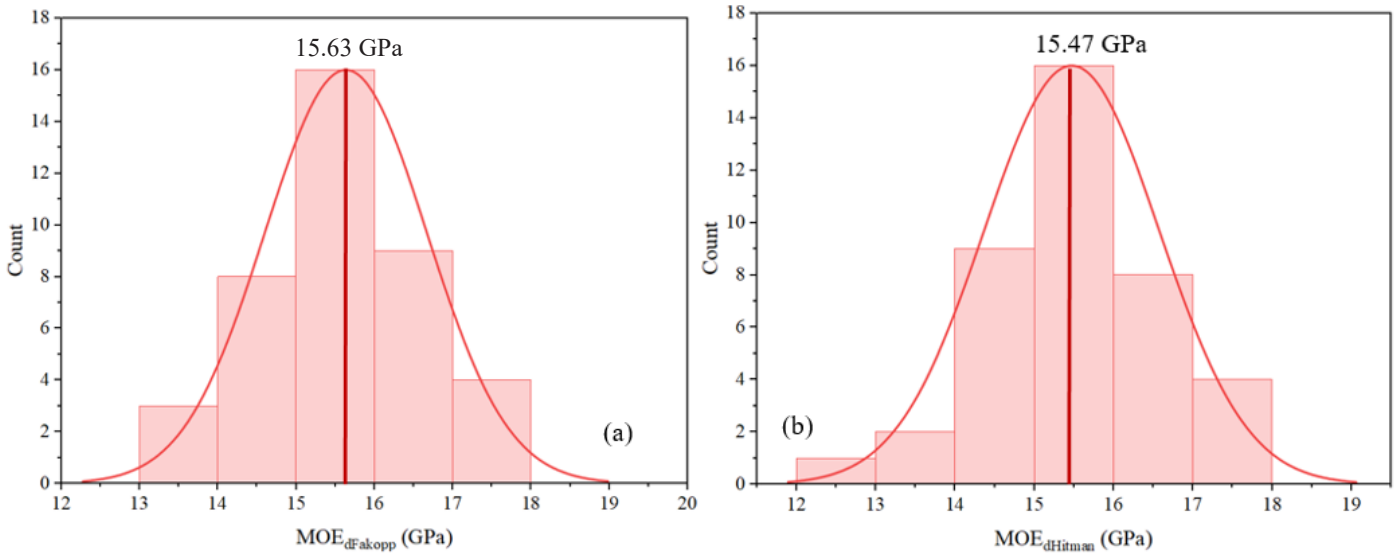

Figure 6. Distribution of the MOE$_d$ using (a)Fakopp (MOE$_{dFakopp}$,); (b) Hitman (MOE$_{dHitman}$) measurements of 40 LVL billets.

Shapiro-Wilk normality test was conducted on the MOE$_{dFakopp}$ values using OriginPro software, resulting in a p-value of 0.84 (> 0.05), indicating a normal distribution for MOE$_{dFakopp}$ values.

Figure 6b presents the distribution of the dynamic MOE of the same 40 LVL billets evaluated using the Hitman device. The results ranged from 12 to 17 GPa, with a mean value of 15.47 GPa (± 1.10 GPa) and a coefficient of variation of 7.11%. The Shapiro-Wilk test for MOE$_{dHitman}$ values yielded a p-value of 0.9, indicating a normal distribution.

Both nondestructive testing devices yielded similar mean values for the dynamic MOE of the LVL. This consistency suggests that both devices provided a reliable evaluation of the mechanical properties of the LVL billets. A regression analysis and paired t-test were conducted using OriginPro software to investigate whether these observed similarities were statistically significant (Figure 7).

There was a very strong correlation between MOE$_{dFakopp}$ and MOE$_{dHitman}$ (R^2 of 0.83, and Pearson's r of 0.93). The resulting p-value from the paired t-test was 0.0144 (< 0.05), suggesting that the difference between dynamic MOE obtained using these two devices was statistically significant at $\alpha = 0.05$. However, since the difference is minimal (0.16 GPa), the devices are still interchangeable.

The stress wave velocity parallel to the grain generally ranges from 3500 to 5000 m/s for different species, including red maple (Dackermann et al. 2014; Nowak et al. 2021). Figure 8 presents the distribution of stress wave velocity for both measurement methods. The results for the Fakopp device ranged

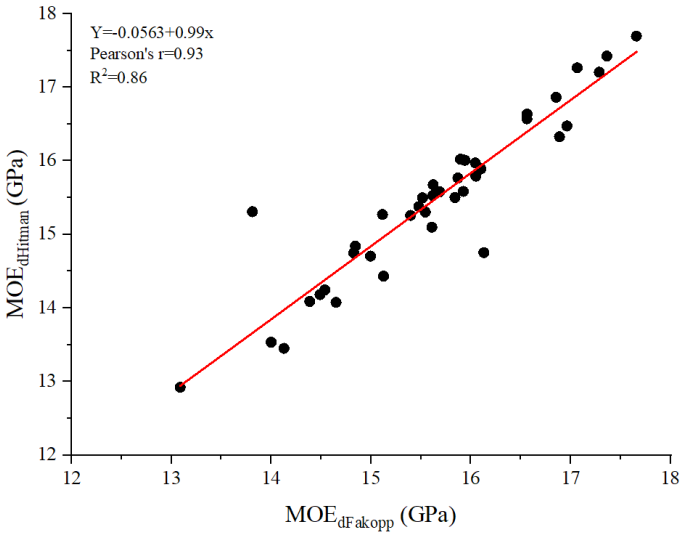

Figure 7. Relationship between MOE$_{dFakopp}$ and MOE$_{dHitman.}$

from 4400 to 5100 m/s, with an average of 4732.89 m/s (± 140.17 m/s) and a coefficient of variation of 2.96% (Figure 12a). Similarly, velocity with the Hitman device (Figure 12b) was 4708.07 m/s (± 164.05 m/s), and a coefficient of variation of 3.48%. According to the Shapiro-Wilk normality test, the results of p-values for stress wave and longitudinal were 0.87 and 0.86, respectively, suggesting a normal distribution. These findings ranged from 4300 to 5100 m/s and are consistent with previous reports by Dackermann et al. (2014).

Effect of the nondestructive evaluation of the veneers on the dynamic MOE of LVL

This section investigates the relationship between the dynamic MOE of the veneer obtained using the stress wave method

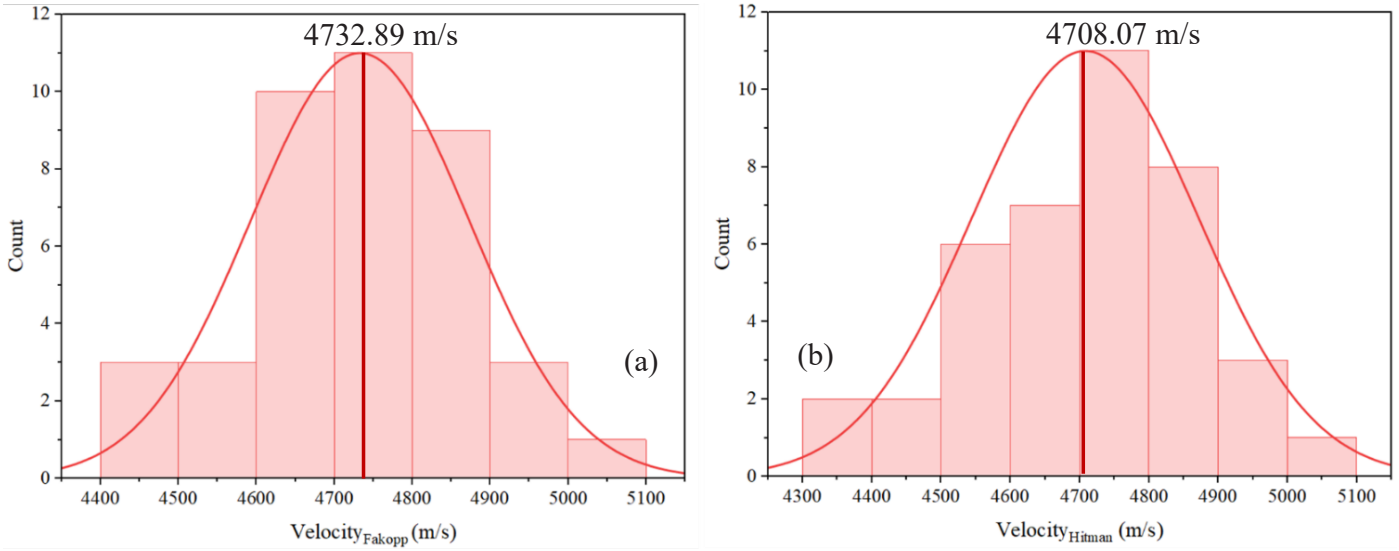

Figure 8. Distribution of the stress wave velocity: (a) V_{Fakopp}; (b) V_{Hitman} of 40 LVL billets.

with the Fakopp device and the dynamic MOE of the final LVL beams obtained through the same measurement method presented in Figure 6a. Although both measurement methods yielded comparable results, the Fakopp device was selected over the Hitman device due to its lower coefficient of variation (6.5% compared to 7%), making it a more reliable choice.

A regression analysis was then conducted using OriginPro software to assess the relationship between the dynamic MOE of LVL and the average dynamic MOE of associated veneers, as presented in Figure 9. The results showed a strong positive correlation between MOE_{dLVL} and $MOE_{dVeneer}$, with a Pearson's r of 0.85. The coefficient of determination ($R^2 = 0.73$) suggested that the MOE_d of the veneers explained 73% of the variability in MOE_{dLVL}.

Similar trends were observed in previous studies, where the stress wave properties of veneers positively influenced the properties of LVL (Del Menezzi et al. 2013). Additionally, Kunesh (1978) found a strong correlation (0.92) between longitudinal stiffness of veneer measured with a dynamic stress wave system and the tensile strength of associated LVL, as well as a high correlation ($R^2 = 0.91$) with LVL bending strength. Wang et al. (2003) found that the dynamic MOE of red maple veneer was well correlated with the bending strength of LVL billets.

Similarly, Zhou et al. (2013) found a strong correlation between MOEd of the veneers and that of the LVL ($R^2 = 0.93$).

Nondestructive testing of LVL billets and their veneers indicated that MOE of the veneers was higher than that of the LVL billets (Table 3), while the velocity of the veneers was

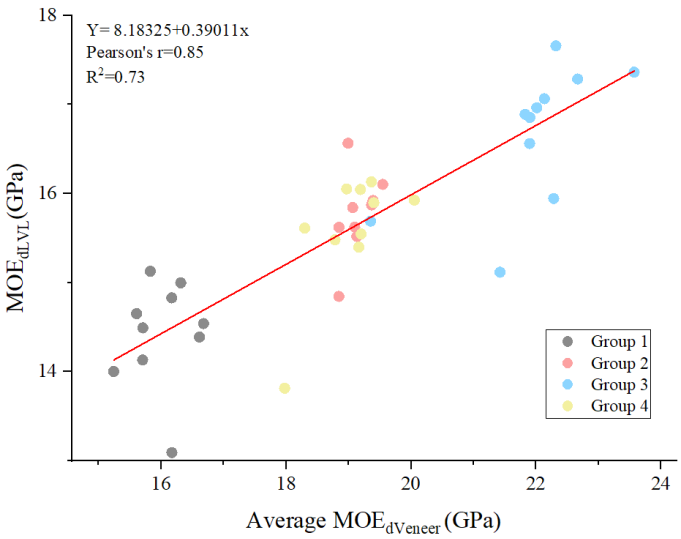

Figure 9. Relationship between MOE_{dLVL} and the average dynamic MOE of 12 associated veneers ($MOE_{dVeneer}$).

slightly greater than that of the LVL billets, even though the same Fakopp NDT method, was used for both materials. The difference could be related to the fixture used for the measurement. We used a fixture and a pendulum for veneers, while pins were used for LVL billets. The other difference could be the composite veneer/glueline composition of the LVL billet, since it is a laminated product; thus, the MOE for the LVL billets is not simply an average of the MOE of the veneers, but also includes the glueline. Conversely, the density of the LVL billets was higher than the average density of associated veneers. The results contrast with the findings of Del Menezzi et al. (2013),

Table 3. — Comparison of density, stress wave velocity, and MOE between LVL and veneers across different MOE groups.

Group	Density				Velocity				Dynamic MOE			
	Veneer		LVL		Veneer		LVL		Veneer		LVL	
	Mean[a]	COV (%)	Mean	COV (%)	Mean	COV (%)	Mean	COV (%)	Mean	COV (%)	Mean	COV (%)
1	571 (12.38)	2.17	692 (32.83)	4.74	5282 (99.37)	1.88	4565 (77.84)	1.7	16 (0.44)	2.75	14 (0.55)	3.95
2	583 (9.26)	1.59	705 (15.98)	2.26	5749 (49.46)	0.86	4728 (72.39)	1.53	19 (0.23)	1.23	15.75 (0.42)	2.66
3	594 (7.86)	2.32	697 (19.51)	4.51	6108 (75.19)	1.23	4904 (57.11)	1.16	22.19 (0.55)	2.50	16.76 (0.70)	4.22
4	584 (7.86)	1.34	695 (19.51)	2.81	5697 (87.58)	1.54	4734 (65.96)	1.39	19.03 (0.55)	2.92	15.58 (0.64)	4.12

a Values represent the means of 120 samples per group while numbers in parentheses represent one standard deviation. COV=coefficient of variation (%).

which observed that the stress wave velocity in the veneers was similar to that in the billets, while the dynamic modulus of elasticity of the billets was higher compared to the veneers.

The comparison between the veneers and LVL billets revealed consistent results across all groups. The MOE of the LVL billets in each group was 12.5% to 24.47% lower than that of the corresponding veneers, with the highest reduction occurring in Group 3.

Opposite results were observed in previous studies (Zhou et al. 2013; Del Menezzi et al. 2013), where MOE of LVL billets was higher than that of the corresponding veneers. This difference could be related to the way the stress wave was introduced into the specimen during testing. The wave in the veneers, which were tightened to a steel fixture using a bolt, was generated by releasing a pendulum that struck the fixture, while the wave for LVL billets was produced by directly hitting a steel pin embedded into the billet. Although the same testing method was used, differences in setup may have influenced wave propagation and the resulting MOE values.

Similarly, stress wave velocity was consistently lower by 13.6% to 19.7% in LVL billets than in veneers, with the higher reduction observed in Group 3. This difference may or may not be attributed to the increased thickness of LVL billets. Several studies have investigated the impact of veneer thickness on the dynamic properties of LVL. De Melo and Del Menezzi (2014) reported that veneer thickness had a significant effect only for specimens tested in the flatwise position, where panels made with thinner veneers exhibited a higher modulus of elasticity. However, Purba et al. (2019) found that the highest static MOE and MOR were associated with the LVL made from 3 mm to 4.2 mm thick veneers, and the lowest MOR was found for the LVL made of the thickest veneer. Previous studies have also found that increasing veneer thickness tends to reduce the shear strength and shear modulus of LVL, particularly when tested in the edgewise direction (Ebihara 1981; Pot et al. 2015).

On the other hand, some studies have reported opposing results, suggesting that increased veneer thickness does not necessarily lead to reduced mechanical performance of the LVL. For instance, a study conducted by Girardon et al. (2016) found that the veneer thickness and bending direction did not significantly influence the average MOE, but rather contributed to greater variability in MOE values. Similarly, Rahayu et al. (2015), examined LVL made from poplar veneers of varying thicknesses and reported that the flatwise MOE was lower than the edgewise MOE, while veneer thickness had no significant effect on the modulus of elasticity.

Therefore, while the effect of veneer thickness on MOE remains uncertain, it may not be the primary factor influencing the observed differences in the dynamic properties of veneer and LVL; other factors could also contribute to these variations. Conversely, the density of LVL billets was higher than that of veneers, as the percentage increase varied from 17.3% to 21.2%, with the highest increase occurring in Group 1. This increase can be attributed to the addition of the adhesive, which has a density of 1.12 g/cm³ (Belaidi et al. 2025a)— which is significantly higher than that of the veneers (0.58 g/cm³)—and can penetrate the porous structure of red maple veneers. In addition, the compression applied during the manufacturing process could reduce the material's volume, leading to densification. Similarly, Zhou et al. (2013) reported that the density of veneers was lower than that of the LVL boards.

When comparing the different groups, a clear trend was observed in which veneers with higher MOE_d resulted in LVL with higher MOE_d. As presented in Table 3, LVL fabricated

with Group 1 veneers, which had the lowest MOE_d (16 GPa), exhibited the lowest MOE_d (14 GPa), while those fabricated with Group 3 veneers, with the highest MOE_d (22 GPa), indicated the highest MOE_d (16 GPa). Stress wave velocity followed a similar pattern, increasing from Group 1 (5282 m/s in veneers, 4565 m/s in LVL) to Group 3 (6108 m/s in veneers, 4904 m/s in LVL). Furthermore, density results varied slightly, with Group 2 having the highest LVL density (704 Kg/m^3), while Group 4 had moderate values for both veneers and LVL.

The mixed group, in which high-grade veneers were placed on the outer layers while medium—and low-grade veneers formed the core, had a MOE_{dLVL} and $MOE_{dVeneer}$ closer to those of Group 2 (medium grade).

These findings highlight the significant effect of MOE of the veneer on LVL performance. Veneers with higher MOE resulted in LVL billets with high MOE_d, while billets fabricated with low-MOE veneers showed lower MOE_d values. A similar conclusion has been reported by Pu and Tang (1997) confirming that veneer quality directly influenced the mechanical properties of LVL billets.

A study carried out by Harding and Orange (1998), on LVL made from *Pinus radiata* found that the lay-up sequence had little to no effect on the physical and mechanical performance of the LVL. A similar conclusion was drawn by Lara Palma and Ballarin (2011) in their study on LVL made from *Eucalyptus grandis*, finding no evidence that the placement of lower-quality veneer on the surface layers affected the performance of the wood panels.

Effect of veneer density and stress wave velocity on MOE_{dLVL}

Veneer density and stress wave velocity are key factors influencing the dynamic modulus of elasticity of the LVL, which directly affects the performance and reliability of the final product. The effect of density and stress wave velocity of veneers on the MOE_{dLVL} was investigated through regression analysis, as shown in Figure 10, using OriginPro software.

Table 4 provides a detailed summary of the statistical results. The regression analysis for density of veneer showed a moderate correlation, with a Pearson's r of 0.62 and R^2 value of 0.38, indicating that density explains 38% of the variation in MOE_{dLVL}. The relationship is statistically significant, as shown by an F-value of 23.61 and a p-value of <0.0001.

In comparison, velocity shows a stronger correlation with MOE_{dLVL}, with a Pearson's r of 0.81 and an R^2 value of 0.66,

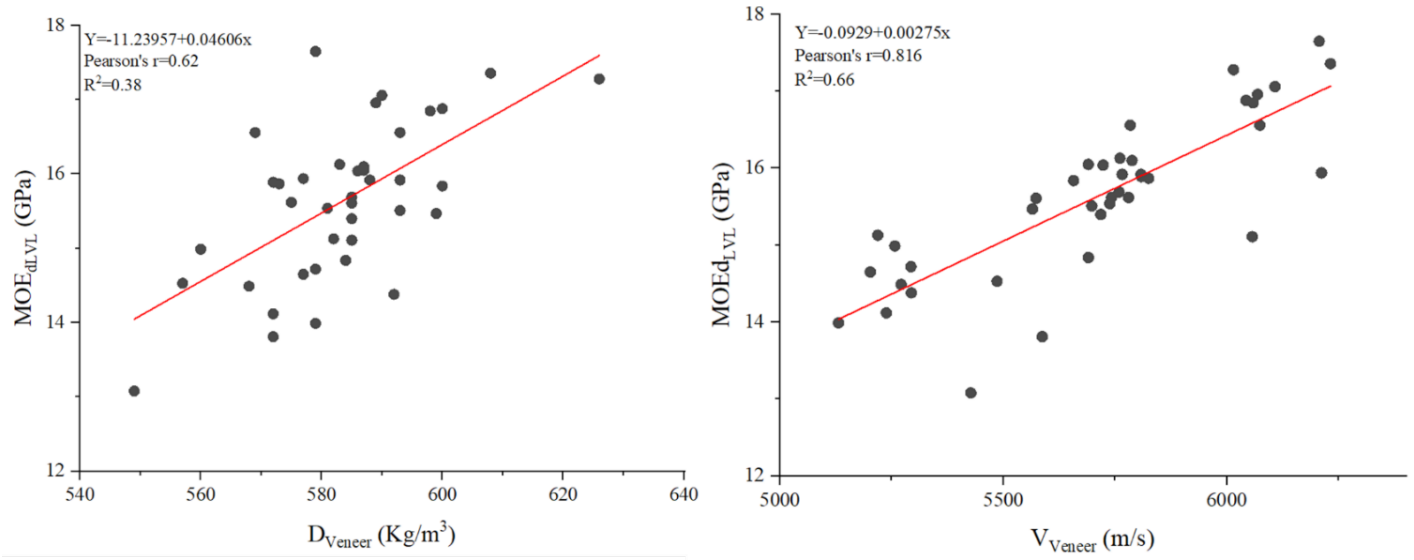

Figure 10. Relationship between density and velocity of veneers with the dynamic modulus of elasticity of LVL.

Table 4. —Regression results of velocity and density on MOE_{dLVL}

MOE_{dLVL}	Equation of regression	Pearson's r	R^2	F value	P value
Density (kg/m^3)	Y= -11.23957+0.04606x	0.62	0.38	23.61493	<0.0001*
Velocity (m/s)	Y= -0.0929+0.00275x	0.81	0.66	76.04058	<0.0001*

* Significant at ≤ 0.05

meaning that 66% of the variation in MOE_{dLVL} can be attributed to velocity. The higher F-value of 76.04 and the p-value of <0.0001 further confirm the statistical significance of this relationship. These results suggest that while both density and velocity influence MOE_{dLVL}, velocity is a more dominant predictor.

Figure 11 presents the regression analysis between the stress wave velocity (V_{LVL}) and the density of the LVL (D_{LVL}) using OriginPro software. The results revealed a very weak correlation, with a Pearson's r of -0.135 and a coefficient of determination of 0.018.

Similar findings were reported by Zhou et al. (2017), who observed a weak correlation between velocity and density of poplar veneer. This can be explained by the fact that density reflects the proportion of solid cell material present in the wood structure (Zhou et al. 2017; Machado et al. 2014). However, several studies (Lasserre et al. 2009; Hernández 2007; Zhou et al. 2017; Hasegawa et al. 2011) have highlighted that wave velocity can be influenced by other factors, including microfibril angle, grain angle, and fiber length, which affect the propagation of the stress wave. Furthermore, Machado et al. (2014) reported that this weak correlation highly depends on the species.

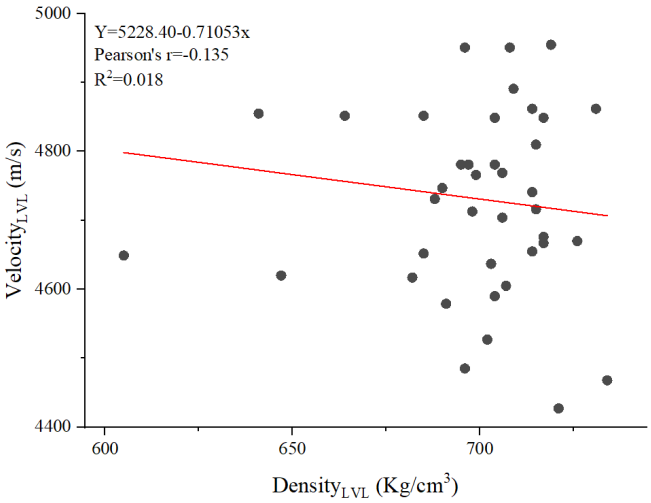

Figure 11. Relationship between density and velocity of the LVL.

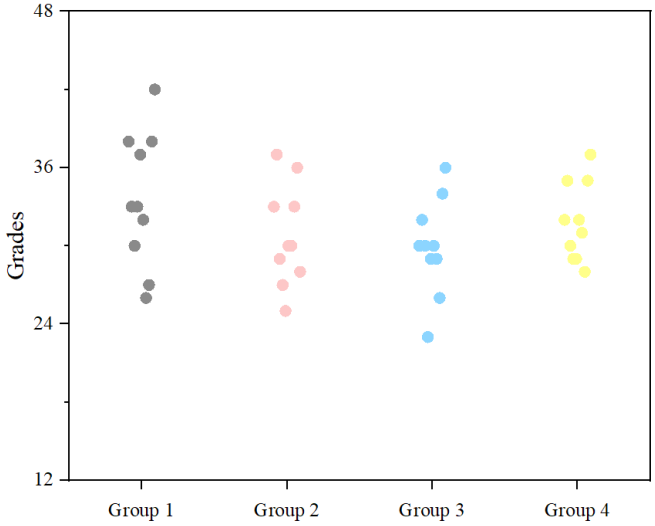

Figure 12. Distribution of LVL billet grading value based on veneer composition.

Effect of the Veneer visual grade on the mechanical properties of LVL

Based on the visual grading of veneers, a grading score was assigned to each 12-layer LVL billet. The distribution of LVL billet grading score for the four groups is presented in Figure 12. The grading scores ranged from 24 to 36, indicating that most billets were composed of mid-range veneer grades (B and C), with fewer high-quality grade A veneers or low-quality grade D veneers. The variability observed within each group may be attributed to the random arrangement of veneers during the manufacturing process of LVL billets, leading to differences in the final grading scores.

It was expected that LVL billets made with Group 3 veneers, which had the highest MOE_d, would achieve higher grading scores, while those fabricated with Group 1 veneers would exhibit the lowest grading scores due to their use of veneers with the lowest MOE_d. The grading numbers for LVL billets made with Group 2 and Group 4 veneers were expected to fall between those of groups 1 and 3. However, the actual distribution of grading numbers suggests that most LVL billets fell within the medium range, from 24 to 36.

While the grading score provides an overview of the veneer quality composition in the LVL billets, it was also important to examine the effect of LVL grade number on the mechanical properties of the final product. A regression analysis was conducted between the LVL grade number and its associated dynamic modulus of elasticity, using OriginPro software, as shown in Figure 13.

The regression analysis showed a weak correlation between the two parameters, with a Pearson's r of -0.268 and a coefficient of determination of 0.07, suggesting that only 7% of the variation of the MOE_{dLVL} can be explained by the presence of defects, indicating that the grading alone does not strongly predict the MOE_{dLVL}.

The presence of the weak correlation was unexpected, as higher-grade veneers were assumed to enhance the mechanical properties of the LVL billets. This suggests that other factors, such as veneer orientation, adhesive type, and natural variabil-

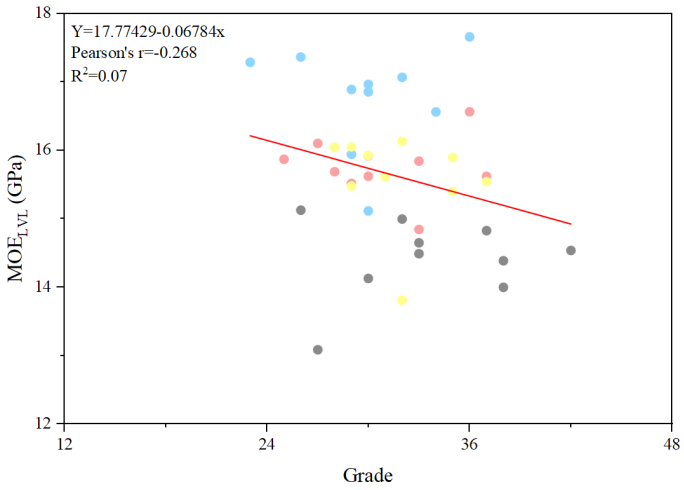

Figure 13. Relationship between LVL grading score and its associated MOE_{dLVL}.

ity in wood properties, may have influenced the mechanical performance of the LVL billets.

According to Bucur (2006), in addition to the natural imperfections, cracks and fiber deviation can also affect the stiffness of wood material (Bucur 2006). Similarly, studies by Kollmann (1951) and Eberhardsteiner (1995) have shown that fiber and microfibril angles also play a critical role in determining the stiffness and strength of wood.

Conclusion

The study investigates the relationship between the mechanical properties of individual veneers and the overall structural performance of LVL billets using two nondestructive evaluation tools—the Fakopp Microsecond Timer and the Hitman HM200. The veneers were classified by dynamic MOE into low, medium, high, and mixed groups.

The key findings are summarized as follows:

1. A strong correlation was found between MOE of veneers (MOE_{dLVL}) and the resulting LVL billets ($MOE_{dVeneer}$), with a correlation coefficient (r) of 0.85 and an R^2 value of 0.73. This indicates that veneer properties significantly influence LVL performance.

2. MOE values obtained from the Fakopp and the Hitman HM200 devices showed a strong correlation ($r = 0.93$, $R^2 = 0.86$), confirming the reliability and consistency of both measurement approaches.

3. The LVL billets exhibited a noticeable reduction in MOE compared to their source veneers, ranging from 12.5% to 24.47%, with the greatest reduction observed in high-grade veneer group.

4. Within each group, higher veneer MOE corresponded to higher LVL MOE, indicating that higher-quality veneers resulted in stronger LVL billets. Conversely, lower-quality veneers resulted in weaker LVL billets.

5. The mixed group, where high-grade veneers were placed on the outer layers and medium- and low-grade veneers formed the core, produced MOE values (19 GPa for veneer, 15.58 GPa for LVL) comparable to the medium-grade group (19 GPa for veneer, 15.75 GPa for LV), suggesting an efficient use of mixed-quality veneers.

6. A weak correlation was observed between the grading score and the dynamic modulus of elasticity of the LVL ($r = -0.26$, $R^2 = 0.07$), indicating that grading score alone is not a reliable predictor of LVL stiffness.

The findings of this study provide practical insights into veneer selection and layup strategies to enhance LVL performance and improve wood utilization efficiency.

Acknowledgments

The authors acknowledge the support from the USDA Forest Service Forest Products Laboratory in Madison, Wisconsin as a major contributor of technical assistance, advice, and guidance to this research. In accordance with Federal law and U.S. Department of Agriculture policy, this institution is prohibited from discriminating on the basis of race, color, national origin, sex, age or disability. (Not all prohibited bases apply to all programs.) To file a complaint of discrimination: write USDA, Director, Office of Civil Rights, Room 326-W, Whitten Building, 1400 Independence Avenue, SW, Washington, D.C. 20250 9410 or call (202) 720-5964 (voice and TDD). USDA is an equal opportunity provider and employer. The authors also acknowledge the support from Great Lake Veneer and Henkel for supplying wood veneers and adhesive. This publication article is a contribution of the Forest and Wildlife Research Center at Mississippi State University.

References

Arriaga F, Wang X, Íñiguez-González G, Llana DF, Esteban M, Niemz P (2023) Mechanical Properties of Wood: A Review. Forests 14(6):1202. https://doi.org/10.3390/f14061202

Belaidi D, Lamichhane A, Pradhan S, Mohammadabadi M, Shmulsky R, Wang X (2025a) Effect of adhesives on bonding performance of softwood and hardwood plywood. Forest Prod J 75(1):16–25, p. 17. https://doi.org/10.13073/FPJ-D-24-00044

Belaidi D, Mohammadabadi M, França F, Shmulsky R, Wang X, Seale RD (2025b) Destructive and nondestructive e-rating of red maple veneers. Forest Prod J 75(2):195–205. https://www.doi.org/10.13073/FPJ-D-25-00015

Bucur, V (2006) Acoustics of Wood. 2nd ed. Springer, Berlin.

Cavalli A, Togni M (2013) How to improve the on-site MOE assessment of old

timber beams combining NDT and visual strength grading. Nondestruct Test Eval 28(3):252–262. https://doi.org/10.1080/10589759.2013.764424

Chen Y, Guo W (2016) Mechanical properties evaluation of two wood species of ancient timber structure with nondestructive testing methods. BioRes 11(3):6600–6612.

Dackermann U, Crews K, Kasal B, Li J, Riggio M, Rinn F, Tannert T (2014) In situ assessment of structural timber using stress-wave measurements. Mater Struct [Materiaux et Constructions] 47(5):787–803. https://doi.org/10.1617/s11527-013-0095-4

De Melo RR, Del Menezzi CHS (2014) Influence of veneer thickness on the properties of LVL from Paricá (*Schizolobium amazonicum*) plantation trees. Eur J Wood Wood Prod *72*(2):191–198. https://doi.org/10.1007/s00107-013-0770-8

Del Menezzi C, Mendes L, de Souza M, Bortoletto G (2013) Effect of nondestructive evaluation of veneers on the properties of laminated veneer lumber (LVL) from a tropical species. Forests 4(2):270–278. https://doi.org/10.3390/f4020270

Divós F, Tanaka T (2005) Relation between static and dynamic modulus of elasticity of wood. Acta Silv Lign Hung 1:105-110. https://doi.org/10.37045/aslh-2005-0009

Divos F, Tanaka T (1997). Lumber strength estimation by multiple regression. Holzforschung 51(5):467–471. https://doi.org/10.1515/hfsg.1997.51.5.467

Eberhardsteiner J (1995). Biaxial testing of orthotropic materials using electronic speckle pattern interferometry. Measurement 16(3):139–148. https://doi.org/10.1016/0263-2241(95)00019-4.

Ebihara T (1981) Shear properties of laminated-veneer lumber (LVL) [in Japanese]. J Jpn Wood Res Soc [Mokuzai Gakkaishi] 27(11):788–794.

Gao Z, Gong M (2021) Strand-based engineered wood products in construction. In: Engineered Wood Products for Construction. IntechOpen. https://dx.doi.org/10.5772/intechopen.100324.

Gong M (2019) Lumber-based mass timber products in construction. In: Concu G, ed. Timber Buildings and Sustainability. Rijeka: IntechOpen; 2019. pp. 7-16. DOI: 10.5772/ intechopen.85808

Girardon S, Denaud L, Pot G, Rahayu I (2016) Modelling the effects of wood cambial age on the effective modulus of elasticity of poplar laminated veneer lumber. Ann For Sci 73(3):615–624. https://doi.org/10.1007/s13595-016-0569-y

Hasegawa M, Takata M, Matsumura J, Oda K (2011) Effect of wood properties on within-tree variation in ultrasonic wave velocity in softwood. Ultrasonics 51(3):296–302. https://doi.org/10.1016/j.ultras.2010.10.001

Harding OV, Orange RP (1998) The effect of juvenile wood and layup practices on various properties of radiata pine laminated veneer lumber. Forest Prod J 48(7/8):63–70

Hernández RE (2007) Influence of accessory substances, wood density and interlocked grain on the compressive properties of hardwoods. Wood Sci Technol 41(3):249–265. https://doi.org/10.1007/s00226-006-0114-5

Kimmel JD, Janowiak JJ (1995) Red maple and yellow-poplar LVL from ultrasonically graded veneer. Forest Prod J 45(7/8):54–58.

Kollmann F (1951) Technologie des Holzes und der Holzwerkstoffe [Technology of Wood and Wood-based Materials], Springer, New York.

Kloiber M, Reinprecht L, Hrivnák J, Tippner J (2016) Comparative evaluation of acoustic techniques for detection of damages in historical wood. J Cult Herit 20(July-Aug):622–631. https://doi.org/10.1016/j.culher.2016.02.009

Kunesh RH (1978) Using ultrasonic energy to grade veneer. Pp 275–278 in Proc 4th Symp on NondestructiveTesting of Wood, August 28–30, 1978, Vancouver, WA. Washington State University, Pullman, WA

Lamichhane A, Pradhan S, Belaidi D, Mohammadabadi M (2025) Engineered wood cellular beams: Influence of corrugated panels layout on structural performance. Structures 73(March):108460. https://doi.org/10.1016/j.istruc.2025.108460Lasserre JP, Mason EG, Watt MS, Moore JR (2009) Influence of initial planting spacing and genotype on microfibril angle, wood density, fibre properties and modulus of elasticity in *Pinus radiata* D. Don corewood. For Ecol Manag 258(9):1924–1931. https://doi.org/10.1016/j.foreco.2009.07.028

Lara Palma HA, Ballarin AW (2011) Physical and mechanical properties of LVL panels made from *Eucalyptus grandis* (in Portuguese). Ci Flo 21(3):559–566. https://doi.org/10.5902/198050983813

Liu Z, Liu Y, Yu H, Yuan J (2006) Measurement of the dynamic modulus of elasticity of wood panels. Front For China 1(4):425–430. https://doi.org/10.1007/s11461-006-0048-y

Machado JS, Louzada JL, Santos AJA, Nunes L, Anjos O, Rodrigues J, Simões RMS, Pereira H (2014) Variation of wood density and mechanical properties of blackwood (*Acacia melanoxylon* R. Br.). Mater Des 56 (April):975–980. https://doi.org/10.1016/j.matdes.2013.12.016

McGavin RL, Leggate W (2019) Comparison of processing methods for small-diameter logs: Sawing versus rotary peeling. BioRes 14 (1):1545–1536. https://doi.org/10.15376/BIORES.14.1.1545-1563

Miclea C, Tanasoiu V, Miclea C, Tanasoiu C (2002) Nondestructive testing techniques and piezoelectric ultrasonics transducers for wood and built in wooden structures. JOAM 4(4). https://www.researchgate.net/publication/253713113

Németh R, Rademacher P, Hansmann C, Bak M, Báder M (2021) 9th Hardwood Proceedings − Part II. With Special Focus On "An Underutilized Resource: Hardwood Oriented Research." 2021 Hardwood Conference Proceedings, 9.

Nowak T, Patalas F, Karolak A (2021) Estimating mechanical properties of wood in existing structures—selected aspects. *Materials*, *14*(8). https://doi.org/10.3390/ma14081941

Pajchrowski G, Noskowiak A, Lewandowska A, Strykowski W (2014) Wood as a building material in the light of environmental assessment of full life cycle of four buildings. Constr Build Mater 52, 428–436. https://doi.org/10.1016/j.conbuildmat.2013.11.066

Pot G, Denaud L-E, Collet R (2015) Numerical study of the influence of veneer lathe checks on the elastic mechanical properties of laminated veneer lumber (LVL) made of beech. Holzforschung 69:337–345. https://doi.org/10.1515/hf-2014-0011

Pradhan S, Lamichhane A, Belaidi D, Mohammadabadi M (2024) The effect of different densification levels on the mechanical properties of southern yellow pine. Sustainability (Switzerland), 16(15). https://doi.org/10.3390/su16156662

Pu J, Tang CR (1997) Nondestructive evaluation of modulus of elasticity of southern pine LVL: effect of veneer grade and relative humidity. Wood Fib Sci 29(3):249–263.

Purba CYC, Pot G, Viguier J, Ruelle J, Denaud L (2019) The influence of veneer thickness and knot proportion on the mechanical properties of laminated veneer lumber (LVL) made from secondary quality hardwood. Eur J Wood Wood Prod 77(3), 393–404. https://doi.org/10.1007/s00107-019-01400-3

Rahayu I, Denaud L, Marchal R, Darmawan W (2015) Ten new poplar cultivars provide laminated veneer lumber for structural application. Ann For Sci 72(6):705–715. https://doi.org/10.1007/s13595-014-0422-0

Redman A (2020) *International Hardwood Veneer Grading Rules*. Burapha Agro-Forestry. https://www.buraphawood.com/application/files/5515/8866/5232/20200421_International_hardwood_veeer_grading_comparison.pdf

Ross RJ (2015) Nondestructive evaluation of wood: Second edition.

Ross RJ, Erickson JR, Brashaw BK, Wang X, Verhey SA, Forsman JW, Pilon CL (2004) Yield and ultrasonic modulus of elasticity of red maple veneer. Forest Prod J 54(12):220–225.

Teles RF, Del Menezzi C, Souza M, Souza F (2010) Effect of nondestructive testing of laminations on the bending properties of glulam beams made from louro-vermelho (*Sextonia rubra*) Cerne, Lavras 16(1/Mar):77–85. https://doi.org/10.1590/S0104-77602010000100009

Turkot CG, Seale RD, Entsminger ED, França FJN, Shmulsky R (2020). Nondestructive evaluation of red oak and white oak species. Forest Prod

J 70(3:370–377. https://doi.org/10.13073/FPJ-D-20-00015

USDA Forest Service, Forest Products Laboratory, General Technical Report, FPL-GTR-238, 2015; 176 p. https://doi.org/10.2737/FPL-GTR-238

Vössing KJ, Niederleithinger E (2018) Nondestructive assessment and imaging methods for internal inspection of timber. A review. Holzforschung 72(6):467–476). https://doi.org/10.1515/hf-2017-0122

Wang X, Ross RJ, Brashaw BK, Verhey SA, Forsman JW, Erickson JR (2003). Flexural properties of laminated veneer lumber manufactured from ultrasonically rated red maple veneer: A pilot study. Res. Note FPL-RN-0288. Madison, WI: USDA Forest Service, Forest Products Laboratory. 5 p. https://www.fpl.fs.usda.gov/documnts/fplrn/fplrn288.pdf.

Wang X, Ross RJ, Green DW, Brashaw B, Englund K, Wolcott M (2004) Stress wave sorting of red maple logs for structural quality. Wood Sci Technol 37:531–537. https://doi.org/10.1007/s00226-003-0202-8

Winchester N, Reilly JM (2020) The economic and emissions benefits of engineered wood products in a low-carbon future. Energy Econ 85:104596. https://doi.org/10.1016/j.eneco.2019.104596)

Xue B, Hu Y (2013) Analysis of the microstructure and mechanical properties of laminated veneer lumber. BioRes 8(2):2681–2695. https://bioresources.cnr.ncsu.edu/resources/analysis-of-the-microstructure-and-mechanical-properties-of-laminated-veneer-lumber/

Zhou Z-R, Zhao M-C, Gong M, Wang Z (2017) Variation of density and dynamic modulus of elasticity of poplar veneer and its impact on grade yield. BioRes 12(1):1344–1357. https://bioresources.cnr.ncsu.edu/resources/variation-of-density-and-dynamic-modulus-of-elasticity-of-poplar-veneer-and-its-impact-on-grade-yield/

Zhou Z-R, Zhao M-C, Wang Z, Wang BJ, Guan X (2013) Acoustic testing and sorting of Chinese poplar logs for structural LVL products. BioRes 8(3):4101–4116. https://bioresources.cnr.ncsu.edu/resources/acoustic-testing-and-sorting-of-chinese-poplar-logs-for-structural-lvl-products/

Particle board production using paper mill waste sludge and European black pine (*Pinus nigra* A.) wood chips

Selim Karahan *
Gumushane University
Kurtun Vocational School, Forestry Department
Gumushane, Türkiye
Email: selimkarahan@msn.com

Muharrem Tekel
Gumushane University
Kurtun Vocational School, Forestry Department
Gumushane, Türkiye
Email: muharrem.tekel@hotmail.com

(Received 27 February 2025)

Abstract. Paper mills use excessive amounts of water throughout production to produce paper. While mills treat water for reuse, sludge is generated and must be processed as a waste, along with some washing water. In this study, waste sludge from a kraft process mill mixed with up to 40% black pine (*Pinus nigra*) wood chips was investigated for multi-purpose board production using urea formaldehyde resin and ammonium chloride as a hardener. The panels were pressed at 150°C for 7 minutes between 2.4 MPa and 2.6 MPa. The resulting panels were 18 mm thick, with a density of from 0.69 gr/cm^3 to 0.71 g/cm^3. Measurements of density, moisture, water absorption, thickness swelling, modulus of rupture, modulus of elasticity and internal bond strength to the surface were carried out on the particle board panels. The results indicated that panels could be used for general purposes.

Keywords: Paper mill; Waste sludge; Particle board; Physical properties; Mechanical properties

Introduction

Shortages of wood fiber in some regions have encouraged the use of waste products for panel production (Lee et al. 2022). The increasing need for raw materials in the panel production sector has encouraged exploration of other cellulosic resources including agricultural residues and coconut fiber (Table 1). However, these materials may be less compatible than forest-derived residues. One possible alternative fiber source originates from the pulp and paper industry. The pulping process produces a sizable volume of fibers that are unsuitable for paper production (Naik et al. 2004).

These fibers are often burned in the pulp liquor regeneration process, but they might also be used to supplement fiber supplies for panel production. However, this sludge also contains inorganic substances that may be incompatible with composite production.

The objective of this study was to evaluate the potential for using waste sludge from the pulp and paper industry as a partial substitute for wood chips in particleboards.

Materials and methods

Waste sludge from kraft paper mill wastewater was provided by Kahramanmaraş Paper Industry and Trade Inc. (KMK Paper, Kahramanmaraş, Türkiye). The mill processed mixed softwood species. The sludge was dried at 70°C and then broken into pieces and pulverized. Black pine (*Pinus nigra* A.) sawdust was dried at 70°C to between 1% and 2% moisture content then mixed with the sludge at five different ratios (Table 2).

Panels were produced with three layers. The 0.8–1.5 mm thick outer layers were composed entirely of black pine sawdust with 10%–11% urea formaldehyde resin (Table 3). The core consisted of the black pine/pulp sludge mixture along with 8%–9% resin (m/m). The resin contained 55% solids urea formaldehyde and 33% ammonium chloride.

The 40 by 40 cm panels were formed and then cold pressed before being hot pressed for 6 to 7 minutes at 150°C and at 2.4 MPa to 2.6 MPa to a target thickness of 18 mm. The den-

* Corresponding author

Table 1. The alternative plant sources used by some researchers for particleboard production.

Alternative sources	Researchers
Corn stalk, cotton stalk, pepper stalk, wheat stalk, sunflower stalk	Guler and Ozen (2004); Bektas et al. (2005); Alma et al. (2005); Guler et al. (2006); Oh and Yoo (2011); Bektas et al. (2020)
Peanut, hazelnut husk, peanut shell, yellow pine	Guler et al. (2009); Mankowski and Laskowska (2021)
Sugarcane, hemp grass, flax, hemp, kenaf	Jianying et al. (2003); Kalaycıoğlu and Nemli (2006)
Licorice root, rice pad	Guler (2015)
Coconut skin and fiber	Khedari et al. (2003); Khedari et al. (2004)
Needle leaves, pine cones	Nemli and Aydın (2007); Buyuksari et al. (2010)
Kiwi pruning waste, grass waste, tea waste, vine waste	Nemli et al. (2003); Nemli et al. (2009)

sity of the resulting panels ranged from 0.69 g/cm^3 to 0.71 g/cm^3. Ten panels were fabricated for each wood/sludge ratio. The panels were conditioned for 3 weeks at 20°C and 65% relative humidity, in accordance with Turkish Standard (TSE) TS 642 ISO 554 (1997). The conditioned panels were cut into samples for evaluating thickness swelling, water absorption, flexural properties, and internal bond strength, according to EN 326-1:1999 (TSE - TS EN 326-1 1999), Wood-based panels- Sampling, cutting and inspection - Part 1: Sampling test pieces and expression of test results (CEN, Ankara) (Table 4).

Moisture content of the panels was determined using European Standard (EN) 322 (TSE - TS EN 322 1999). Briefly, samples were weighed, oven dried at 104°C and weighed. Density was determined by measuring panel dimensions and weighing each sample according to Standard EN 323 (TSE - TS EN 323 1999).

Flexural properties were determined according to EN 310 (TSE - TS EN 310 1999). Load was applied at a constant rate throughout the experiment, and the loading head speed was adjusted to reach the maximum force (in 60±30) seconds. Load and deflection were continuously monitored, and the resulting load/deflection curve was used to calculate modulus of elasticity (MOE) and modulus of rupture (MOR).

Thickness swelling and water absorption were determined by weighing and measuring the thickness of samples prior to immersion in distilled water. Sample mass and thickness were measured after 2 and 24 hours of immersion.

Internal bond strength was measured according to Standard EN 319 (TSE - TS EN 319 1999). Samples were glued to aluminum blocks, allowed to cure, and then pulled apart. The load required to fail the specimens was defined as the shear capacity.

The data were averaged and then subjected to an analysis of variance. Differences between means were subjected to a Duncan's mean separation test ($\alpha = 0.05$).

Table 2. Proportions of waste sludge and black pine chips used to fabricate panels.

Board type	Waste sludge (%)	Black pine chips (%)
A	0	100
B	10	90
C	20	80
D	30	70
E	40	60

The densities of the boards obtained with waste sludge and European black pine wood chips were 0.69 g/cm^3–0.71 g/cm^3.

Table 3. Properties of the urea formaldehyde resin used to fabricate the panels.

Property	UF
Solids (%)	55±1
Density (g/cm^3)	1.20
pH	8.5
Viscosity (cps)	160
Ratio of water tolerance	10/27
Reactivity	35
Free formaldehyde (%)	0.15
33% NH_4CI content (max, %)	1
Gel point (100°C)	25–30
Storage time (25°C, max day)	90
Flowing point (25°C)	20–40

Table 4. Dimensions and number of replicates per treatment used to assess panel properties.

Test	Dimensions (mm)	Replicates/ Treatment	Test standard
Thickness swelling	18	10	TSE - TS EN 317 (1999)
Density	18	10	TSE - TS EN 323 (1999)
Water absorption	18	10	TSE - TS EN 317 (1999)
Flexural properties	18	10	TSE - TS EN 310 (1999)
Internal bond	18	10	TSE - TS EN 319 (1999)

Results and discussion

Thickness swelling after 2 hours of immersion was lowest in the all-wood panel and steadily increased with increasing pulp sludge content (Table 5). The presence of any sludge produced a significant increase in thickness swelling, with the largest swelling in the 40%/60% sludge/wood panels. Panel thicknesses continued to increase with the additional 22 hours of soaking, but the trends were the same. Standard EN 317 (TSE - TS EN 317 1999) limits swelling to 14% after 24 hours of immersion, meaning that none of the panels met this standard, including the all-wood one.

Water absorption followed trends that were similar to those for swelling, with steadily increasing absorption with increased sludge content. Once again, absorption increased significantly with increased sludge content. The results suggest that any sludge reduces panel properties. This problem might be overcome by adding more resin to the furnish.

Kalaycıoğlu (1992) determined that water intake of panels composed of tobacco stem and tea factory waste was 60%–71% after 24 h, and thickness increased 22%–37%. Filiz et al. (2011) determined that the low-density particle boards produced from tea plant wastes swelled between 17% and 34.8%, while Sevinçli (2014) reported that swelling of medium density boards composed of lavender plant and red pine chips was between 34.36% and 76.98%.

The addition of pulp sludge also negatively affected flexural properties, with significant losses in both MOR and MOE with increasing pulp content (Table 6). There was a 16% loss in MOR when 10% sludge was substituted and a nearly 60% loss in MOR when 40% sludge was substituted. EN 310 (TSE - TS EN 310 1999) specifies a minimum MOR of 10 MPa for 13 to 20 mm thick boards and 11 MPa for interior equipment such as furniture, meaning that only 10% sludge could be added without reducing this property below acceptable levels. Similarly, MOE significantly declined by 14.8% with 10% sludge and 60.9% when 40% sludge was substituted. EN 310 (TSE - TS EN 310 1999) specifies a minimum MOE of 2300 MPa in dry conditions and 1950 MPa in humid environments for 13 to 20 mm thick panels. Once again, addition of 10%

Table 5. Effect of increasing sludge content on thickness swelling and water absorption of particleboards subjected to EN 317 (TSE - TS EN 317 1999).*

Immersion time (Hr)	Sludge/Wood (%)	Thickness swelling (%)		Water absorption (%)	
		Mean	Range	Mean	Range
2	0/100	8.98 (1.07) [a]	8.18-9.77	9.88 (1.18)[a]	9.00-10.75
2	10/90	12.06 (1.36)[b]	11.26-12.86	13.27 (1.50)[b]	12.39-14.14
2	20/80	12.28 (1.03)[b]	11.48-13.07	13.51 (1.13)[b]	12.63-14.38
2	30/70	14.46 (1.35)[c]	13.66-15.25	15.90 (1.49)[d]	15.02-16.77
2	40/60	16.16 (1.37)[d]	15.36-16.95	17.77 (1.51)[e]	16.89-18.65
24	0/100	38.10 (5.76)[e]	34.53-41.67	41.92 (6.33)[f]	37.99-45.84
24	10/90	52.19 (4.90)[f]	48.62-55.75	57.41 (5.39)[g]	53.48-61.33
24	20/80	60.11 (6.19)[g]	56.42-63.67	66.12 (6.81)[h]	62.19-70.04
24	30/70	61.46 (3.90)[g]	57.89-65.68	67.68 (4.29)[h]	63.68-71.53
24	40/60	67.40 (6.79)[h]	63.83-70.97	74.14 (7.48)[i]	70.21-78.07

* Values represent means of 10 replicates per sludge/wood ratio, while figures in parentheses represent one standard deviation. Values followed by the same letter do not differ significantly by Duncan's Least Significant Difference Test ($\alpha = 0.05$).

Table 6. Effect of increasing sludge content on flexural properties (MOR, MOE) and internal bond (IB) of particleboards subjected to EN 310 (TSE - TS EN 310 1999) and EN 319 (TSE - TS EN 319 1999).*

Sludge/Wood (%)	Modulus of Rupture (MPa)		Modulus of Elasticity (MPa)		Internal Bond Strength (MPa)	
	Mean	Range	Mean	Range	Mean	Range
0/100	13.34 (1.59)[d]	11.67-15.01	2743.1 (292.1)[d]	2364-3071	0.4335 (0.0482)[e]	0.37-0.48
10/90	11.22 (0.83)[c]	10.35-12.09	2336.7 (105.8)[c]	2211-2497	0.3627 (0.0476)[d]	0.30-0.43
20/80	7.63 (1.09)[b]	6.48-8.78	1753.6 (155.9)[b]	1506-1980	0.2897 (0.0531)[c]	0.24-0.36
30/70	6.62 (0.67)[ab]	5.91-7.33	1688.9 (305.9)[b]	1199-1992	0.2295 (0.0424)[b]	0.20-0.29
40/60	5.50 (0.82)[a]	4.63-6.36	1073.3 (209.9)[a]	810-3071	0.1940 (0.0595)[a]	0.13-0.28

* Values represent means of six replicates per sludge/wood ratio, while figures in parentheses represent one standard deviation. Values followed by the same letter do not differ significantly by Duncan's Least Significant Difference Test ($\alpha = 0.05$).

sludge resulted in an acceptable panel, while further increases produced unacceptable losses in MOE.

Internal bond (IB) followed similar trends, with significant losses in properties with increasing sludge content. The standard (TSE - TS EN 319 1999) calls for IBs of 0.36 MPa and 0.29 Mpa (Table 6).

Kalaycıoğlu (1992) determined that the MOR values of tobacco stalk and tea factory waste panels were between 12.68 MPa and 16.87 Mpa, while IB values were between 0.360 MPa and 0.438 MPa. Aras et al. (2014) found an MOE of 970 MPa in boards produced from 100% pine nut cones with a density of 0.70 g/cm^3.

The minimum IB on the surface is 0.24 MPa for 13 mm and 20 mm general purpose particle boards used in dry conditions, while this value increases to 0.35 MPa for panels used in interior equipment (including furniture) or other load bearing panels in dry conditions. In this case, the addition of 20% sludge still resulted in panels that met some of the requirements for some applications, but further sludge addition resulted in significant declines in IB that would make the panels unacceptable for most uses.

Conclusions

The addition of 10% pulp sludge to the core of black pine particleboard resulted in panels that still met the requirements for thickness swelling/water absorption, flexural properties, and IB, but further sludge content significantly reduced most properties below acceptable levels. The results suggest that pulp sludge could be used as an extender at low concentration. However, the effect of sludge addition on other panel properties needs to be evaluated, including odors and resistance to biodeterioration.

Authorship contributions

SK: Conceptualization, Data curation, Formal Analysis, Methodology, Project administration, Software, Supervision, Validation, Visualization, Writing – original draft, Writing – review & editing. MT: Investigation, resources and Funding acquisition.

References

Alma MH, Kalaycıoğlu H, Bektaş I, Tutus A (2005) Properties of cotton carpel-based particle boards. Ind Crops Prod 22(2):41–149. https://doi.org/10.1016/j.indcrop.2004.08.001

Aras U, Kalaycıoğlu H, Yel H (2014) Some of the Particleboards Produced from Pistachio Pine Cones Properties, 3rd International Symposium on Non-Wood Forest Products, 8–10 May 2014, Kahramanmaras. https://www.researchgate.net/publication

Bektas I, Tutus A, Ugur C (2020) Investigation of the conformity of some mechanical properties of particle boards produced from cotton stalks to standards. Turk J For 21(4):445–450 (in Turkish). https://doi.org/10.18182/tjf.741237

Bektas I, Guler C, Kalaycıoğlu H, Mengeloglu F, Nacar M (2005) The manufacture of particleboards using sunflower stalks (*Helianthus annuus* L.) and poplar wood (*Populus alba* L.). J Compos Mater 39(5):467–473. https://doi.org/10.1177/0021998305047098

Buyuksari U, Ayrilmis N, Avci E, Koc E (2010) Evaluation of the physical, mechanical properties and formaldehyde emission of particleboard manufactured from waste stone pine (*Pinus pinea* L.) cones. Bioresour Technol 101(1): 255–259. https://doi.org/10.1016/j.biortech.2009.08.038

Filiz M, Usta P, Turgut Sahin H (2011) Evaluation of some technical properties of particle board obtained from melamine, urea formaldehyde glue, red pine and tea wastes. Suleyman Demirel University J. Sci. Inst. 15(2): 88–93. https://search.trdizin.gov.tr/dergi

Guler C, Ozen R (2004) Some properties of particleboards made from cotton stalks (*Gossypium hirsitum* L.). Holz Roh Werkst 62(1):40–43. https://doi.org/10.1007/s00107-003-0439-9

Guler C, Bektas I, Kalaycıoğlu H (2006) The experimental particleboard manufacture from sunflower stalks (*Helianthus annuus* L.) and calabrian pine (*Pinus brutia* T.). Forest Prod J 56(4):56–60 (in Turkish). https://www.researchgate.net/publication/290846093_Manufacturing_of_particleboard_from_sunflower_stalks_Helianthus_annuus_L_using_urea-formaldehyde_resin

Guler C, Copur Y, Buyuksari U (2009) Producıng particleboards from hazelnut (*Coryllus avellana* L.) husk and European black pine (*Pinus nigra* A.). Wood Res 54 (1):125–132. http://www.woodresearch.sk/wr/200901/12.pdf

Guler C (2015) Production of particleboards from licorice *Glycyrrhiza glabra* and European black pine (*Pinus nigra* A.) wood particles. Sci Res Essay 10(7):273–278 (in Turkish). https://doi.org/10.5897/SRE2015.6193

Jianying X, Guenping H, Wong ED, Kawai S (2003) Development of binderless particleboard from kenaf core using steam injection pressing. J Wood Sci 49(4): 327–332. https://doi.org/10.1007/s10086-002-0485-7

Kalaycıoğlu H (1992) Evaluation of Vegetable Wastes in Particle Board Industry, ORENKO'92 National Forest Products Industry Congress, Proceedings, Volume I: 288–292, 22–25 September 1992, Trabzon, Türkiye. https://avesis.ktu.edu.tr/yayin/661c5cb6-7dcf-4795-ad04-51dfbd7451a6/bitkisel-atiklarin-yongalevha-endustrisinde-degerlendirilmesi-orenko-92-ulusal-orman-urunleri-endustrisi-kongresi, Turkish

Kalaycıoğlu H, Nemli G (2006) Producing composite particleboard from kenaf (*Hibiscus cannabinus* L.) stalks. Ind Crops Prod 24(2): 177–180. https://doi.org/10.1016/j.indcrop.2006.03.011

Khedari J, Choroenvai S, Hirunlabh J (2003) New insulating particleboard from durian peel and coconut coir. Build Environ 38(3): 435–441. https://doi.org/10.1016/S0360-1323(02)00030-6

Khedari J, Nonkangrob N, Hirunlabh J, Teekasap S (2004) New lost-cost insulating particleboards from mixture of durian peel and coconut coir. Build Environ 39: 59–65. https://doi.org/10.1016/j.buildenv.2003.08.001

Lee SH, Lum WC, Boon JG, Kristak L, Antov P, Pedzik M, Rogozinski T, Taghiyari HR, Lubis MAR, Fatriasari W, Yadav SM, Chotikhun A, Pizzi A (2022) Particleboard from agricultural biomass and recycled wood waste: a review. J Mater Res Technol 20:4630–4658. https://www.sciencedirect.com/science/article/pii/S2238785422013990

Mańkowski P, Laskowska A (2021) Compressıve strength parallel to grain of earlywood and latewood of yellow pine. Maderas-Cienc Tecnol (23):57:1–12. https://doi.org/10.4067/s0718-221x2021000100457

Naik TR, Friberg TS, Chun Y-C (2004) Use of pulp and paper mill residual solids in production of cellucrete. Cem Concr Res 34(7):1229–1234. https://doi.org/10.1016/J.CEMCONRES.2003.12.013

Nemli G, Kirci H, Serdar B, Ay N (2003) Suitability of kiwi (*Actinidia sinensis* P.) prunings for particleboard manufacturing. Ind Crops Prod

17(1): 39–46. https://doi.org/10.1016/S0926-6690(02)00057-2

Nemli G, Aydin A (2007) Evaluation of the physical and mechanical properties of particleboard made from the needle litter of *Pinus pinaster* ait. Ind Crops Prod 26(3):252–258. https://doi.org/10.1016/j.indcrop.2007.03.016

Nemli G, Demirel S, Gumuskaya E, Aslan M, Acar C (2009) Feasibility of incorporating waste grass clippings (*Lolium perene* l.) in particleboard composites. Waste Manage 29(3):1129–1131. https://doi.org/10.1016/j.wasman.2008.07.011

Oh YS, Yoo JY (2011) Properties of particleboard made from chili pepper stalks. J Trop For Sci 23(4):473–477. https://www.jstor.org/stable/23617062#metadata_info_tab_contents

Sevin***çli*** Y (2014) Examination of Mechanical and Physical Properties of Chipboard Produced from Waste Lavender Plant, Master's Thesis (ref. 353534), Institute of Science, SDU, Isparta, Türkiye. https://tez.yok.gov.tr/UlusalTezMerkezi/tezSorguSonucYeni.jsp

TSE - TS EN 310 (1999) Wood based panels- determination of modulus of elasticity in bending and of bending strength. EN 310. 1999. TSE: Ankara, Türkiye. https://standards.globalspec.com/std/1069407/ts-en-310

TSE - TS EN 317 (1999) Particleboards and fiberboards, determination of swelling in thickness after immersion. EN 317. 1999. TSE: Ankara, Türkiye. https://standards.iteh.ai/catalog/standards https://standards.globalspec.com/std/1061255/ts-en-317

TSE - TS EN 319 (1999) Particleboards and fiberboards, determination of tensile strength perpendicular to plane of the board. EN 319. 1999. TSE: Ankara, Türkiye. https://standards.globalspec.com/std/1047172/ts-en-319

TSE - TS EN 322 (1999) Wood-based panels- Determination of moisture content. EN 322. 1999. TSE: Ankara, Türkiye. https://standards.globalspec.com/std/1061664/ts-en-322

TSE - TS EN 323 (1999) Wood- Based panels- Determination of density. EN 323. 1999. TSE: Ankara, Türkiye. https://standards.globalspec.com/std/1048860/ts-en-323

TSE - TS EN 326-1 (1999) Wood- Based panels- Sampling, cutting and inspection- Part 1: Sampling test pieces and expression of test results. EN 326-1. 1999. TSE: Ankara, Türkiye. https://standards.globalspec.com/std/1057682/ts-en-326-1

TSE TS 642 ISO 554 (1997) Standard atmospheres for conditioning and/or testing; Specifications. TS 642-ISO 554. 1997. TSE: Ankara, Türkiye. https://standards.globalspec.com/std/1072284/ts-642-iso-554

The impact of water exposure on the mechanical properties of a wood-plastic composite

Antypas Imad Rezakalla *
Associate Professor
Don State Technical University
Gagarin Square 1, Rostov-on-Don
Russian Federation
E-mail: imad.antypas@mail.ru

(Received 19 March 2025)

Abstract. Processed and unprocessed polypropylene samples reinforced with various proportions of pine and beech wood were manufactured using pressure molding and subjected to various mechanical tests. Increasing the percentage of wood particles regardless of the wood species was associated with increased density and hardness of the wood-plastic composite, while tensile strength, deformation at fracture, and elastic limit decreased with increasing particle size. Higher moisture contents were associated with increases in both tensile strength and elastic limit.

Keywords: Wood-plastic composite; Polypropylene; Black pine; European beech; Mechanical properties; Wood particles; Polymer; Moisture effects

Introduction

There has been a growing trend to use wood waste in various industrial sectors such as construction, agriculture, forestry, automotive, and others. This trend reduces waste, conserves valuable material resources, creates new materials, or can improve properties of already existing materials (Perišić et al 2024; Rezakalla and Dyachenko 2022).

An important use of various forms of wood waste (such as pellets or fibers) is as a polymer filler in the production of wood/plastic composites (WPC). Adding wood particles creates composites with the necessary mechanical and physical properties required for specific applications under specific working conditions (Perišić et al. 2024; Rezakalla and Dyachenko 2022). These materials tend to be much more resistant to moisture absorption than the parent wood.

Wang and Morrell (2004) found slow moisture uptake in long-term immersion of two commercial WPCs (Trex® and Strandex®), but significant accumulation in the outer 5 mm layer at levels sufficient for fungal decay (Wang and Morrell 2004). Moisture mapping revealed that Strandex® absorbed water more slowly, with both brands showing moisture gradients capable of supporting fungal growth near the surface.

Wang and Morrell (2005) investigated the effects of moisture and temperature cycling on the durability and mechanical properties of wood-plastic composites (WPCs). Their study found that repeated wet-dry and freeze-thaw cycles degraded the material's strength and stiffness, while increasing water absorption and swelling. These results underscore the environmental vulnerabilities of WPCs and emphasize the need for enhanced material formulations to improve performance in outdoor applications.

Wang et al. (2020) investigated water absorption in wood-polypropylene composites with 15–45 wt% wood content and found that showing Fickian diffusion behavior accelerated at higher temperatures (23°C, 60°C, 80°C). Water absorption reduced mechanical properties, with 45% wood composites losing 32% tensile strength and 47% modulus of elasticity, while flexural strength showed similar degradation. Dynamic material analysis confirmed water's plasticizing effect, emphasizing the trade-off between wood content and moisture-induced property loss in WPCs.

* Corresponding author

Wood and Fiber Science, 57(4), 2025, pp. 205–212
https://doi.org/10.22382/wfs-2025-18

Kord (2011) examined the influence of different proportions of fixed-sized beech particles combined with polypropylene, using citric acid as a binder, on the hardness of samples manufactured through pressure molding. He concluded that increasing the percentage of wood was associated with increased hardness. This finding was further corroborated by Kaymakçi and Ayrilmiş (2013) who also reported that increased wood content was associated with increased water absorption and changes in thickness.

Lin et al. (2023) evaluated a polypropylene (PP)-based WPC prepared using twin-screw extrusion, and the effects of adding maleic anhydride (MAH) and wood flour on the properties of the WRC, prepared at ratios of 5, 6, 7, 8, 9, and 10% by weight of MAH. Increasing MAH was associated with an initial increase in tensile strength, but further additions resulted in declines, while water absorption decreased. Tensile strength also initially increased with increased wood flour, then declined, and water absorption increased by 62% when the wood flour content exceeded 10% by weight.

Cavus and Mengeloğlu (2020) examined the effect of particle size (0.074–0.841 mm) and 3% MPP on neat PP and recycled PP (rPP) wood-plastic composites containing 40% mahogany wood flour. Smaller wood particles enhanced density, stiffness (flexural/tensile modulus), and impact strength, while MAPP improved interfacial adhesion, boosting strength properties but reducing elongation. Scanning electron microscopy (SEM) revealed optimized particle-matrix bonding with MAPP, though rPP composites showed slightly reduced performance versus virgin PP.

Bhaskar et al. (2021) examined the influence of various types of polymer binders (PP, polyvinyl chloride, polyethylene vinyl acetate, and polyethylene naphthalate) on WPC properties. Polyvinyl acetate polymer had a significant impact on tensile strength, bending strength, and impact resistance properties.

These studies suggest the potential for adjusting WPC composition to minimize water absorption and thereby reduce any potential effects on mechanical properties. The objective of this study was to assess the influence of water exposure on the mechanical properties of WPCs.

Materials and methods

Material Preparation

Wood Particles

Black pine (*Pinus nigra* L.) particles (L = 300 -800 µm) with a density of 0.45 g/cm^3, and hardwood particles (L = 100-800 µm) from beech (*Fagus sylvatica* L) with a density of 0.65 g/cm^3 were obtained from a cutting and furniture finishing operation. Particle size distributions were determined by weighing a series of sieves with different diameters. The particles were added and the sieves were vibrated for 3 minutes, after which the amount of particles retained in each sieve was weighed (Figure 1).

Particles larger than 600 µm were removed, since previous studies have shown that moisture absorption increases with increasing particle size (Bhaskar et al. 2021; Abdul Rahman et al., 2023).

The particles were oven-dried at 100°C for 120 minutes and then placed in vacuum sealed bags to minimize moisture absorption. The bags were stored in a cool/dry location until needed.

Polymer granules

Primary polypropylene (PP) particles were obtained from SABIC PP 520 L (Saudi Basic Industries Corporation, Riyadh, Saudi Arabia) with the following characteristics: density: 0.910 g/cm^3; melting point: 160°C; Shore D hardness: 70; tensile strength (ISO 527): 32 MPa; flexural modulus (ISO 178): 1300 MPa.

Particles from recycled plastic industry waste polymer plants (Re-PP) had the following characteristics: density: 0.910 g/cm^3; melting point: 20 g/10 min; Shore D hardness: 70; tensile strength 25 MPa; flexural modulus 1300 MPa.

Coupling agent

Abietic acid was ground to a fine powder and used as a coupling agent for wood and polymers. This organic material had an average melting point of 140°C, density of 1.06 g/cm^3, and was insoluble in water (Ataman Chemicals, Turkey).

Manufacturing of casting molds

The sample injection mold was designed using the ANSYC program, following specifications described in ASTM Standard D-638 (2003). The mold was then manufactured using a CNC machine and subsequently assembled.

Manufacturing of wood-plastic composites (WPC)

The materials were used to assess the effects of different wood/plastic ratios on WPC properties (Table 1).

Injection Process

The materials were thoroughly mixed before being introduced into the funnel of a Qingdao Tongsan extruder operated at 450 kPa for 10 s (Qingdao Tongsan Plastic Machinery Co, Ltd, China). The materials were held at 450 kPa for 4 s before being extruded through the system, with temperatures held at 170°C

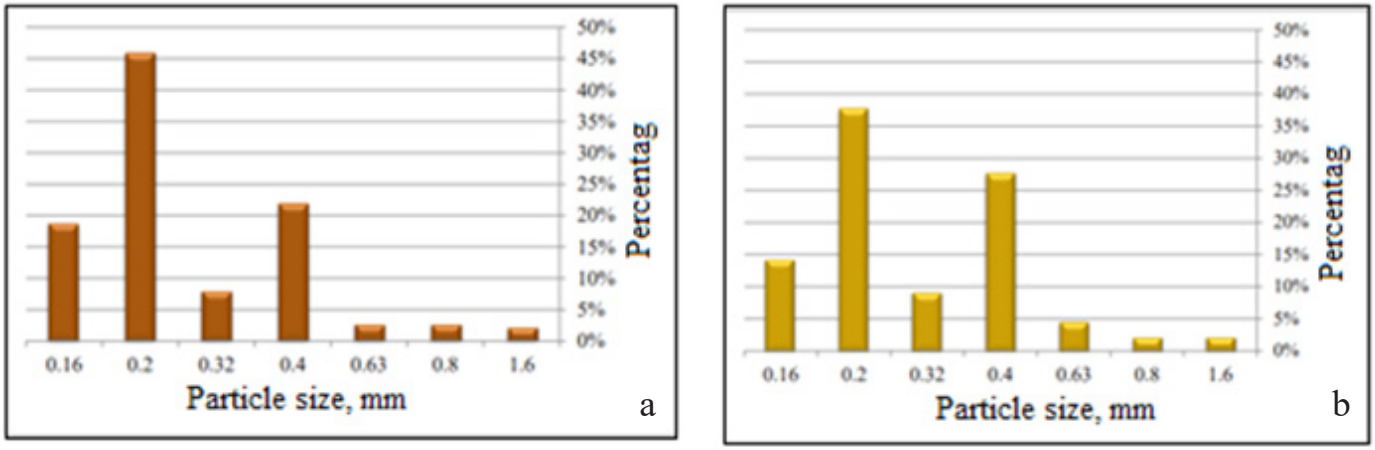

Figure 1 Wood Particle Size Distribution in (a) beech or (b) pine.

for the feed, and 190°C for zone 1, zone 2, and the nozzle. The samples were cooled for 15 seconds and then stored at 23 ± 2°C and 50 ± 5% RH until tested (Figure 2).

Experiments

Density determination test

Sample density was determined by weighing (nearest 0.005 g) and then determining volume by water displacement. Density tests were conducted on three samples of each material and averaged.

The influence of immersion time on density

WPC samples were weighed and immersed in distilled water according to ASTM Standard D-1037 (1999), with three samples taken for each reinforcement ratio. After the desired immersion time, the samples were removed, liquid water was wiped off, and the samples were weighed (nearest 0.001 g) and their dimensions measured. This process was repeated after 0.5, 1, 7, and 14 days, and the data were used to calculate density.

Hardness test

Hardness was assessed on three samples of each material according to ASTM Standard D-2240 (2003). Five readings were taken per sample using a Shore Type HD 3000 Durometer (Hildebrand Korsklldelumd, Germany) at a pressure force of 5000 g, with a measurement displacement of 2.5 mm, an indenter at 30°, and a measuring range of 10–90 (LABOMAT Equipment and Specialties, France).

Tensile test

The tensile strength was assessed according to ASTM Standard D-638 (2003) on a CY -6120 Tensile tester with a 50 kN load cell (Chun Yen Testing Machines Co., Ltd., Taiwan). Tensile tests were conducted on three samples of each material, and the average value of the results was taken after calculating

Table 1. Proportions of components used to manufacture wood-plastic composites.

Sample code	Wood particles, Wt%	Polymer, Wt%	
		Virgin (%)	Recycled (%)
PP15/Pine	15	83	—
PP30/Pine	30	68	—
PP45/Pine	45	53	—
PP15/Beech	15	83	—
PP35/Beech	30	68	—
PP45/Beech	45	53	—
RePP15/Pine	15	—	83
RePP30/Pine	30	—	68
RePP45/Pine	45	—	53

2% mass/mass of coupling agent was added to all mixtures.

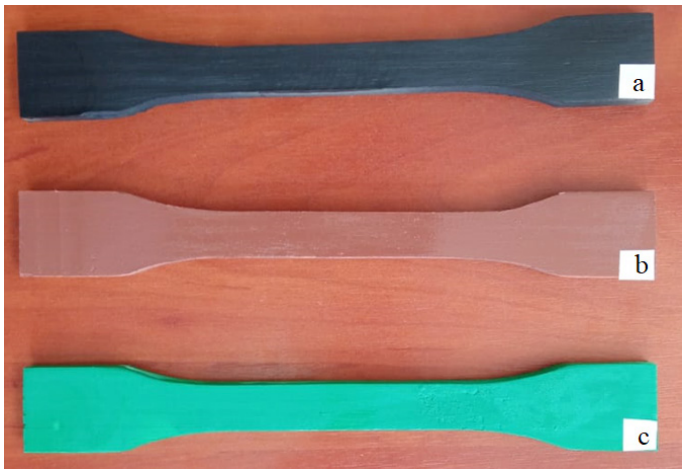

Figure 2. Samples of wood-plastic composite containing (a) pine, (b) beech, or (c) recycled PP with pine.

the deviation and confidence. (Example: for the sample PP/15 pine, average μ = 22.6 MPa, standard deviation σ ≈ 1.14 MPa → 22.6 ± 1.0 MPa (95% confidence)).

Results and discussion

Density

Density increased 9.35% with the addition of 45% pine and 10.45% with the addition of 45% beech (Figure 3). This density increase was somewhat lower at low reinforcement ratios, as it was only 0.6% for 15% pine wood and 1.15% for beech wood fiber reinforcement. Increased density of the WPC reflects the compression of the denser wood cell wall (Maldas et al. 1989).

Production processes that use high pressure, such as injection molding at 5 bar, exert pressure on the cell walls, leading to increased density of wood particles and, consequently, increased WPC density (Amos et al. 2012; DeArmitt 2017).

There was a marked increase in density of the recycled polypropylene, starting at 2.6% with the addition of 15% pine and reaching 13% with the addition of 45% pine. Recycled polypropylene generally had a higher density than virgin polypropylene due to the presence of materials added during earlier production.

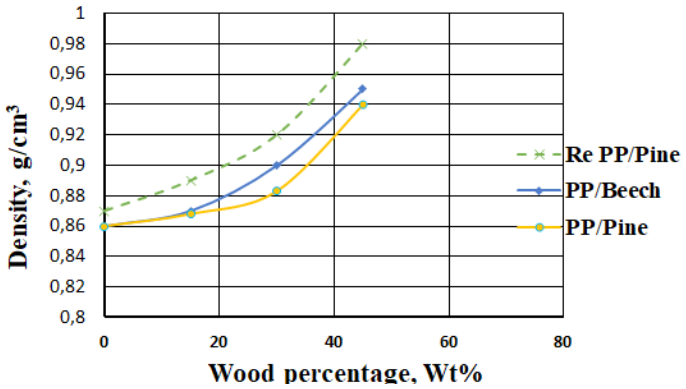

Figure 3. Effect of different proportions of pine or beech particles on density of the resulting WPC.

The influence of immersion time on density

Water absorption increased as the percentage of wood particles increased (Figure 4). Water absorption in composite materials is primarily associated with cellulose and hemicellulose because they contain a large number of easily accessible hydroxyl groups. Since wood naturally has a high water-absorption capacity, an increase in the ratio of wood particles results in a corresponding increase in water absorption of the WPC. It is important to note that the polypropylene exhibits almost

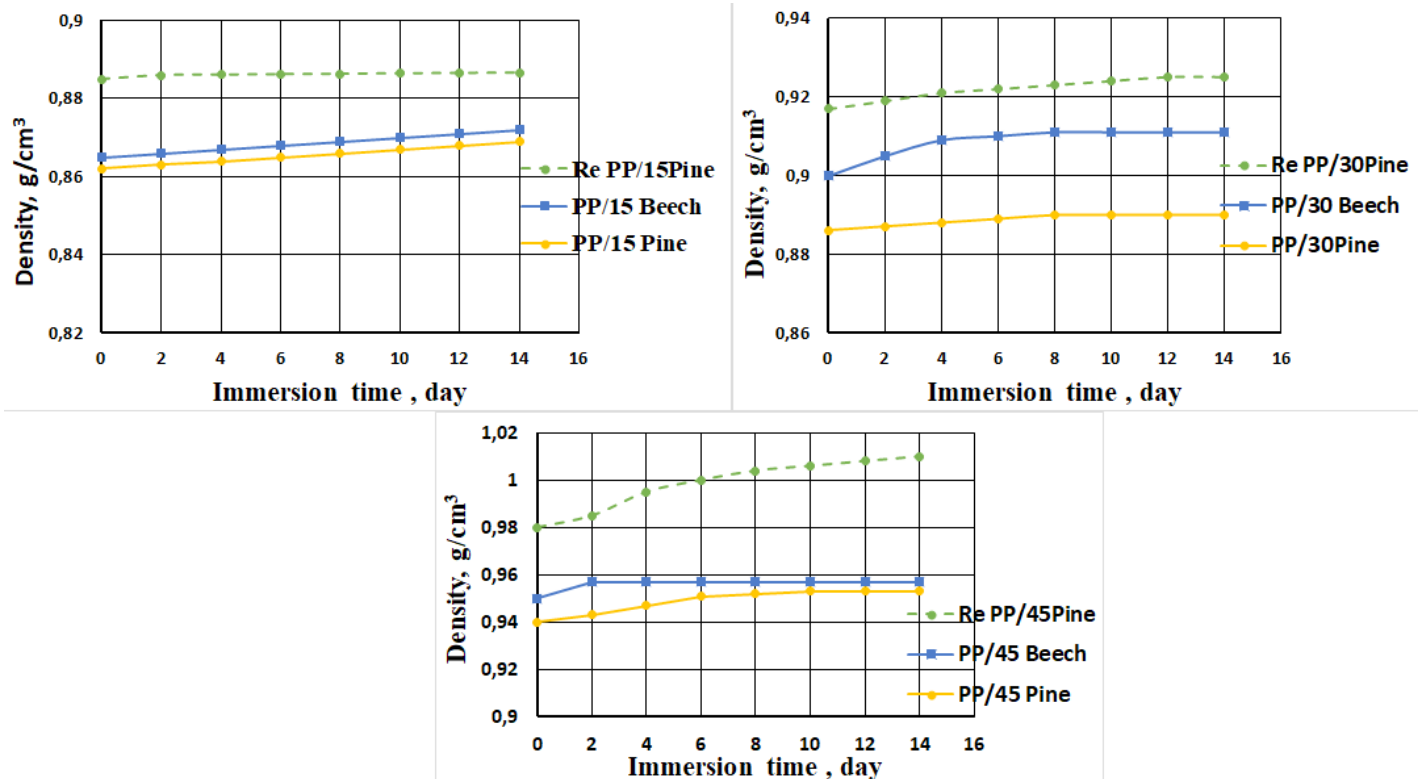

Figure 4. Effect of water immersion on density of WPCs with different ratios of wood particles and polypropylene.

negligible water absorption compared to wood during the specified immersion time, which aligns with the findings of previous research (Kord 2011; Cavus and Mengeloğlu 2020).

The RePP45/Pine samples had a greater water absorption capacity, as their density increased by 3.2%, while the PP15/Beech samples were less water-absorbent, with their density increasing by only 0.12%.

Influence of reinforcement percentage on hardness

WPC hardness increased with increased wood particle level for both wood species. The increase was 21% when reinforced with 45 wt.% pine wood particles and 22.6% when reinforced with 48 wt.% beech wood particles. A similar result was observed when comparing virgin and recycled PP. Hardness increased by 21% with 45 wt.% pine wood particles using virgin PP, and by 14% when using recycled PP (Figure 5).

There was no difference in hardness in WPC samples immersed for 14 days (Table 2).

Hardness increased linearly with increasing WPC density, with the derivative of hardness, with respect to density, being greater than zero, indicating a linear function (Figure 6).

Tensile test

The tension tests were used to derive mechanical behavior curves (Figure 7). Tensile strength, fracture strain, and yield strength all decreased with increased wood content, while modulus of elasticity increased. Increased MOE with increased wood content reflects that ability of wood to stiffen the PP, but these materials disrupt the PP, reducing tensile strength (Figure 8) (Gnatowski 2002).

Influence of the recycled polymer on tensile properties

Overall, mechanical properties were higher when using primary PP compared to recycled PP at the same wood level

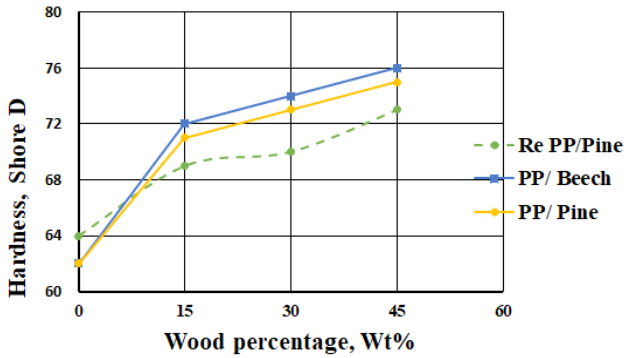

Figure 5. Effect of increasing wood levels on hardness of WPCs prepared using virgin or recycled PP.

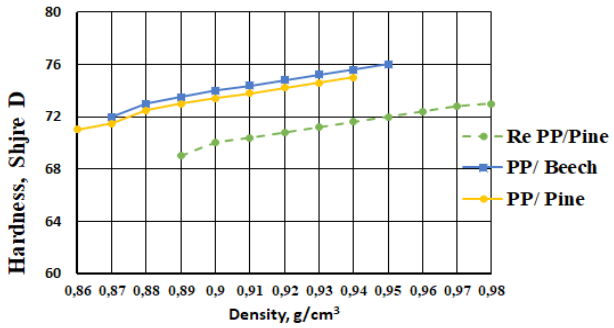

Figure 6. Relationship between density and hardness of WPCs containing different ratios of wood.

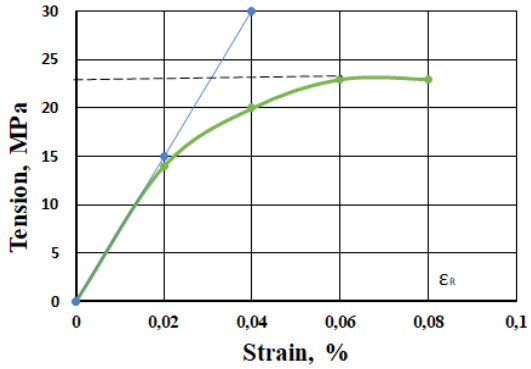

Figure 7. Example of a stress-strain curve of a wood-plastic composite reinforced with 15% pine.

Table 2. Change in WPC hardness over time samples immersed in water for up to 14 days.

Sample code	Hardness (Shore D)				
	Pre-immersion	0.5 day	1 day	7 days	14 days
PP15/Pine	71	70	69	70	70
PP30/Pine	73	73	72	72	73
PP45/Pine	75	75	75	74	74
PP15/Beech	72	72	71	72	71
PP30/Beech	74	74	74	74	74
PP45/Beech	76	75	75	75	75
Re PP15/Pine	69	69	69	69	69
Re PP30/Pine	70	70	71	70	70
Re PP45/Pine	73	72	72	71	71

Values represent means of 3 replicates per material and time (ASTM D-1037)

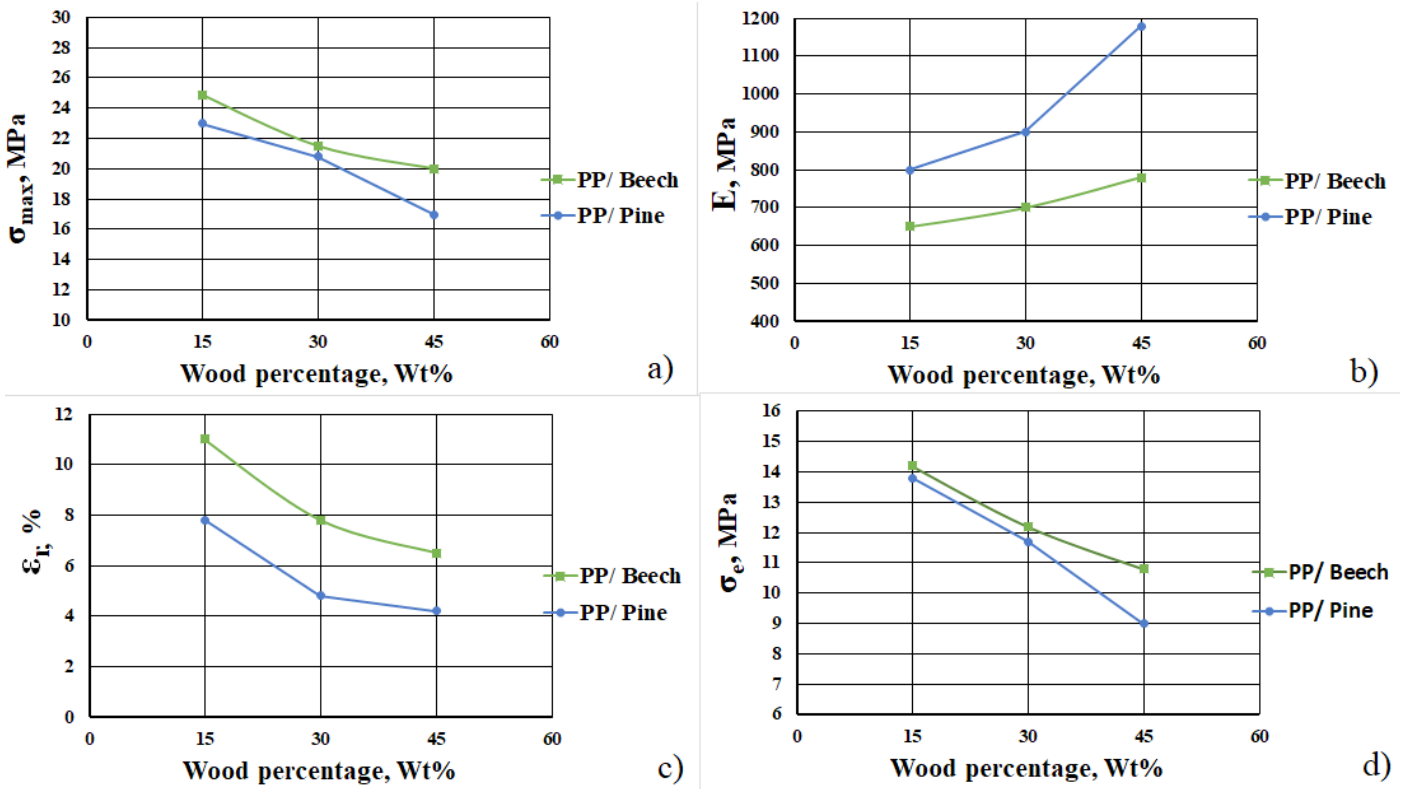

Figure 8. Effect of increased proportions of wood particles in a WPC on (a) tensile strength, (b) modulus of elasticity,(c) fracture strain, and (d) yield strength for WPC at different blending ratios of pine and beech wood particles.

(Figure 9). This could be attributed to impurities present in the recycled polymer, which negatively affect the adhesion between components and weakened the interfacial surfaces, aligning with the findings of previous research (Kord et al. 2011). Additionally, differences in the structures of primary and recycled polypropylene may also play a role.

The influence of immersion time on tensile mechanical properties

Maximum stress and yield stress both increased with immersion time, while MOE initially declined then increased slightly over time (Figure 10).

From Figure 10a, it can be observed that, at the beginning of the immersion, the maximum stress decreased in magnitude. The resistance of composite materials reflects the quality of the interfacial surfaces between components, which allows for the transfer of stress from the binder material to the support. The strength of this bond contributes to improved resistance. However, during immersion, water was absorbed by the wood, leading to distortions at the interface or failure of the bond between the polymer and the wood, resulting in degradation of the surface and a decrease in resistance. As the immersion time increased and exceeded 2 days, the wood continued to absorb more water, causing the particles to swell and fill the voids in their structure, which hindered the sliding of polymer chain molecules and ultimately increased the tensile strength.

MOE tended to decrease at the start of immersion and then increased slightly with additional immersion time (Figure 10b). The initial declines may be due to hydrogen bonding between water molecules and wood fibers. However, in the presence of moisture, these bonds break, forming new hydrogen bonds with water molecules, which leads to a decrease in mechanical properties. Subsequent swelling of wood particles within the PP matrix may account for the slight increase in MOE with longer immersion times.

Increased moisture content at the start of immersion led to increased elongation, due to slippage between water and wood, resulting in a weakening of the bond between the polymer and the wood (Figure 10b). However, the elongation values for all reinforcement ratios decreased when the immersion time reached approximately 1 day. This decrease was associated with the swelling of the wood and the filling of voids in the interfacial surfaces between the polymer and the wood. The higher the wood particle content, the lower the elongation at failure. However, elongation again increased after 2 days of immersion.

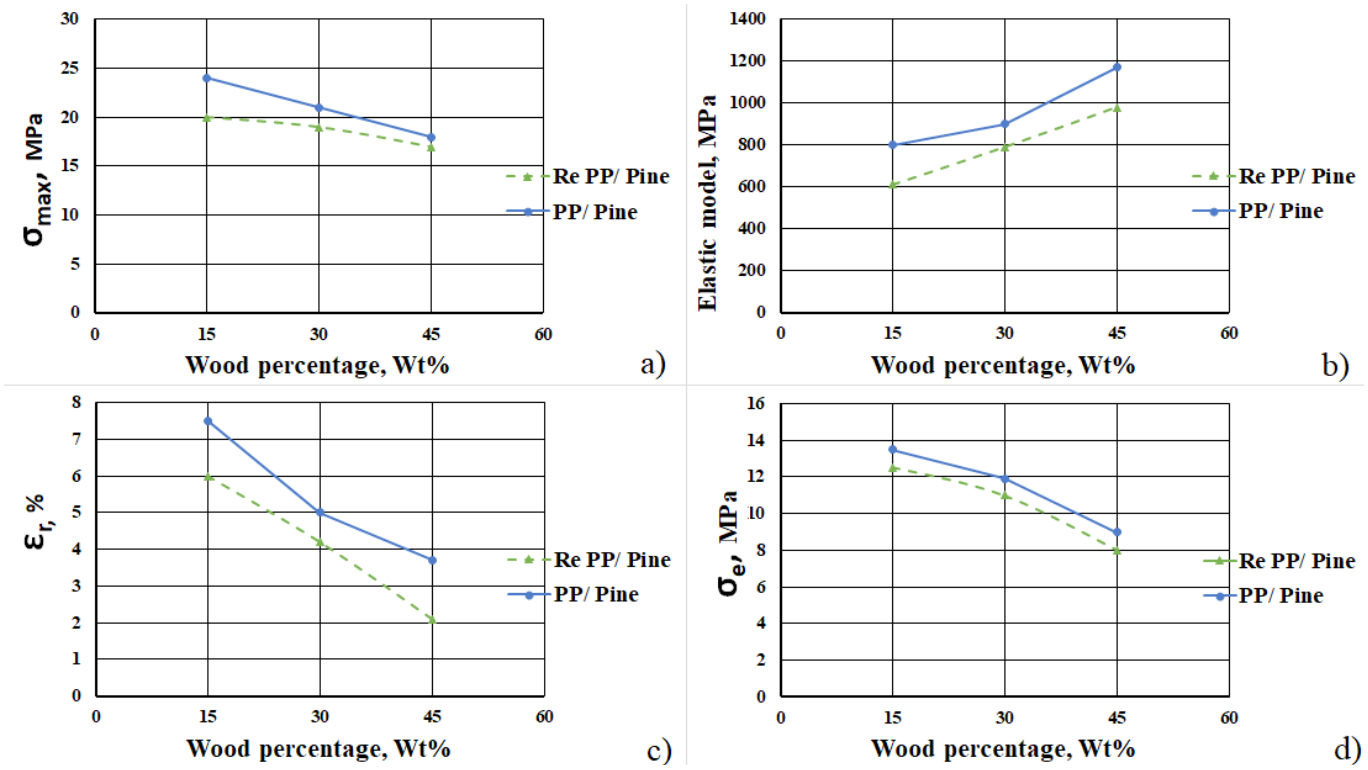

Figure 9. Effect of the use of virgin or recycled polypropylene on (a) tensile strength, (b)modulus of elasticity, (c) fracture strain, and (d) yield strength in tension of WPCs with different ratios of pine.

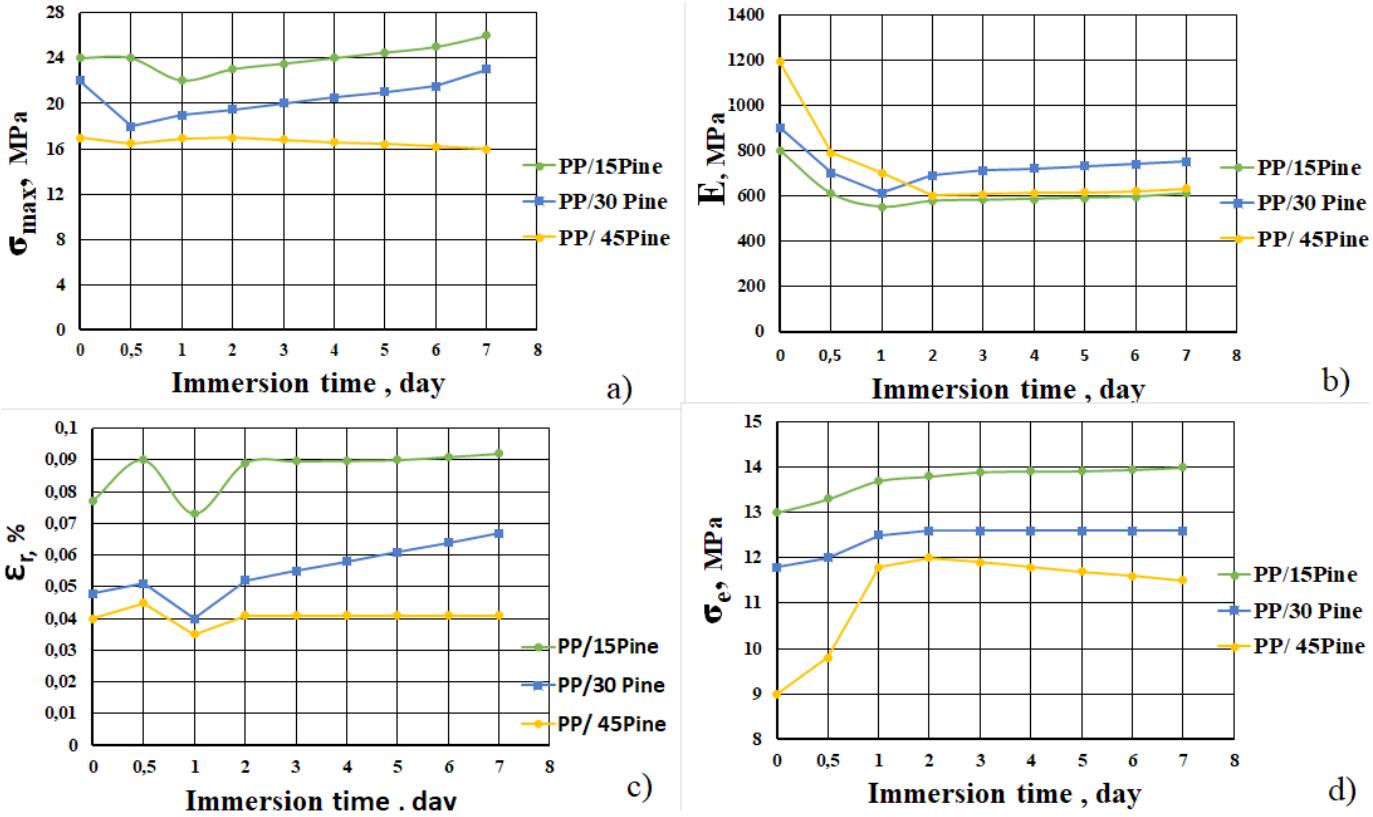

Figure 10. Effect of water immersion time on (a) maximum stress, (b) modulus of elasticity, (c) fracture strain, and (d) yield strength for WPCs made from primary and recycled PP with different ratios of pine particles.

Conclusions

Wood plastic composite hardness and density improved with increasing wood filler percentage, with the hardness of reinforcing materials directly impacting final product performance. A 2-week immersion had minimal effect on hardness, regardless of specific component ratios or material combinations.

Particle size analysis revealed that larger particles adversely affected several key properties, including ultimate strength, failure deformation characteristics, and elastic limit performance. Conversely, stiffness measurements showed consistent enhancement with greater wood content across all tested formulations.

Failure deformation and elastic limit increased at lower moisture levels, while tensile strength and elastic modulus decreased. High moisture environments produced the opposite effect, elevating both tensile strength and elastic limit.

Recycled PP composites exhibited similar performance trends to virgin material counterparts, but the properties were reduced, possibly because the parent materials in the recycle products had extra additives.

These findings provide valuable insights for optimizing WPC formulations to meet specific engineering requirements. The consistent, predictable relationships observed between processing parameters and final product characteristics offer manufacturers reliable guidelines for material development and application-specific tuning of composite properties. The comprehensive results establish a foundation for further research into advanced WPCs and their practical implementations.

Recommendations

Further investigate the optimal ratios of wood particles to plastic in order to enhance specific mechanical properties such as tensile strength, elasticity, and hardness.

Study the effects of different types of binding materials and their impact on the bonding quality of wood-plastic composite components.

References

Abdul Rahman A, Adeboye OJ, Adebayo A, Salleh MR (2023) Behaviour and some properties of wood plastic composite made from recycled polypropylene and rubber wood. Jordan J Mech Ind Eng 17(2):281–287.

Amos SE, D'Souza A, Yalcin B, Ista TK, Clemons CM (2012) Processing behavior, morphology and benefits of using low density hollow glass microspheres in polymer wood composites. In: Proceedings of the 11th international conference on wood and biofiber plastic composites & nanotechnology in wood composites symposium. 2011 May 16-17; Madison, WI. 3M Energy and Advanced Materials, and USDA Forest Service, Forest Products Laboratory. Madison, WI. https://www.fpl.fs.usda.gov/documnts/pdf2011/fpl_2011_amos001.pdf

ASTM D 638-03 (2003) Standard Test Method for Tensile Properties of Plastics, ASTM International, West Conshohocken.

ASTM D 2240-97 (2003) Standard Test Method for Rubber Property -Durometer Hardness, ASTM International, West Conshohocken.

ASTM D 1037- 99 (1999) Standard Test Methods for Evaluating Properties of Wood-Base Fiber and Particle Panel Materials, ASTM International, West Conshohocken. https://store.astm.org/d1037-12r20.html

Bhaskar K, Jayabalakrishnan D, Vinoth Kumar,M, Sendilvelan S, Prabhahar M (2021) Analysis on mechanical properties of wood plastic composite. Materials Today 45(7):5886-5891. https://doi.org/10.1016/j.matpr.2020.08.570

Cavus V, Mengeloğlu F (2020) Effect of wood particle size on selected properties of neat and recycled wood polypropylene composites. BioRes 15(2):3427–3442.

DeArmitt C (2017) Functional fillers for plastics. Pp 517–532 in Applied Plastics Engineering Handbook (second edition), ed. Myer Kutz. Elsevier eBooks, 437. https://doi.org/10.1016/b978-0-323-39040-8.00023-7

Gnatowski M (2002) Water Absorption and Durability of Wood Plastic Composites, Polymer Engineering Company Ltd, Canada.

Kaymakçi A, Ayrilmiş N (2013) Determination of the relationships between Brinell hardness and tensile strength of wood plastic composites. PRO LIGNO 9(4):430-434. https://www.proligno.ro/en/articles/2013/4/Kaymakci_final.pdf

Kord B (2011) Effect of wood flour content on the hardness and water uptake of thermoplastic polymer composites, World Appl Sci J 12(9):1632–1634. https://www.idosi.org/wasj/wasj12(9)/41.pdf

Kord B, Danesh MA, Veysi R, Shams M (2011) Effect of virgin and recycled plastics on moisture sorption of nanocomposites from newsprint fiber and organoclay. BioRes 6(4):4190–4199. https://doi.org/10.15376/biores.6.4.4190-4199

Lin Z, Xiang Q, Xu DE (2023) Study on water resistance of polypropylene based wood-plastic composites used in building. Compos Adv Mater 32:1–9. https://doi.org/10.1177/26349833231218017

Maldas D, Kokta BV, Daneault C (1989) Thermoplastic composites of polystyrene: effect of different wood species on mechanical properties, J Appl Polym Sci 38(3):413. https://doi.org/10.1002/app.1989.070380303

Perišić S, Kalevski K, Grujić A, Nedeljković D, Stajić-Trošić J, Radojević V (2024) Effect of moisture on the mechanical properties of wood-plastic composites hybridized with metal grid layers. Polymers 15(24):4705. doi: 10.3390/polym15244705

Rezakalla AI, Dyachenko AG (2022) Physical and mechanical properties analysis of wood-waste composite panels. Materiale Plastice 59(2):61–72. https://doi.org/10.37358/MP.22.2.5585

Wang W, Morrell, JJ (2004). Water sorption characteristics of two wood-plastic composites. Forest Prod J 54(12):209–212. https://ir.library.oregonstate.edu/concern/articles/sf2685560

Wang W, Morrell JJ (2005) Effects of moisture and temperature cycling on material properties of a wood/plastic composite. Forest Prod J 55(10):81–83.

Wang W, Guo X, Zhao D, Liu L, Zhang R, Yu J (2020) Water absorption and hygrothermal aging behavior of wood-polypropylene composites. Polymers 12(4):782. https://doi.org/10.3390/polym12040782https://doi.org/10.3390/polym12040782